Heat-Mediated Optical Manipulation

Zhihan Chen[†],
Materials Science & Engineering Program, Texas Materials Institute, and Walker Department of Mechanical Engineering, The University of Texas at Austin, Austin, Texas 78712, United States

Jingang Li[†],
Materials Science & Engineering Program, Texas Materials Institute, and Walker Department of Mechanical Engineering, The University of Texas at Austin, Austin, Texas 78712, United States

Yuebing Zheng
Materials Science & Engineering Program, Texas Materials Institute, and Walker Department of Mechanical Engineering, The University of Texas at Austin, Austin, Texas 78712, United States

Abstract

Progress in optical manipulation has stimulated remarkable advances in a wide range of fields, including materials science, robotics, medical engineering, and nanotechnology. This Review focuses on an emerging class of optical manipulation techniques, termed heat-mediated optical manipulation. In comparison to conventional optical tweezers that rely on a tightly focused laser beam to trap objects, heat-mediated optical manipulation techniques exploit tailorable optothermo–matter interactions and rich mass transport dynamics to enable versatile control of matter of various compositions, shapes, and sizes. In addition to conventional tweezing, more distinct manipulation modes, including optothermal pulling, nudging, rotating, swimming, oscillating, and walking, have been demonstrated to enhance the functionalities using simple and low-power optics. We start with an introduction to basic physics involved in heat-mediated optical manipulation, highlighting major working mechanisms underpinning a variety of manipulation techniques. Next, we categorize the heat-mediated optical manipulation techniques based on different working mechanisms and discuss working modes, capabilities, and applications for each technique. We conclude this Review with our outlook on current challenges and future opportunities in this rapidly evolving field of heat-mediated optical manipulation.

Graphical Abstract

Corresponding Author: **Yuebing Zheng** – Materials Science & Engineering Program, Texas Materials Institute, and Walker Department of Mechanical Engineering, The University of Texas at Austin, Austin, Texas 78712, United States; zheng@austin.utexas.edu.
[†]Z.C. and J.L. contributed equally to this work.

The authors declare no competing financial interest.
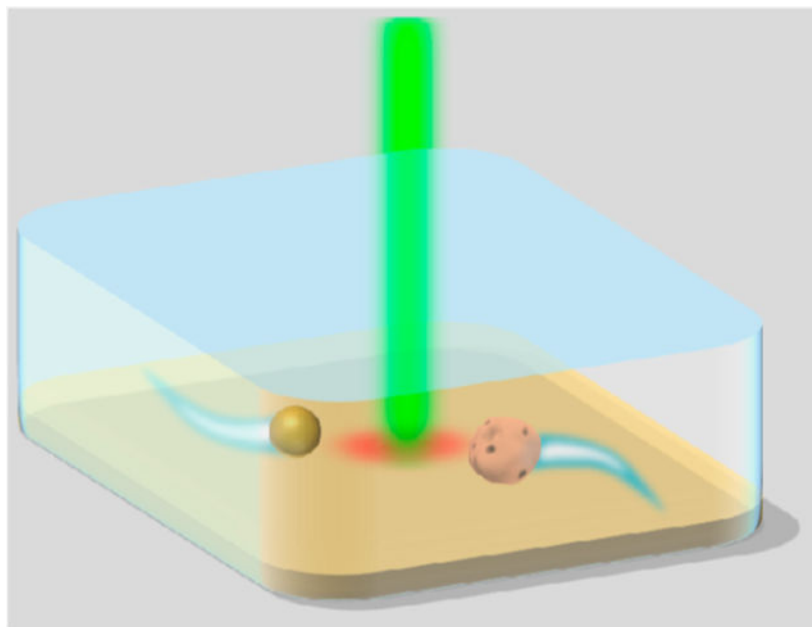
1. INTRODUCTION

Precise manipulation of nanomaterials is instrumental in nanofabrication,[1–3] robotics,[4,5] material characterization,[6–8] and fundamental sciences.[9,10] Many approaches have been proposed for this purpose. For instance, optical tweezers exploit optical gradient forces from a tightly focused laser beam to trap small objects.[11,12] Alternatively, directed migration in a temperature or concentration gradient field, also known as thermophoresis or diffusiophoresis, is widely applied for the concentration of nanoparticles and biomolecules.[13,14] Electrophoretic and dielectrophoretic forces are also commonly used to trap or separate different objects in an external electrical field.[15–17] In addition, efficient manipulation of micro/nano-objects has been demonstrated with magnetic[18] and acoustic fields.[19,20] Among them, optical approaches are highly attractive due to their remote and noncontact operation, single-particle resolution, and high manipulation precision. Proposed by Ashkin in 1970,[11] optical tweezers have been extensively applied in broad fields and were awarded the Nobel Prize in Physics in 2018 for their applications in the study of biological systems.[21] However, conventional optical tweezers suffer from high operational power, the optical diffraction limit, and the requirement of a difference in refractive indexes of the solution and target objects.[22] To enhance the versatility of optical manipulation, structured light with tailorable optical intensity, phase, and polarization has been extensively applied.[23–25] In addition to the gradient forces, optical torques,[26–28] optical pulling forces,[29–31] and optical binding forces[32–34] are realized with structured light for optical rotation,[35–37] particle transport,[38–40] and colloidal self-assembly.[41–44]

Recent efforts have shown that multiple forces or fields can be coupled to develop hybrid manipulation methods with additional flexibility and advantages over the techniques based on single forces. For example, the integration of optical tweezers and dielectrophoresis leads to the invention of optoelectronic tweezers, which can overcome both the high operating

power in optical tweezers[45–47] and the requirement of sophisticated electrical circuits in dielectrophoretic manipulation[48] to achieve on-demand manipulation of objects with low optical power.[49,50] In another example, optofluidics, i.e., the integration of optics and fluidics, has demonstrated faster delivery and more stable trapping of target analytes at the sensing/imaging locations compared with conventional fluidic platforms, which can remarkably enhance the analytical capabilities.[51–53]

In the late 19th century, a series of physical phenomena on the thermal migration of objects were discovered. In 1856, Ludwig reported thermophoresis in liquid mixtures, while Tyndall independently observed thermophoresis in gas mixtures in 1870.[54] In 1877, Tore described the movement of carbon particles in the direction of light, which was marked as the first observation of photophoresis.[55] Subsequently, more thermal effects, including thermally induced diffusiophoresis, natural convection, and Marangoni convection, were discovered. Recently, various heat-mediated optical manipulation techniques have been proposed and developed via the integration of optics and thermal physics.[56] Here, we refer to "heat-mediated optical manipulation" as a category of optical manipulation techniques that are enabled by the synergy of optics (including optical forces, optical heating, and optical cooling) and temperature-gradient-induced mass transfer. Owing to the entropically favorable photon–phonon conversion and tailorable thermal management, the desired temperature field can be readily created and dynamically controlled with low optical intensity and simple setups.[57–59] By exploiting the various thermal forces and motions such as thermophoresis, photophoresis, and convective flows in the light-controlled temperature field, researchers have achieved versatile manipulation of various objects with diverse materials, shapes, and sizes (ranging from nanoscale to macroscale) in different environmental media.[60,61] With tunable manipulation modes, including trapping, nudging, pulling, and rotating, many applications are proposed to advance the fields of nanofabrication, nano-medicine, chemical and biological sensing, robotics, and fundamental investigation of physics, chemistry, and biology.

This Review provides a comprehensive overview of heat-mediated optical manipulation (Figure 1). We introduce the fundamentals of opto-thermomechanics involved in the manipulation processes, including optothermal conversion, thermophoresis, diffusiophoresis, photophoresis, optothermal flows, and optothermal deformation. We further discuss the design rationales and capabilities of different heat-mediated optical manipulation techniques based on their distinct mechanisms and highlight their implementations in architected nanomaterials and artificial robotics. Finally, we present our perspectives on the merits, challenges, and future directions of heat-mediated optical manipulation.

2. PHYSICAL MECHANISMS

In this section, we briefly introduce major physical mechanisms involved in heat-mediated optical manipulation techniques. We start with the basic principles of optical heating and cooling. Then, different optothermo–matter coupling phenomena, including thermophoresis, diffusiophoresis, thermoelectricity, optothermal convection flows (i.e., natural convection, optothermally induced Marangoni convection, and electrothermoplasmonic flow), and optothermal shape deformation, are discussed.

2.1. Optical Heating and Cooling

2.1.1. Optical Heating.—Most materials, including metals, polymers, and ceramics, can absorb light at certain wavelengths under ambient conditions. The absorbed photon energy leads to the excitation of electrons, and the subsequent nonradiative decay of the excited electrons converts the energy to heat. Common photothermal materials include (1) metals such as gold (Au)[62] and chromium (Cr);[14] (2) carbon-based materials such as reduced graphene oxide (rGO),[63] carbon nanotubes (CNTs),[64] and graphene nanoplatelets;[65] (3) organic materials such as polydopamine (PDA)[66] and azobenzene;[67] and (4) other materials such as amorphous silicon,[68] titanium oxide[69] and nitride,[70] lead sulfide,[71] and light-absorbing liquids.[72]

Metals are most extensively used for optical heating via visible or near-infrared (NIR) laser irradiation, which is also known as plasmonic heating. Specifically, localized surface plasmons of metallic nanostructures can be excited upon light illumination, which increases the frequency of collisions between the conductive electrons and lattice atoms and promotes photon–phonon conversion. Consequently, a temperature gradient field is built around the illuminated region of the metallic nanostructure, which is given by[57,59]

$$\rho C_P \frac{\partial T(r)}{\partial t} - \nabla \cdot [\tau \nabla T(r)] = q \tag{1}$$

where ρ, C_P, and τ are the density, specific heat capacity at constant pressure, and thermal conductivity of the irradiated region, respectively; t is the irradiation time; and q is the volumetric heat-generation density that stems from the optical heating of the nanostructures. When the plasmonic heating reaches a steady state, the temperature gradient field is given by[73]

$$\nabla \cdot [\tau \nabla T(r)] = -q = -\frac{1}{2} Re(J \cdot E^*) \tag{2}$$

where **J** and **E** are the electronic current density and electric field inside the metallic nanostructure, respectively. More details on plasmonic heating can be found in refs 59, 74, and 75.

Nanostructured photothermal materials are commonly used to sustain a strong temperature gradient field via optical heating for enhanced manipulation. For instance, a bulk Au thin film is usually less effective due to its high thermal conductivity, which makes it difficult to obtain a steady and strong temperature gradient field. Instead, many Au nanostructures are designed to improve the localized heating for the establishment of a desired temperature field, including Au nanoparticle linear arrays,[76] Au nanoparticle random arrays,[77] Au nanorod arrays,[62] Au nanohole arrays,[78] and Au nanopyramidal dimer arrays.[79] Moreover, some anisotropic nanostructures (e.g., Au nanorod arrays) can respond differently to the polarization of the incident light, providing an extra degree of freedom to modulate the temperature gradient fields for versatile optical manipulation.[62] Photothermal materials can serve as the substrate and heating source for heat-mediated optical manipulation of target objects. Alternatively, the manipulated objects can be doped or coated with light-absorbing materials to serve as self-heating sources for heat-mediated optical manipulation.[80]

2.1.2. Optical Cooling.—In addition to heat generation via photon–phonon conversion, light-induced heat dissipation has been demonstrated for solid-state materials, i.e., optical cooling or laser refrigeration.[81,82] Optical cooling of a solid crystal can be realized by anti-Stokes fluorescence. Briefly, the incident photons excite electrons from the ground state to the excited state. The excited electrons absorb lattice phonons and spontaneously emit new photons with a larger energy than that of the incident photons, which takes away thermal energy from the crystal lattice and leads to its internal cooling.[82] More details about optical cooling can be found in refs 82–85.

Optical cooling was predicted by Pringsheim in 1929[86] and experimentally demonstrated by Epstein et al. in 1995 using ytterbium (Yb)-doped fluorozirconate glass.[87] Since then, laser refrigeration of ytterbium-doped crystals has been extensively investigated,[88–92] and the record shows optical cooling of ytterbium-doped yttrium lithium fluoride ($YLiF_4$) crystals to ~91 K from room temperature.[93] In addition, Xiong and co-workers demonstrated laser cooling of a cadmium sulfide semiconductor[94] and organic–inorganic lead halide perovskites[95] based on anti-Stokes fluorescence. Recently, Pauzauskie and co-workers demonstrated laser refrigeration of ytterbium-doped nanocrystals in liquid media.[96,97] Similar to optical heating, the local cooling of crystals in solutions can also be harnessed to facilitate optical manipulation of micro- or nanoscale objects.[98]

2.2. Thermophoresis

Thermophoresis, also known as thermodiffusion, thermal diffusion, or the Ludwig–Soret effect, is one typical type of phoretic motion.[99–103] It describes the thermally directed migration of colloidal species in the fluidic environments under a temperature gradient field (Figure 2a). When a particle is in a thermal gradient field, excess hydrostatic pressure occurs within a thin layer at the particle/solvent interface, i.e., electrical double layers, which leads to an anisotropic pressure tensor in the vicinity of the particle surface. Accordingly, the particle moves toward the direction of decreasing the interfacial free energy.[104] In general, the drift velocity u for a particle is given by

$$u = -D_T \nabla T \qquad (3)$$

where D_T is the thermophoretic mobility and ∇T is the temperature gradient. For a diluted suspension, the mass flow J is expressed as $J = -D\nabla c - cD_T \nabla T$, where D is the Brownian diffusion coefficient and c is the particle concentration. At the steady state ($J = 0$), ∇c is given by[101]

$$\nabla c = -c\frac{D_T}{D}\nabla T = -cS_T \nabla T \qquad (4)$$

where $S_T = D_T/D$ is the Soret coefficient. Because different colloidal species have Brownian diffusion coefficients D with differences up to several orders of magnitude, the Soret coefficient S_T provides a more general description of thermophoretic migration. When $S_T > 0$, suspended particles are thermophobic and move from the hot region to the cold region; otherwise, particles are thermophilic and move from the cold region to the hot region with $S_T < 0$. In general, most colloidal particles are thermophobic under ambient conditions.[102]

The magnitude of S_T also indicates the scale of the particle concentration gradient in a temperature field.

Thermophoresis in liquids is complex, and a general physical model is still missing. The Soret coefficient S_T has been found to be synergistically determined by a number of parameters, including the particle/solvent interfacial properties,[105,106] environmental temperature,[100,107] size of the particle,[108] and hydrodynamic boundary effects.[109,110] For example, Piazza and co-workers found that the Soret coefficient was a function of the solution ionic strength and the Debye length in sodium dodecyl sulfate (SDS) micellar solution or a mixture of SDS and dodecylmaltoside.[99,111] Putnam et al. revealed the pH-dependence of the S_T of suspended polystyrene (PS) latex colloids.[112] In addition, the sign of S_T, namely, the moving direction of the colloidal particles under a temperature gradient, can be reversed by changing the environmental temperature, which has been experimentally validated in different colloids, including lysozyme proteins,[100,113] PS beads,[111–114] micelles,[111] DNAs,[115] and Ludox particles.[116] More detailed and comprehensive discussion on thermophoresis can be found in a review by Piazza and Parola.[102]

2.3. Thermoelectricity

Thermophoretic migration can be regulated by adding ions into colloidal particle suspensions[117] through the establishment of thermoelectric fields.[118] In brief, depending on their Soret coefficients,[119] different ions migrate at different velocities and directions under a temperature gradient via thermophoresis, leading to a spatial separation of ion species with opposite charges. Consequently, when the ionic redistribution reaches a steady state in a closed system, a thermoelectric field E_T is established, which is also termed the Seebeck effect (Figure 2b),[120]

$$E_T = S \nabla T = \frac{k_B T \nabla T}{e} \frac{\sum_i Z_i n_i S_{Ti}}{\sum_i Z_i^2 n_i} \tag{5}$$

where S is the Seebeck coefficient, T is the environmental temperature, i indicates the ionic species, k_B is the Boltzmann constant, e is the elementary charge, and Z_i, n_i, and S_{Ti} represent the charge number ($Z_i = \pm1$ for positive and negative monovalent ions), the concentration, and the Soret coefficient of i species, respectively.

Considering the Seebeck effect, Würger proposed a general empirical fitting expression for thermophoresis,[118,121]

$$D_T = \frac{\varepsilon \zeta^2}{3\eta T} - \frac{\varepsilon \zeta}{\eta} S \tag{6}$$

where ζ is the surface potential of the particle and ε and η are the permittivity and viscosity of the solution, respectively. The first term corresponds to the thermo-osmotic flow,[122,123] which is always positive. The second term is related to the thermoelectric field and the surface charge of the suspended particle, which can be either positive or negative. Many works have reported the reversible thermal migration of micron-sized particles by altering the concentration of different ions such as H^+ and OH^- ions.[111–113,117,124] By controlling

the types of ions and the surface charge of the particles, one can achieve on-demand trapping or propelling of colloidal particles under a light-directed thermoelectric field. Interestingly, thermoelectric fields can also arise from the polarization of pure solvent (e.g., water) under the temperature field.[125–127] In addition, the thermoelectric effect can be controlled by other factors, including temperature,[128,129] particle–solvent interface,[114] colloidal size,[130] and particle concentration,[131,132] which is discussed in detail in refs 118 and 133.

2.4. Diffusiophoresis

Diffusiophoresis describes the transport of colloidal particles under a concentration gradient of the solute (Figure 2c), which is induced by the slip velocity at the particle–liquid interface.[103] This phenomenon was first discovered by Derjaguin et al. in 1947.[134] It can be observed in both electrolyte[135,136] and nonelectrolyte solutions.[137] The former stems from a synergistic effect of local electric and pressure fields in the electric double layer of suspended colloids, and the latter is only driven by the pressure field. Specifically, diffusiophoresis in the electrolyte can be interpreted as the combination of thermoelectricity (see section 2.3) and a pressure gradient resulting from the tangential concentration gradient within the electric double layer. Note that diffusiophoresis in nonelectrolyte solutions also stems from the pressure gradient; however, this pressure gradient mainly originates from the steric repulsion[138] or van der Waals attraction.[139,140] As summarized by Kumar and co-workers,[141] diffusiophoresis is influenced by three factors: (1) the concentration gradient of the solute, (2) the zeta potential of the colloids, and (3) the difference in Brownian diffusion coefficients (D) of the electrolytes. The establishment of molecular solute concentration gradients (i.e., ∇c) can be achieved in different ways, including molecular exclusion, chemical reaction, and solubility variation. In heat-mediated optical manipulation, the concentration gradient of molecules is mainly ascribed to the temperature-dependent solubility or thermal migration under a temperature gradient.

Depletion attraction is a typical type of diffusiophoretic force,[142] which is generated from the concentration gradient of suspended small molecules in the colloid–molecule mixture. The small molecules can also be replaced by nonadsorbing polymers, micelles, or nanoparticles to provide depletion forces.[14,143,144] Depletion attraction is widely exploited in heat-mediated optical manipulation to offer interparticle and particle–substrate bonding forces for the controlled optical assembly and printing of colloidal particles onto the substrates.[145,146] Specifically, under a temperature gradient, different components possess different drift velocities based on their thermophoretic mobilities. Because small molecules commonly have a larger Brownian diffusion coefficient D, they migrate faster than colloidal particles, which induces a steady concentration gradient parallel to the temperature gradient. This concentration gradient of small molecules exerts osmotic pressure to drive suspended colloids toward the molecule-depleted region by the depletion force.

2.5. Photophoresis

Photophoresis describes the directed movement of light-absorbing particles suspended in a fluid (mostly in the gas), which is attributed to the momentum transfer between the particle and the surrounding molecules (Figure 2d). Photophoresis can be induced by the temperature difference (T) or the thermal accommodation coefficient difference (a) of the

particle.[55,147] Here, the thermal accommodation coefficient $a = (T - T_0)/(T_w - T_0)$, where T_w, T, and T_0 are the temperatures of the particle, the incident molecules, and the leaving surrounding molecules during the molecule–particle collision, respectively.[148]

For the first type of photophoretic force, T is a variable while a is a constant (denoted as ΔT photophoretic force). When an illuminated light-absorbing particle has a higher temperature at one side than the other side along the direction of light propagation, the ambient molecules around the hot side will absorb greater energy and exert a larger force on the particle than the cold side, leading to a net photophoretic force toward the cold side.[149] Depending on the temperature distribution around the particle, photophoretic forces can either push or pull the particle along the light-propagation direction, corresponding to positive or negative photophoresis, respectively.

For the second type of photophoretic force, T is a constant around the particle as the particle is homogeneously heated, while a is a variable (denoted as Δa photophoretic force). The Δa photophoretic force points from the higher-a side to the lower-a side and is highly related to the surface properties of the particle. Therefore, owing to the different surface properties and compositions of the particles, Δa results in net momentum transfer between the particle and the surrounding molecules, enabling directional motions of the particle in gas. Note that the moving direction under the Δa photophoretic force can be complicated due to the highly variable surface properties of the objects.

2.6. Natural Convection

Natural convection describes a type of fluidic flow resulting from the density gradient (i.e., $\Delta \rho$) of the fluid. Commonly, the density gradient of the fluid can be controlled by local heating, where the fluid's density decreases as the temperature rises. When the heated fluid with a lower density moves upward due to Archimedes' force, the neighboring denser (colder) fluid flows toward the heating source due to fluid continuity. The fluid at the heating region continues to be heated and moves upward, leading to a convective flow (Figure 2e). It is worth noting that, unlike the aforementioned phoretic motions driven by the particle–liquid interfacial forces, natural convection can occur solely within the fluid regardless of the suspended objects.

Donner et al. have conducted comprehensive studies on the natural convection induced by plasmonic heating.[150] For nanoscale heating sources, the natural convection is usually too weak for efficient manipulation of nanoscale objects. For example, for a Au disc with a size below 200 nm, the fluid velocity seldom exceeds 10 nm/s, even if the temperature reaches the boiling point.[150] Thus, arrays of light-absorbing nanostructures have been widely used to enhance natural convection.[79] In addition, the height of the microchannel or fluid chamber plays a vital role as a smaller height can suppress the vertical temperature gradient and thus weaken the natural convection.[150] Furthermore, Roxworthy et al. have distinguished between Rayleigh–Bénard convection and thermoplasmonic convection under the scope of natural convection.[151] Both have radially symmetric toroidal flow patterns. Rayleigh–Bénard convection stems from an instability in a channel with a uniformly heated bottom surface, which requires a large temperature increment across the whole fluid cell to induce the instability and a Rayleigh number larger than ~1700.[152] In contrast, thermoplasmonic

convection is generated by spatially nonuniform heating of plasmonic nanostructures, which is irrelevant with instability and only requires a Rayleigh number larger than 0.

2.7. Marangoni Convection

Marangoni convection describes the mass transfer at the fluid–fluid interface due to a gradient of surface tension, which is mainly induced by the stress discontinuity at the interface of two fluids. Marangoni convection can stem from both the concentration gradient and the thermal gradient, where the latter is also termed thermocapillary convection.[153] The temperature-dependent Marangoni convection is typically described by[154]

$$\tau_S = \eta \frac{\partial u_s}{\partial N} = - k_T \nabla T_S \qquad (7)$$

where τ_S is the shear stress at the interface, η is the dynamic fluid viscosity, u_s and N are the tangential velocity and normal vector to the surface, respectively, k_T is the temperature coefficient of the surface tension, and ∇T_S is the temperature gradient at the surface. In brief, when a fluid–fluid interface (typically liquid–gas interface) is heated, the interface with a higher temperature possesses a lower surface tension. As the fluid is directed toward the region of higher surface tension, the Marangoni convective flow will move along the temperature gradient near the interface. Due to the fluid continuity, the overall Marangoni convection behaves as a type of recirculation flow (Figure 2f), which can be exploited to manipulate objects with various materials, sizes, and shapes.

2.8. Electrothermoplasmonic Flow

The electrothermoplasmonic (ETP) flow represents the directed motion of asymmetrically heated fluid triggered by the electrical body force. When a laser beam illuminates a plasmonic nanostructure, a highly localized heating of fluid is generated surrounding the plasmonic hotspot, which leads to local gradients in the fluid's permittivity ($\nabla \varepsilon$) and electrical conductivity ($\nabla \sigma$). By applying an alternating current (ac) electric field, the electric body force of the fluid leads to a drag force to transport the suspended particles toward the hotspot (Figure 2g). The time-averaged electrical body force per unit volume is expressed as[155]

$$\langle F_{\mathrm{ETP}} \rangle = \frac{1}{2} \epsilon \left[\frac{(a-b)}{1 + (\omega \epsilon / \sigma)^2} (\nabla T \cdot E) E - \frac{1}{2} a \left| E \right|^2 \nabla T \right] \qquad (8)$$

where $a = (1/\epsilon)(\partial \epsilon / \partial T)$, $b = (1/\sigma)(\partial \sigma / \partial T)$, ϵ and σ are the fluid's permittivity and electrical conductivity, respectively, E is the applied electric field, and ω is the frequency of the ac electric field. The velocity of the ETP flow can be easily tuned by the frequency and amplitude of the ac electric field.

2.9. Optothermal Shape Deformation

Light-driven shape deformation can be divided into optothermal and optomechanical shape deformation. Optomechanical shape deformation is mainly attributed to the photoisomerization[156–162] and photodimerization[163,164] of certain molecules. For instance,

the isomerization from trans to cis isomer of diacrylate azobenzene derivatives leads to the geometrical change, which can induce the strain gradient in liquid crystals and actuates their bending behavior.[165] The mechanisms of optothermally induced shape deformation (Figure 2h) are typically classified into four categories:[166–168] (1) volume expansion (as in polydimethylsiloxane (PDMS)); (2) phase transition (as in liquid crystals, shape memory polymers/alloys, and melting polymers); (3) molecular sorption/desorption (as in poly(*N*-isopropylacrylamide)); and (4) surface acoustic waves (as in Au nanowires). In general, inhomogeneous temperature fields along the objects are demanded, which can be fulfilled by (1) asymmetric coating or doping of light-absorbing materials and (2) spatial or temporal modulation of incident light. Optothermal shape deformation leads to the storage and release of strain energy, which can be exploited for the versatile manipulation of objects.

3. OPTICAL MANIPULATION BASED ON THERMOPHORESIS

When a temperature gradient is established in a solution upon laser irradiation, the suspended objects influenced by the temperature gradients can undergo directed thermophoretic migration toward either the hot region or the cold region depending on the signs of thermophoretic mobilities D_T (or Soret coefficient S_T). Because most objects, including synthetic particles, live cells, and vesicles, have a positive D_T, they are intrinsically repelled by optical heating or trapped by optical cooling. Through rational design and control of the heating laser beam, the target objects can be manipulated by the thermophoretic repelling force to achieve trapping and light-directed swimming. Interestingly, some objects also show a negative D_T to be trapped by laser heating through engineering the solvent–object interfaces. Along with the advantages of low-power and simple optics, optothermophoretic manipulation is applicable to a wide range of objects.

3.1. Optothermophoretic Swimmers

Artificial swimmers, which mimic the swimming behaviors of microorganisms in nature, represent a series of automotive devices that self-propel in liquid media, which are finding applications in biomedical engineering, sensing, and environmental remediation.[169–172] Light-fueled swimmers are attractive because they can be made of various materials and can be remotely controlled with simple experimental setups.[24,173–176] Moreover, the inherent optical heating effects in optothermal swimmers can facilitate photothermal therapy in disease theranostics.[177]

Optothermophoretic swimmers have been developed based on the thermophobic nature of target objects. Specifically, the light-directed motion of swimming objects in a solution is fueled by laser heating, which is usually termed self-thermophoresis.[178] To function as an optothermophoretic swimmer, an object should have an asymmetric optothermal response to build a local temperature gradient under light irradiation. Three approaches have been developed to achieve this goal: (1) swimmers have symmetric shapes with asymmetric absorptivity (e.g., Janus particles[179]); (2) swimmers have asymmetric shapes with a uniform decoration of light-absorbing materials (e.g., tubular rockets[180]); and (3) homogeneous swimmers undergo temporally and/or spatially nonuniform laser illumination.[10,181,182]

In the first approach, Janus particles, which usually consist of a low-light-absorption core particle (e.g., silica or PS) with a partial coating of high-light-absorption materials (e.g., Au)[178,183–185] or two interconnected individual parts with different light absorptions (e.g., Au spheres attached with DNA origami)[186–188], have been widely investigated. Typically, when a laser beam uniformly irradiates a Janus particle, a temperature gradient is built surrounding the particle (Figure 3a). The resultant thermo-osmotic fluid flow drives the Janus particle to move along the temperature gradient.[123,178,189] Recently, Heidari et al. demonstrated that the velocity of phoretic swimmers could be controlled by the thermo-osmotic flow near the substrate/water interface, which could be tuned via the functionalization of the substrate.[190] While most self-thermophoretic swimmers are thermophobic and swim from the hot region to the cold region, they can be engineered to be thermophilic by introducing a thermoelectric field.[107,112,191]

Optothermophoretic swimmers can achieve macroscopic directional movements with extremely high swimming speeds. Xuan et al. developed self-thermophoretic Janus Au-silica particles with different diameters of 50, 70, and 120 nm.[184,192] When the Janus particles were irradiated by the NIR femtosecond laser beam, self-propulsion of the particles was triggered based on self-thermophoresis. Directional propulsion of the Janus particles was realized with a rapid swimming velocity up to 950 body lengths/s (Figure 3b). More interestingly, the Janus swimmers modified with a macrophage cell membrane could actively seek cancer cells and percolate cell membranes under NIR light illumination, which paved the way for light-controlled drug delivery.[192]

Because Janus swimmers can only maintain the directional movement in a short time scale due to the rotational Brownian motion,[178] adaptive control strategies were proposed to navigate swimmers to achieve continuous directional swimming.[10,179,183,193,194] For instance, Bregulla et al. developed a feedback-control method to achieve the directed propulsion and precise transport of Janus particles to a target position.[179] This method consisted of three steps: (1) when the heating laser was off, the orientation of the Janus particle changed randomly due to the rotational Brownian motion; (2) when the orientation was toward the target under an acceptance angle range, the laser was switched on to trigger the propulsion; and (3) once the particle lost the track to the target, the laser beam was turned off and the loop was returned to step 1 (Figure 3c). Alternatively, Ilic et al. developed dual-wavelength optothermophoretic swimmers featuring two absorbing caps composed of different materials (i.e., Au and titanium nitride) that could absorb laser beams of different wavelengths for self-propulsion.[70] By switching two laser beams based on the predesigned algorithms, the swimmers were delivered to the target positions without the need for real-time imaging and feedback control. In addition to single swimmers, collective behaviors of optothermophoretic Janus particles were also studied,[195–197] facilitating the development of autonomous manipulation of multiswimmers and even swarm intelligence.

Alternatively, a temperature gradient required for optothermophoretic swimmers can also be created by laser heating of colloidal particles with asymmetric shapes.[180,198] He and co-workers developed polymeric tubular rockets with Au nano-shells (Figure 3d), which could self-propel in the solution or cell culture media via optothermophoresis.[180] The temperature distribution of the tubular rockets is shown in Figure 3e, indicating a higher

temperature increment at the small front opening than that of the large rear opening. In addition, the temperature inside the tube was much higher than that outside the tube. By controlling the on/off state of the incident laser, a rocket with a body length of ~10–12 μm could swim in the direction toward the small opening at a speed of up to 160 μm s^{-1} (Figure 3f). Similarly, Kim et al. developed a head–tail structure with asymmetric light absorption to achieve self-thermophoretic rotational motions.[199]

In an example of the third type of self-thermophoretic swimmers, swimming was realized with uniformly Au-coated melamine resin microspheres through temporally asymmetric laser heating.[10] The homogeneously decorated particles were thermophobic, and their propulsion direction was the vector from the laser-heated circumferential spot to the particle center. By parallelly changing the positions of laser beams to push the particles according to the real-time optical images, multiple microswimmers were successfully localized to the predesigned positions. The real-time tracking feedback loop was then employed to investigate the information flows among the active swimming particles by pairwise control. The control system dynamically steered the position of each particle to keep the distance between two neighboring particles at a constant value r_{eq} (Figure 3g). Two or three active particles could form structures where all average interparticle distances were equal to r_{eq}. When the number of particles exceeded three, the formed structures could not have identical interparticle distances due to the structural confinement in two dimensions (Figure 3h). The underlying mechanism of the symmetric self-thermophoretic swimmers has been further illustrated.[200] Moreover, the study of swimmers integrated with machine learning could shed light on the understanding of adaptive and collective behaviors of microsystems.[201,202]

Self-propelled optothermophoretic swimmers have been widely explored for biomedical applications due to their remote and chemical-free control, high-speed motion, and inherent heating for photothermal therapy. In addition, an NIR laser is usually used to drive thermophoretic swimmers to avoid photodamages to the biological tissues. Li et al. exploited tubular rockets for in vivo transportation with high speeds (~2.8 mm s^{-1}) and real-time tracking at high resolution (~3.2 μm).[203] To achieve fast swimming in the highly viscous blood, microscale rockets with three tubes were designed (Figure 4a) that showed a much higher speed than those of microrod and single-channel tubular rockets due to the increasing quantity of the propulsion channel and the light-excitation interfacial area. This microrocket could also be applied underneath a shallow tissue (less than ~1 mm), such as the ear of an anesthetized mouse, where it could be tracked via photoacoustic imaging (Figure 4b). Cui et al. exploited mesoporous Au-silica half-shell swimmers for in vivo photothermal therapy and chemotherapy in a biofilm (Figure 4c).[204] The mesoporous structure facilitated the loading of vancomycin, while the Au-coating enabled self-thermophoresis upon NIR laser irradiation. The experimental results showed that this microswimmer could penetrate quickly into the biofilm and release the encapsulated vancomycin without damaging healthy tissue due to the localized temperature rise (~45 °C). Because of their strong optothermal response, optothermophoretic swimmers assisting photothermal tumor therapy was also proposed.[205,206] In addition, He et al. utilized Janus-particle-based swimmers composed of polyelectrolyte multilayers and superparamagnetic iron oxide nanoparticles for laser-assisted tissue welding.[207] The Janus particles could self-propel into the wound guided by thermophoresis and an external magnetic field (Figure 4d). The Janus particles with active

navigation are promising for tissue welding, especially when the bleeding of wounds is too strong, because the light-powered Janus particles can move with speeds up to hundreds of micrometers per second to rival the bleeding flow.

3.2. Optothermophoretic Tweezers

Apart from the optothermophoretic swimmers that are nudged away from the heating laser beams, the target objects can also be trapped and dynamically controlled under the light-induced temperature fields, leading to the realization of thermophoretic tweezers. Two different approaches have been proposed: (1) establishing a ring-shaped temperature field where the inner region is cold to trap thermophobic objects; and (2) trapping objects with interfacial-entropy-driven negative D_T at the laser-heating spot.

For the first approach, Cichos and co-workers developed a thermophoretic trapping platform for thermophobic objects through dynamic laser heating of ringlike arrays of plasmonic nanostructures as substrates.[208–211] In brief, because thermophobic objects were repelled away from the laser-heating spot (Figure 5a), they could be confined inside a plasmonic ringlike nanostructure by rotating the heating laser at certain frequencies (Figure 5b).[208] A single amyloid fibril was also successfully trapped based on this method to study the growth, secondary nucleation, or fibril breakup.[212] Apart from trapping the objects at the center of ringlike nanostructures, different trapping modes were realized by controlling the temperature gradient fields based on the feedback control of the heating laser.[210] Through tracking the position of target particles by real-time imaging, one could direct the laser beam on certain parts of the heating nanostructure via a two-dimensional (2D) acousto-optic deflector, enabling offset, double-well, and ring-shape thermophoretic trapping of 200 nm colloids (Figure 5c). Additionally, Nedev et al. demonstrated thermophoresis-assisted three-dimensional (3D) optical trapping of Janus particles via the synergy of thermophoretic force, optical gradient force, and optical scattering force.[213]

Optothermophoretic trapping and tweezing can also be achieved by exploiting the negative thermophoretic mobilities of colloidal particles and cells under certain conditions. Accordingly, upon laser heating, direct optothermophoretic trapping[214] and assembly[77,215] of colloids and cells can be achieved without the need for additional feedback control. Lin et al. developed optothermophoretic tweezers to trap charged particles at the laser-heating region by exploiting the entropic response and the permittivity gradient at the particle–solvent interface under a thermal gradient.[214] The thermophoretic mobility of a particle is given by[113]

$$D_T = -\frac{\varepsilon}{2\eta T}\frac{2\Lambda_1}{2\Lambda_1 + \Lambda_P}\left(1 + \frac{\partial \ln \varepsilon}{\partial \ln T}\right)\zeta^2 \tag{9}$$

where ε is the solvent permittivity, η is the solvent viscosity, and Λ_1 and Λ_P are the thermal conductivities of the solvent and particle, respectively. In bulk water, $\frac{\partial \ln \varepsilon}{\partial \ln T}$ equals -1.4 at room temperature, which corresponds to a positive D_T. For a charged particle in water, the polarized water molecules were adsorbed on the particle surface with specific orientations based on electrostatic interactions. An electric double layer formed at the particle–water

interface with a highly ordered inner layer and a loosely oriented outer layer (Figure 6a). These structured water molecules created an abnormal permittivity gradient with a positive $\frac{\partial \ln \varepsilon}{\partial \ln T}$ value and a resultant negative D_T. Thus, the particle would migrate from the cold to the hot region to be trapped at the laser beam by optical heating.

To achieve dynamic manipulation of objects, a thermoplasmonic substrate composed of quasi-continuous Au nanoislands (AuNIs)[77,216] is used to generate spatially continuous hotspots.[217–219] The trapped objects could be manipulated to any location by arbitrarily scanning the heating laser or moving the sample stage. The versatilities of optothermophoretic tweezers were demonstrated by parallelly manipulating and patterning PS beads of different sizes into diverse patterns (Figure 6b). Peng et al. further investigated the working principle of optothermophoretic tweezers in various nonionic liquids at the molecular level.[220] The results showed that the driving forces were derived from a layered structure of solvent molecules at the particle–solvent interface, and the trapping stability of the particles could be improved by engineering the particle hydrophilicity, particle surface charge, solvent type, and ionic strength on the layered interfacial structures.

Additionally, optothermophoretic tweezers were exploited to manipulate biological cells with negative surface charges due to the existence of phospholipid bilayers.[221] A digital micromirror device (DMD) was integrated into the optical setup to achieve versatile manipulation of biological cells (Figure 6c). Figure 6d shows the parallel trapping of yeast cells into a "NANO" pattern and the dynamic transformation of cell assemblies from a "Y" pattern to a "T" pattern. Besides biological cells, lipid vesicles with similar phospholipid bilayers were also manipulated by optothermophoretic tweezers.[222] Compared with conventional optical tweezers, the optothermophoretic tweezers do not rely on the refractive index contrast between trapped objects and the environment. In addition, they require a much lower operation power (2–3 orders of magnitude lower) and less rigorous optical setups than optical tweezers.

Optothermophoretic manipulation has also been realized at the macroscopic scale. Kavokine et al. demonstrated a centimeter-scale motion of a vial triggered by collective optothermophoretic trapping of nanoparticles (Figure 7a).[71] When a laser beam irradiated a vial containing high-concentration lead sulfide nanoparticles, the irradiated particles absorbed the incident light and served as the heating sources. In the meantime, other particles got trapped in the laser-heating region via thermophoresis. As the local concentration of nanoparticles increased up to a point beyond Jean's instability, the collective motion of the particles was induced, endowing sufficient momentum to push the vial away from the laser (Figure 7b). This work revealed the potential applications of heat-mediated optical manipulation in the macroscopic world.

3.3. Opto-Refrigerative Tweezers

Taking advantage of the common thermophobic nature, Li et al. developed opto-refrigerative tweezers (ORT) to trap and manipulate nano-objects at the laser-generated cold region via the optical refrigeration and thermophoresis synergy (Figure 8a).[98] A quasi-continuous layer of Yb-doped YLiF$_4$ nanocrystals was used as the substrate, where localized laser cooling

could be achieved under the irradiation of a 1 020 nm laser (Figure 8b). Nanoparticles with a positive Soret coefficient could be trapped at the laser spot by thermophoretic forces and dynamically transported along the substrate. On the basis of a temperature gradient field, ORT permitted long-range trapping of nanoparticles with a weakly focused laser beam, which could reduce the photon degradation of target objects. In addition, the trapping of objects by ORT in the low-temperature region could avoid potential photothermal damages. Thus, ORT present a noninvasive optical manipulation tool for fragile nanoparticles and biomolecules. As a demonstration, a fluorescent nano-particle trapped by ORT showed enhanced stability compared to that by optical tweezers due to the suppression of both photobleaching and thermal bleaching (Figure 8c and d).

4. OPTO-THERMOELECTRIC MANIPULATION

Upon laser heating in electrolyte solutions, the thermophoretic migration of cations and anions leads to the ionic spatial redistribution to establish thermoelectric fields.[118] The optothermoelectric fields have been widely exploited to trap and manipulate a variety of charged colloidal particles. With a rational design of electrolyte solutions and particle surface charges, optothermoelectric approaches can achieve on-demand manipulation of objects with a wide range of materials, shapes, and sizes. By further exploiting the depletion attraction at the particle–particle and particle–substrate interfaces, optothermoelectric assembly and printing of colloidal matter, which provide versatile tools for bottom-up nanofabrication, have been demonstrated. Furthermore, the concept of opto-thermoelectric microswimmers has been developed to actively control the rotating and swimming states of Janus particles for effective target delivery.

4.1. Opto-thermoelectric Tweezers

Thermoelectric fields have been widely employed to manipulate charged molecules,[120] colloidal particles,[117] and micelles.[223] Lin et al. developed opto-thermoelectric nanotweezers (OTENT) to achieve trapping and manipulation of diverse colloids.[224] Optothermal substrates (e.g., AuNIs and Au nanorod arrays) were used as the heating sources, which facilitated the generation of a temperature gradient under laser illumination. A cationic surfactant, cetyltrimethylammonium chloride (CTAC), was used to modify all suspended particles with a positive surface charge (Figure 9a). Interestingly, CTAC molecules above the critical micelle concentration (0.13–0.16 mM) in solutions self-assembled into positive micelles (Figure 9b). The CTAC micelles and Cl^- ions served as two counterions to create a thermoelectric field in OTENT.[225] Specifically, under a laser-generated temperature gradient, both CTAC micelles and Cl^- ions migrated from the hot to the cold region, i.e., moving away from the laser beam. Because S_T (micelle) $\gg$ S_T (Cl^-), positive CTAC micelles moved faster and further than Cl^- ions, leading to a thermoelectric field pointing toward the laser beam because of their spatial separation.[226] Consequently, the positively charged objects could be trapped at the laser spot with thermoelectric forces (Figure 9c). It should be noted that CTAC can be replaced by biocompatible surfactants such as poly(diallyl dimethylammonium chloride) for biological applications.[226] OTENT can be applied to manipulate colloidal particles with a wide range of materials, sizes, and shapes at the single-particle resolution with a low optical power (0.05–0.4 mW·μm^{-2})

that is 2–3 orders of magnitude lower than that of optical tweezers.[227] By integrating OTENT with a DMD, the researchers demonstrated parallel manipulation of different metal nanoparticles with a size down to ~100 nm (Figure 9d). In addition to a single focused laser beam, Kotnala et al. used a multiple-mode fiber to generate a large thermal speckle field with a diameter over 100 μm for the large-scale optothermoelectric trapping of multiple particles.[228] Integrated with a microfluidic system, this optothermal speckle field demonstrated size-selective nanoparticle filtration by the interplay of the Stokes drag force and the thermoelectric force.

To further improve the light-to-heat conversion and enhance the thermal gradient for more precise opto-thermoelectric trapping, Liu et al. exploited plasmonic nanoantennas as optothermal nanoradiators to overcome the optical diffraction limit in OTENT (Figure 9e).[62] Due to the anisotropic optothermal response of the nanoantennas, the thermoelectric field and the resultant trapping stiffness could be tuned by the polarization of the laser beam, which enabled the directed transport of nanoparticles on rationally designed nanoantenna arrays. For instance, by fabricating a T-shape pattern and a triangle-shaped pattern with gold nanorod antennas, linear and circular transport of nanoparticles, respectively, was achieved by altering the polarization of the laser beam (Figure 9f). Moreover, the use of a femtosecond laser could further enhance its capability to trap single quantum dots with a size down to ~30 nm.

OTENT can be further extended as a 3D manipulation technique. Kotnala et al. achieved opto-thermoelectric fiber tweezers by transplanting the AuNIs substrate to a flexible fiber platform integrated with a three-axis stage (Figure 10a).[229] Because the core of the fiber and the laser beam were always aligned, the thermoelectric field was fixed at the center of the fiber tip, which could be dynamically shifted in 3D by moving the three-axis stage. Two operation modes with different incident directions of the laser beam (i.e., normal versus parallel to the substrate) could be achieved (Figure 10b). Single-particle delivery was demonstrated by trapping the nanoparticle at the fiber tip and moving the fiber to a target vesicle with controllable speed and spacing (Figure 10c). Alternatively, Lin et al. reported the 3D opto-thermoelectric manipulation of light-absorbing silicon nanoparticles (SiNPs) by exploiting the self-generated thermoelectric field.[146] Upon laser radiation, a temperature gradient field was built on the SiNP because of the asymmetric heating along the beam-propagation direction. Because the illuminated pole was hotter than the rear pole, the spatial redistribution of CTAC micelles and Cl$^-$ ions led to a thermoelectric field pointing against the beam-propagation direction (Figure 10d). Considering the positively charged SiNP adsorbed with CTAC molecules, the opto-thermoelectric force would pull the SiNP against the beam direction (Figure 10e). As shown in Figure 10f, a laser-coupled, tapered optical fiber with a low numerical aperture was used to demonstrate long-distance opto-thermoelectric pulling. The pulling velocity of SiNPs could be tuned by altering the laser-power intensity and the concentration of CTAC. In addition, the synergy of the optothermoelectric pulling force and the optical scattering force acted as the out-of-plane restoring force to maintain the particle in the trap. Accordingly, 3D manipulation of SiNPs was achieved when moving the laser focal plane in the Z direction. The SiNP particle with the self-generated opto-thermoelectric field could further function as an optothermal shuttle to trap and transport nonlight-absorbing particles such as PS beads (Figure 10g).

4.2. Opto-thermoelectric Assembly

When two particles are trapped at the laser spot in the optothermoelectric field, the CTAC micelles at the interparticle gap will drift away via thermophoresis, resulting in a depletion attraction force to bind two particles together (Figure 11a).[230,231] This micelle-mediated colloidal bonding can be maintained even after the temperature gradient is removed. By trapping and placing single particles one by one, diverse colloidal superstructures of arbitrary configurations were built with various particles as the building blocks (Figure 11b). 3D assembly of colloidal structures was also achieved by incorporating an optical scattering force to push the particle to the upper layer (Figure 11c). In addition, the assembled colloidal structures could be disassembled and then reassembled into other configurations. As a demonstration, Lin et al. mimicked the configuration of chiral molecules and applied this opto-thermoelectric assembly technique to build reconfigurable chiral meta-molecules using colloidal particles as the meta-atoms (Figure 11d).[232] Discrete particles were successfully assembled into different chiral structures and reassembled into their opposite enantiomers (Figure 11e). The measured differential scattering spectra under circularly polarized light illumination presented multiple bisignate chiral modes with high-quality factors. Moreover, the optical chirality of meta-molecules could be tuned by both geometric and compositional asymmetries, which provided a promising platform to investigate the origin of chirality at a colloidal scale.[233] Furthermore, the assembled colloidal structures could be immobilized on substrates via the depletion attraction at the particle–substrate interface.[145] Alternatively, Peng et al. demonstrated the opto-thermoelectric assembly of colloidal superstructures in a photocurable hydrogel solution, where the assembled superstructures could be fixed on the substrate via cross-linking of hydrogels.[234]

4.3. Opto-thermoelectric Swimmers

Peng et al. exploited the opto-thermoelectric fields to activate the rotation and directional navigation of Janus microswimmers (Figure 12a).[235] Specifically, when a focused laser beam illuminated a PS-Au Janus particle, an asymmetric temperature profile and a resultant thermoelectric field were generated in the CTAC solution (Figure 12b). The thermoelectric force always pointed from the cold to the hot region, where the X component attracted the particle to the beam center and the Y component made the particle drift toward the Au-coated hemisphere (Figure 12c). Therefore, the Janus particle could be stably rotated around the laser beam by the synergy of the thermoelectric force F_t, the optical force F_0, and the Stokes drag force F_d (Figure 12d). A rotation rate of ~40 rpm was achieved with a laser power of 1.9 mW. Interestingly, the angle θ between the PS/Au interface and the substrate remained close to 90° during the rotation. This self-alignment behavior of the Janus particle could be explained by calculating the thermoelectric torque as a function of angle θ, which showed that $\theta = (3/8)\pi$ or $(5/8)\pi$ was more energetically favorable than the other angles (Figure 12e). Meanwhile, the Janus particle could be nudged by another defocused laser beam via self-thermophoresis (see section 3.1). By switching the rotating and nudging states of the Janus particle via a feedback-control algorithm, the particle achieved efficient target delivery in a fuel-free fluid environment (Figure 12f).

5.   OPTOTHERMAL DIFFUSIOPHORETIC MANIPULATION

The key to the optothermal diffusiophoretic manipulation of objects in solutions is the establishment of a concentration gradient of solutes upon laser heating. Two approaches have been proposed so far: (1) exploiting thermophoretic motion of molecules to build a concentration gradient and (2) using a binary critical mixture that can be thermally decomposed to generate a local concentration gradient around the target objects. The first approach is suitable for the concentration and assembly of colloidal particles and biological objects at a large scale, while the second one can be used to develop optothermal microswimmers and microengines.

5.1.   Optothermal Diffusiophoretic Concentration and Assembly

Various objects, including colloidal particles,[14,144] DNA/RNA,[236,237] and biological cells,[238,239] can be concentrated or assembled with high throughput via the optothermally induced depletion force. For instance, Jiang et al. demonstrated the concentration of 100 nm PS beads at the laser-heating region in a polyethylene glycol (PEG) solution (Figure 13a).[14] Under the laser-generated temperature gradient, PEG molecules migrated away from the laser beam to the cold region via thermophoresis, which established a concentration gradient (Figure 13b) and created a depletion force to drive suspended PS beads to the laser-heating spot. This depletion-based trapping is applicable to various objects and is highly dependent on the size and concentration of depletants. Maeda and co-workers carried out a series of studies on the manipulation of biological materials via a depletion force.[236–239] Representatively, it was found that, upon laser heating in a microchannel (Figure 13c), DNA molecules could form different structures in PEG solutions (Figure 13d) that were dependent on the DNA length and PEG volume fraction (Figure 13e).[236,237] Ring-shaped structures of DNA molecules were formed due to the balance between the attractive depletion force and the repelling thermophoretic force. In another example, Deng et al. assembled 1.6 μm silica microspheres into an ordered close-packed structure using 12 nm magnetic nanoparticles as the depletants (Figure 13f).[144]

5.2.   Optothermal Diffusiophoretic Swimmers

Diffusiophoretic swimmers based on catalytic reactions have been widely investigated.[240] Recently, diffusiophoretic swimmers have also been realized in a chemical-fuel-free environment by optothermally demixing a binary mixture around a Janus particle (Figure 14a).[241,242] Unlike the catalytic swimmers that consume chemical fuels such as hydrogen peroxide, optothermal diffusiophoretic microswimmers based on local demixing are fuel-free, and the mixing–demixing processes are reversible. Bechinger and co-workers developed optothermal diffusiophoretic microswimmers in a binary critical mixture of water and 2,6-lutidine by laser-heating-driven asymmetric local demixing at Janus particles.[181] Upon laser illumination, a temperature gradient field was generated in the proximity of a Janus particle. Once the temperature around the absorbing coating exceeded the critical temperature T_c (307 K) of the binary mixture (Figure 14b), the solution in the vicinity of the coating separated into two immiscible phases. The resultant localized concentration gradient induced a tangential gradient of pressure at the particle surface and led to the directional drifting of the Janus particle. It is worth noting that the moving direction of the Janus

particle can be altered by modifying its local surface hydrophilicity[241] or surface charge,[243] as the Janus particle always swims toward the region rich in 2,6-lutidine. The effect of thermophoresis has been excluded via a control experiment with the same setup in pure water, where directed motions were not observed.[241]

The optothermal diffusiophoretic microswimmer system has served as a versatile platform to investigate phototaxis,[181,244] gravitaxis,[245] and various collective behaviors[246–249] of self-propelled colloidal particles. As for phototaxis, it has been found that light gradient fields can better navigate the optothermal diffusiophoretic swimmers.[181] Specifically, Janus particles under a monotonic light intensity gradient ∇I can be reoriented against the gradient due to the broken axial symmetry of the slip velocity, which stems from the inhomogeneous heating of the metallic cap. To overcome the rotational Brownian motion, periodic sawtooth-like light profiles were created to achieve directional transport of the Janus particle over arbitrary distances (Figure 14c). When the time to travel through each light-intensity segment was less than its reorientation time τ_ω, the particle could achieve rectified motion over long distances (Figure 14d). Furthermore, Lozano and Bechinger revealed that the microswimmers could respond to light pulses phototactically, which moved either along or counter to the pulse with respect to the pulse velocity and the particle's size, shape, and swimming velocity.[244] For the study of gravitaxis, Ten Hagen et al. exploited Janus structures with homogeneous mass density but asymmetric shapes to achieve gravitactic swimming (both upward and downward motions) in a binary mixture, revealing that the swimming behaviors related to gravitational fields of some motile microorganisms in nature could be purely attributed to their asymmetric shapes.[245] Moreover, collective behaviors of self-propelled particles and living microorganisms have also been studied based on microswimmers. For instance, Lavergne et al. exploited the microswimmer system with feedback rules to study the collective behaviors in living systems in response to visual perception. It was revealed that the motility change of individual objects as a function of an anisotropic and long-range perception of the environment can lead to robust group formation and cohesion.[248]

5.3. Optothermal Diffusiophoretic Rotors

We define rotors as artificial particles or structures that can stably rotate around certain axes.[250] Micro/nanoscale rotors can be achieved via different stimuli, including acoustic,[251] electric,[252] magnetic,[18] chemical,[253] optical,[254] and optothermal fields,[235,255–257] which have shown promising applications in robotics,[258,259] nanosurgery,[260] and microfluidics.[261] Schmidt et al. developed a microscopic rotor based on the optothermal diffusiophoresis, which can achieve an extremely high rotation speed.[255] Briefly, a silica microsphere with randomly distributed iron oxide inclusions was initially trapped by optical forces. Because more heat was generated on the side closer to the laser beam, an asymmetric temperature profile was established surrounding the particle. The resultant diffusiophoretic force had an opposite direction to the optical force, driving the particle away from the laser beam (Figure 15a). By tailoring the laser power intensity, the particle could find an off-axis position, where the diffusiophoretic force was balanced by the optical force. Owing to small asymmetries in the composition of the particle, a net diffusiophoretic force was also generated in the tangential direction, which drove the particle to rotate around the optical

axis (Figure 15b). The rotation rate of this microengine could reach 4 600 rpm with high conversion efficiency at a laser power of a few milliwatts. The efficiency of this rotor can further be tuned by the laser power, the ambient temperature, and the mixture criticality. Alternatively, optothermal diffusiophoretic microrotors in the same critical mixture were realized by designing an asymmetric L-shaped particle with selective Au deposition (Figure 15c).[262]

6.   PHOTOPHORETIC MANIPULATION

Photophoretic manipulation describes the optical trapping and manipulation of light-absorbing objects via photophoretic force, which can be achieved in either gaseous or liquid media. Photophoretic manipulation is applicable to objects with variable materials, shapes, and sizes such as carbon spheres,[263,264] clusters of carbon nanotubes,[265,266] biological smut spores,[267] and millimeter-sized absorbing plates.[268] A traditional Gaussian laser beam can be exploited to achieve photophoretic trapping.[269,270] To make the trapping more stable, intensity minima of the light fields are usually demanded because the light-absorbing particle tends to be transversally repelled from the high-light-intensity region to the low-light-intensity region.[271] Accordingly, various structured light configurations have been proposed, including optical bottle beams,[272–274] optical vortices,[275] doughnut beams,[276] speckle fields,[277,278] and many others.[279,280]

On the basis of the photophoretic force induced by the temperature difference (i.e., ΔT photophoretic force), Shvedov et al. achieved meter-scale transportation of ~10 μm objects in a gas medium by trapping the particle inside a vortex beam.[149] Later, the same group reported the pulling and pushing of predesigned Au-coated hollow glass spheres in the air by toggling the doughnut polarized laser beam between azimuthal polarization and radial polarization.[276] When the particle was stably confined in the intensity minimum of the doughnut beam, its moving direction was primarily determined by the thickness of the Au coating. Specifically, a thin-Au-coated hollow glass sphere can be regarded as semitransparent with more light absorbing at the nonillumination side, resulting in a pulling force toward the laser source. However, a particle with a thick-Au-coating layer is highly opaque with most of the incident light being absorbed at the illumination side, so it is pushed along the laser beam. Moreover, for the thin-Au-coated sphere, its moving direction could be further manipulated by switching the polarization of the beam to flip the light-absorption distribution of the sphere (Figure 16a). Photophoretic trapping and manipulation of particles in the air can lead to fascinating applications. For instance, Smalley et al. demonstrated the photophoretic manipulation of single cellulose particles for a volumetric display (Figure 16b).[281] The optical intensity was spatially modulated via the combination of spherical and astigmatic aberrations to enable photophoretic trapping sites. Through scanning the trapped particles rapidly and illuminating them with collinear red, green, and blue lasers (Figure 16c), arbitrary and full-color 3D images that can be seen from all angles were achieved.

One can further combine ΔT photophoretic forces and optical forces to achieve particle manipulation. Lu et al. achieved photophoretic pulling and pushing of a single Au plate on a tapered fiber via the synergy of photophoretic and optical forces (Figure 16d).[282] The evanescent field outside of the fiber became stronger as the plate got closer to the fiber

tip because of the decrease in the diameter of the fiber. Therefore, the temperature of the front side of the Au plate was considerably higher than that of the back side, resulting in a photophoretic pulling of the plate toward the light source. When the Au plate was pulled to the middle of the fiber, the photophoretic force was negligible due to a small temperature difference while the optical force became larger, which pushed the plate away from the light source. The simulated total light-induced forces showed that the Au plate could move back and forth on a tapered fiber (Figure 16e), which was validated experimentally (Figure 16f).

In addition, photophoretic force induced by the difference of thermal accommodation coefficients (i.e., α photophoretic force) can be synergized with the T photophoretic force, optical radiation force, and gravitation force to trigger transversal rotation of micron-sized particles.[283,284] Yuan and co-workers exploited the α photophoretic force to achieve 3D manipulation of a microparticle composed of carbon black and silica in pure liquid glycerol.[285,286] Thermal convection and thermophoresis played an insignificant role in this specific system due to the high thermal conductivity of the particles and special thermodynamic properties of liquid glycerol (Péclet number and Reynolds number $\ll 1$ while Prandtl number $\gg 1$). Recently, Bargatin and co-workers demonstrated photophoretic levitation of millimeter-sized mylar films with one side coated with carbon nanotubes (Figure 16g).[287] The coated carbon nanotubes not only enhanced the light-absorption efficiency of the whole film but also increased the collision time between incident gas molecules and the film, leading to a higher thermal accommodation coefficient than that for the uncoated side. The resultant α photophoretic force could levitate the thin film with a load that was many times the weight of the film (Figure 16h).

7. OPTICAL MANIPULATION BASED ON NATURAL CONVECTION

Natural convection is a type of flow attributed to the density gradient of fluids, which can be achieved upon laser irradiation on absorbing substrates, particles, or solvents. It usually has a toroidal-shaped flow and manipulates suspended particles via the Stokes drag force. However, the manipulation accuracy of single objects by convective flow is relatively low. Natural convection has been widely applied for the large-scale assembly of colloidal particles, as in "optothermal assembly based on natural convection", and the rapid transport of objects toward the plasmonic trapping sites due to its long working range,[150] as in "optical trapping assisted by natural convection". In addition, coordination of natural convection and thermophoresis in a temperature gradient has also been exploited for on-demand manipulation of target objects.[288] It is worth noting that both thermoplasmonic convection (defined as the natural convection induced by the optical heating in metallic nanostructures[151]) and Rayleigh–Bénard convection (defined as the natural convection stemming from the instability of a uniformly heated bottom surface and a Rayleigh number exceeding a certain threshold[152]) can be exploited for the optical manipulation. Without further declaration, the manipulation in the following subsections is based on Rayleigh–Bénard convection.

7.1. Optical Trapping Assisted by Natural Convection

The toroidal-shaped natural convection flow can be directly applied to manipulate single objects.[289] For instance, Cong et al. utilized a Au-coated microwell array for efficient optical trapping and single-cell analysis.[290] The optical heating not only triggered the convective flow to facilitate 3D manipulation of a single cancer cell but also provided a constant-temperature environment for a recombinase polymerase amplification reaction of nucleic acid markers. Kumar et al. exploited natural convection to achieve pitch-rotational motion of upconverting particles and single cells.[291] A hexagonal-shaped particle with a length of 5 μm was rotated 180° within 1 s. The rotation rate could further be tuned by the laser intensity and the thickness of the absorbing layer.

In addition to its direct use in optical manipulation, natural convection can also be applied to assist optical trapping and to overcome the diffusion limit in optical tweezing techniques due to its large working range. Kotnala et al. adopted the natural convective flow to assist plasmonic trapping and sensing of nanoparticles with an ultralow concentration ($<2 \times 10^7$ particles·mL^{-1}) (Figure 17a).[292] A multimode optical fiber coupled with a 532 nm laser beam was utilized to illuminate a large area of Au film with a plasmonic nanoaperture, generating the thermal convective flow for rapid delivery of freely dispersed particles. The delivered particles were then trapped at the nanoaperture by a 1020 nm laser beam via plasmon-enhanced optical forces (Figure 17b). Compared with diffusion-limited trapping, this convection-assisted trapping could reduce the average trapping time by up to 15-fold. In another work, Roxworthy et al. exploited thermoplasmonic convection to assist the plasmonic trapping and sorting based on Au bowtie nanoantenna arrays.[293] At a low laser power, when the optical gradient force was larger than the drag force and scattering force, particles could be trapped near the Au bowtie nanoantennas. When the power increased, the strong convective flow could draw in particles from well outside the laser focal spot and lead to the trapping of multiple particles as a cluster. Because the trapping behavior of different sized particles varied as a function of bowtie number density and laser power, a hybrid phase diagram for particle sorting could be obtained by overlapping two individual trapping diagrams of different sized particles (Figure 17c). As an example, particle sorting by selective trapping of 0.5 μm versus 1 μm PS particles was demonstrated (Figure 17d).

Along with optical trapping and rapid transport assisted by natural convection, the light-induced temperature variation along the convective flow can be exploited for advanced applications. For example, Braun et al. exploited the temperature variation and natural convective flow for DNA replication.[294] Because high- and low-temperature regions existed along the convective cycle, DNA transported by the natural convection flow could be exposed to different temperatures at a certain time, providing suitable environments for its melting and elongation as required by a traditional polymerase chain reaction.

7.2. Optothermal Assembly Based on Natural Convection

Because the natural convective flow has a large working range in solutions and is universally applicable to manipulating various objects, it has been widely exploited for the larger-scale optothermal assembly of colloidal structures.[288,295,296] The heating source for the

optothermal assembly can be (1) predesigned light-absorbing substrates,[79,297] (2) mobile light-absorbing particles,[298] or (3) light-absorbing fluids.[72,299]

As an example of substrate-based optical heating, Shoji et al. fabricated Au nanopyramidal dimer arrays via angular-resolved nanosphere lithography to serve as a template for the optothermal assembly of 2D hexagonal arrays of PS particles.[79] Thermoplasmonic convection was induced via plasmonic heating, facilitating the transport of PS particles toward the plasmonic trapping sites. Lu et al. exploited one-dimensional photonic crystals composed of Si_3N_4 and SiO_2 to generate thermal convection for particle assembly via total internal reflection.[296]

In addition to the predesigned optothermal substrates, the natural convective flow can be generated by optical heating of the suspended nanoparticles or the solvents.[298] For instance, Dinh et al. exploited the suspended Au nanorods as the heating source to induce a thermoplasmonic convective flow for 3D assembly of hydrogel microparticles (Figure 18a).[300] Similarly, Jin et al. assembled Au nanoparticles on a glass substrate via self-generated thermoplasmonic convective flows without chemical ligands or substrate patterning (Figure 18b).[295] The size of the assembly can be controlled by the light intensity and the illumination time. Alternatively, Liu et al. exploited a 1.48 μm fiber laser to heat water to induce natural convection (Figure 18c),[72] which led to a concentration of particles in the vicinity of the fiber tip. By moving the fiber at a proper speed, they separated the particles with different sizes based on their size-dependent gravitational velocity (Figure 18d). As a demonstration, the sorting of 15 and 45 μm PS particles was achieved (Figure 18e).

Upon the generation of thermal natural convection flow, thermophoresis of colloidal particles is unavoidable due to the existence of temperature gradients. When the thermophoretic force and the Stokes drag force induced by natural convective flow are comparable, both should be taken into consideration to fully understand the motion of target objects. Because colloids can be thermophobic or thermophilic depending on the sign of the Soret coefficients, the direction of thermophoretic forces and thermal convection flows can be either the same or the opposite.

When particle assembly is induced by the synergy of natural convection and positive thermophoresis (i.e., moving away from the heating source), ring-shaped colloidal assemblies can be obtained due to the counterbalance between thermophoretic force and Stokes drag force induced by the natural convection (Figure 19a).[68,297,301–304] Flores-Flores et al. further demonstrated the transition from integral assembled structures to ring-shaped ones by increasing the power of the incident laser (Figure 19b).[68] At low optical power (0.8 mW), natural convection was dominant and thermophoresis became trivial, leading to particle accumulation around the laser spot. When the laser power increased to 6 mW, the thermophoretic force was comparable with the Stokes drag force, repelling particles outside the laser spot to form a ring-shaped structure. Similarly, Weinert and Braun developed an optical conveyor through the combination of a bidirectional thermal convective flow and lateral thermophoretic forces to realize the accumulation of 1.5 nm molecules.[305]

In the case of negative thermophoresis (i.e., moving toward the heating source), enhanced optothermal assembly can be achieved by the synergistic effects of thermal convection and thermophoresis. For instance, Brasiliense et al. assembled silver nanoparticles functionalized by dodecanethiols into 3D supercrystals for potential surface-enhanced Raman scattering spectroscopy (Figure 19c).[288] It was found that the thermoplasmonic convection dominated when the Ag nanoparticles were far away from the laser spot, while thermophoresis played a more important role when the particles were in the vicinity of the laser spot (Figure 19d). Wu et al. also demonstrated the large-scale optical assembly of PS particles into needle-like structures in the radial direction with the assistance of negative thermophoresis and thermal convection.[306]

Through the coordination of natural convective flow, negative thermophoresis, and optical force, Ho and co-workers demonstrated long-range and 3D optical trapping of PS beads and *Escherichia coli* (*E. coli*) bacteria (Figure 19e).[307] The convective flow was exploited to transport dispersed particles toward the Au-coated fiber tip. Meanwhile, the thermophoretic force along with the optical force counterbalanced with the drag force from the lateral convection at the near field to achieve particle trapping. Accordingly, the large-scale assembly of PS particles on AuNI substrates was achieved via thermoplasmonic convection, and the assembled structures could be moved by translating the laser spot (Figure 19f).[77]

8. OPTICAL MANIPULATION BASED ON OPTOTHERMALLY INDUCED MARANGONI CONVECTION

Marangoni convection describes a type of flow arising from the surface tension gradient, which can be induced by optothermal effects, concentration gradients of chemicals,[308–310] and catalytic effects for the bubble generation.[311–313] Several types of optothermally induced Marangoni convection have been exploited for heat-mediated optical manipulation. These include convection at optically heated water–oil interfaces and liquid–gas interfaces that are pre-existing in the systems, as well as the convection at optothermally generated vapor bubbles. When a focused laser beam irradiates light-absorbing particles or continuous substrates,[77,314] the local heating causes water evaporation and nucleation of microbubbles at the solid–liquid interface.[315,316] The surface tension gradient along a bubble surface introduces Marangoni convection in solutions, which can rapidly transport suspended objects. Marangoni convection occurring at the planar fluid–fluid interface usually requires less temperature increase and is more suitable for the manipulation of macroscopic objects. In contrast, Marangoni convection induced by localized optothermal bubbles can achieve precise manipulation of the micro/nanoscale objects. Advantages of Marangoni-convection-based optical manipulation include (1) applicability to target objects of variable materials, sizes, and shapes; and (2) strong forces (several orders of magnitude larger than that induced by natural convection) for fast and large-scale particle manipulation. We will discuss optical trapping, assembly, swimming, and rotation based on Marangoni convection.

8.1. Optothermal Trapping, Transport, and Accumulation Based on Marangoni Convection

Marangoni convection at optically generated and controlled optothermal bubbles has been exploited to trap and transport colloidal particles and biological cells.[317–320] Zhao et al. reported the trapping of colloidal particles and biological cells by the optothermal bubble with a balance among the drag force, surface tension force, and pressure force derived from the pressure difference between the gas and the liquid.[318] Noninvasive manipulation was achieved via directly manipulating the bubble as a shuttle for target objects (Figure 20a). Dai et al. demonstrated 3D manipulation of hydrogel microstructures with a size of >10 μm by generating and moving an optothermal bubble. With the bubble under the microstructures, researchers could lift the microstructures for out-of-plane rotation and 3D assembly (Figure 20b and c).[320,321] Apart from the single-bubble manipulation, Ghosh et al. explored the convective flow arising from two adjacent optothermal bubbles for versatile particle manipulation. Self-assembly, sorting, and circular motions of different colloidal particles have been demonstrated by controlling the size and distance of two bubbles.[76] Rahman et al. exploited a spatial light modulator to split a laser beam for independent generation and manipulation of multiple bubbles, which were utilized for in-plane rotation and translation of micro-objects (Figure 20d).[322] Moreover, optothermal bubbles were harnessed to drive the more complex and functional objects like disk-shaped microrobots.[323] The bubble-driven robots could push PS beads and yeast cells toward target locations.

Because of their capabilities of long-range particle transport and efficient particle trapping, optothermal microbubbles have been incorporated into light-driven microrobots to achieve contactless particle loading into and unloading out of the robots. Villangca et al. developed a robot that could load and unload suspended particles with an optothermally induced bubble (Figure 20e).[324] When a microbubble was formed inside a hole of the robot by laser irradiation, Marangoni convection would drag the surrounding particles into the hole of the robot. The trapped objects could be ejected out of the hole by slightly shifting the heating laser beam across the robot body, which was like the action of pumping a syringe (Figure 20f). Compared with the tweezing techniques that trap objects at the laser beam center, such as optical tweezers, optothermophoretic tweezers, and opto-thermoelectric tweezers, optical tweezing assisted by Marangoni convection can keep target objects away from the laser beam to avoid potential photodamages and thermal damages. However, in this case, the resolution of single-object manipulation is commonly limited to the microscale.

Benefiting from the toroidal shape and high velocity of Marangoni convective flow, optothermal bubbles have been widely utilized for rapid accumulation of various objects, such as PS beads,[325,326] quantum dots,[327] metal nanoparticles,[328–331] DNA,[332] living cells,[333] and bacteria,[334,335] and enhancing optical printing, sensing, and chemical reaction. For instance, Uwada et al. exploited the accumulation of glycine molecules and temperature rise in the vicinity of an optothermal bubble to produce glycine crystals.[336] Vélez-Cordero and Hérnandez-Cordero printed entangled arrays of multiwalled carbon nanotubes at an optical fiber tip via a synergy of negative thermophoresis and bubble-induced Marangoni convection.[337] In addition, Iida and co-workers achieved high-density assembly of electric-producing bacteria with a high survival rate on a honeycomb-like film via optothermal

bubbles,[334] which is promising for the development of high-density microbial energy conversion devices. The same group also investigated how surfactants influenced bubble-assisted assembly.[338] It was found that the nonionic surfactant could reduce the bubble size and decrease the convective velocity, which changed the assembly pattern and increased the number of aggregated particles.

Recent years have also witnessed rapid progress in exploiting bubble-based accumulation for sensing applications. Kang et al. exploited optothermal microbubbles to simultaneously aggregate silver nanodecahedra and target molecules to achieve high-sensitivity detection of the molecules with surface-enhanced Raman spectroscopy.[330] Due to the quick accumulation of both the signal-amplification silver nanodecahedra and the molecules assisted by optothermal microbubbles, the Raman signal could be detected within 5 s with the significantly enhanced detection sensitivity. Similarly, Zhao and co-workers used optothermal microbubbles to assemble metal nanoparticles into nanogap-rich superstructures and simultaneously concentrate analytes at the nanogaps for active chemical sensing.[328] With the goal of enhancing sensing based on plasmonic nanoapertures, Kotnala et al. adopted bubble-induced Marangoni convective flow to enhance the trapping efficiency of analytes at the nanoapertures.[292] Recently, Liu et al. demonstrated bubble-mediated accumulation and printing of chiral molecules on plasmonic chiral metamaterials to enhance label-free chiral detection (Figure 21a). As shown in parts b and c of Figure 21, the bubble accumulation of molecules significantly enhanced the detection limit and made it possible to detect various mixtures of chiral biomolecules. Furthermore, Kim et al. exploited a volatile and water-immiscible component called perfluoropentane to demonstrate the generation of microbubbles at a low temperature (~36 °C at the laser beam center) for the fast accumulation and sensing of proteins without any optothermal damage to the biomolecules (Figure 21d).[339] The bubble-induced Marangoni convective flow enhanced the capture efficiency of the proteins by the sensing surface, leading to 1 order-of-magnitude improvement in detection sensitivity and a 30-fold reduction in detection time.

The potential optothermal damage during the vapor-bubble-driven accumulation could also be alleviated by the shrinking surface bubble deposition method. Moon et al. proposed such a method for the low-temperature deposition of DNA-functionalized Au nanoparticles.[340] Vapor bubbles were created by short-time laser irradiation. Once the laser was turned off, suspended particles were printed on the substrate along the bubble surfaces during the bubble shrinkage without additional laser-induced heat. Compared with the optothermal-bubble-assisted printing under continuous irradiation, a stronger fluorescence signal of the printed molecules was detected, validating the low-temperature working manner.

Bubble-assisted Marangoni convection and accumulation can also be applied for optothermal printing of nanomaterials on solid-state substrates for device applications (Figure 22a).[342–345] It has been demonstrated that the toroidal Marangoni convective flow induced by an optothermal bubble can drag various nanomaterials, including PS beads,[325] metallic particles,[331] carbon nanotubes,[346] quantum dots,[347] and soft oxometalates,[348] toward the bubble–substrate interface and immobilize them on the substrate via van der Waals interactions (Figure 22b). The working principle is the same as that for printing molecules on functional substrates for enhanced spectroscopy and sensing.[328,330,339,349,350]

Moreover, an ultra-short lifetime (~100 ns) of the submicrometer vapor bubble[351] facilitates real-time movement of the bubble by scanning the laser beam for continuous printing. Lin et al. demonstrated the printing of single colloidal particles with different sizes and materials into arbitrary patterns on the substrate (Figure 22c).[217] Taking advantage of the programmable control of laser scanning, Bangalore Rajeeva et al. achieved continuous bubble printing of semiconductor quantum dots with high resolution (~650 nm) and high throughput (10^4 μm·s^{-1}).[347] Complicated patterns such as the "Mona Lisa" image were printed with submicron details (Figure 22d). A haptic printing platform was further developed by integrating bubble printing with a smartphone device for free-form patterning of quantum dots.[352] To avoid the pinning of the microbubble in order to realize continuous printing of more uniform and narrower structures, Shpaisman and co-workers modulated the incident laser to better control the construction and destruction of microbubbles.[331]

Beyond printing colloidal particles that have been synthesized previously, bubble printing can be employed for one-step synthesis and structuring of nanomaterials from precursor solutions. For example, Ag rings and ZnO nanocrystals were patterned on substrates via bubble-driven localized ion accumulation and the resultant chemical reaction.[353,354] Conducting polymers (e.g., polypyrrole and polyaniline) were in situ synthesized and patterned on a glass substrate via the fast concentration of pyrrole and aniline by optothermal bubbles.[355,356] Moreover, the synergy of the instantaneous ion saturation and the high temperature around the bubble permits surfactant-free synthesis and simultaneous patterning of an immiscible metallic nanoalloy.[357,358] Linear patterning of rhodium–gold nanoalloys via bubble printing is shown in Figure 22e.[357] High-resolution transmission electron microscopy and energy-dispersive X-ray spectroscopy were performed to validate the formation of nanoalloys (Figure 22f).

Rather than through the generation of optothermal bubbles, Marangoni convective flow can also arise at a pre-existing gas–liquid interface or solid–solid interface that is optically heated.[308,359] For instance, Winterer et al. heated the water near the surface to generate a strong thermocapillary flow at the air–solution interface (Figure 23a).[359] Au nanoparticles were levitated by the thermocapillary flow and then repelled away from the laser spot at the interface due to the toroidal shape of Marangoni flows (Figure 23b). The temperature increase of the solution was only 1.75 K, which made it possible to apply it for biological samples. In another example, Zhang et al. exploited a ringlike laser pattern to establish a closed potential barrier around target objects at the liquid–air interface for stable trapping and manipulation at the interface (Figure 23c), which is similar to the particle manipulation based on multiple optothermal bubbles shown in Figure 20d.[360] Wei and co-workers further demonstrated particle manipulation inside solid fibers based on laser-induced thermocapillary convection.[361] When a functional material-core glass-cladding fiber was heated by a laser, the cladding and the core were locally liquidized when a chain of in-fiber particles was formed due to the penetration wave occurring on the interface (Figure 23d). Marangoni convection was triggered at the heated cladding–core interface, which drove the in-fiber particles to drift along the convective flow (Figure 23e). This manipulation method is independent of the materials, shapes, and sizes of particles and can be used for the assembly of various functional particles inside fibers.

Marangoni convection can also be induced by optically heating liquid droplets in other solvents, which has been used to manipulate the liquid droplets.[362–366] Baroud et al. applied the heat-mediated optical manipulation technique in microfluidics to achieve the formation, transport, fusion, and division of microsized water-in-oil droplets.[367,368] The light absorption of the water droplet was enhanced by adding additional dyes to the droplet. When the droplet was asymmetrically heated by a laser beam, Marangoni convection occurred at the water–oil interface, generating a net force to push the droplet away from the laser beam spot. Accordingly, uneven droplet division was achieved inside the microfluidic channel by applying a heating laser beam at the cross (Figure 24a). de Saint Vincent et al. employed the optothermally induced Marangoni convection to achieve the separation of pure water droplets and water–dye droplets in terms of their difference in light absorption.[369] As the water–dye droplets were heated and repelled by the laser beam due to Marangoni convection, they were separated from nonabsorbing water droplets, enabling continuous sorting of the droplets based on a microfluidic system (Figure 24b). In addition, Kotz et al. exploited the optothermally induced Marangoni effect to achieve the nudging of single water droplets in decanol without microfluidics.[370] Recently, Nagelberg et al. demonstrated the reorientation of Janus emulsion droplets based on the optothermally induced Marangoni forces.[366] It is worth noting that Marangoni convective flow is applicable to both nanoscale and macroscale objects due to its high velocity and large working range.

Another interesting heat-mediated optical approach for the assembly of Au nanoparticles (AuNPs) is enabled by structured-light irradiation coupled with Marangoni convection. For instance, Rodrigo et al. developed a ring-shaped optical field with homogeneous intensity but tailored phase distribution (Figure 25a).[41] AuNPs were propelled around this 2D optical trap, whose velocity was dependent on the optical phase gradient (Figure 25b). When the incident light wavelength matched the plasmonic resonance wavelength of AuNPs, the optical heating of the nanoparticles triggered a strong Marangoni convection flow at the liquid water/superheated water interface around the heated particles. More surrounding AuNPs were then dragged toward the heated particles and assembled into a quasi-stable group (Figure 25c). The size of the assembled group could be controlled by dynamically switching the phase gradient distribution of the incident light.

8.2. Optothermal Swimmers, Oscillators, and Rotors Based on Marangoni Convection

Innovative designs that exploit optothermal Marangoni convection have led to various microscopic and macroscopic swimmers, oscillators, and rotors. Different optothermal swimmers based on Marangoni convection at the fluid–fluid interfaces have been developed, including microscale Janus particles,[371] millimeter-sized photothermal paper,[372] centimeter-sized polymers coated with light-absorbing films,[373] PS-particle-stabilized air bubbles,[374] and millimeter-sized liquid marbles.[375,376] For some of the millimeter-sized or larger swimmers, sunlight or filament lamps can work as the driving light source without the need of a laser.

For example, Okawa et al. demonstrated a light-driven Marangoni swimmer operating at the liquid–air interface (Figure 26a).[377] The swimmer was composed of a PDMS block as the main body with vertically aligned carbon nanotube forests as the light-absorbing film

coated to one side of the block. This design is quite flexible in terms of the swimmer size, swimmer material, liquid, and light source. The size of the swimmer could range from millimeters to tens of centimeters, and the swimming velocity could reach up to 8 cm s^{-1}. In addition, the liquid could be water, isopropyl alcohol, dimethylformamide, etc., and the light source could be either laser or sunlight. Similarly, Liao et al. demonstrated centimeter-sized PDMS swimmers coated with the aligned carbon nanotube films.[373] The swimming velocity reached up to 4.19 cm s^{-1}, which could be tuned by the thickness and alignment direction of the carbon nanotube films as well as the incident laser wavelength.

Interestingly, many of these Marangoni swimmers with a millimeter or larger-scale size can be fabricated on demand with direct writing methods. For example, Sun and co-workers developed a direct laser writing method for the facile fabrication of optothermal Marangoni swimmers with different sizes and shapes.[378] In addition to arbitrarily shaping the swimmers, the laser writing could carbonize polymer materials to obtain light-absorbing and superhydrophobic surfaces that promote optothermal Marangoni convection for powering the swimmers. Wang et al. reported laser-induced graphene (LIG) tape as stick-on optothermal labels that work as light-driven actuators based on the Marangoni effect. They applied direct laser writing to prepare the graphene patterns on PI tapes (Figure 26b).[378] Furthermore, a 3D frog origami with LIG legs was fabricated that underwent directional movement under irradiation with a laser beam, a filament lamp, or sunlight (Figure 26c).

In addition, Fujii and co-workers demonstrated the Marangoni-convection-driven directional movement of millimeter-sized liquid marbles at the water–air interface powered by a heating laser.[375,376] Liquid marbles were liquid drops stabilized by solid powders such as polypyrrole and carbon black. Due to the high light absorption and hydrophobicity, liquid marbles could float and drift at the water–air interface under laser irradiation. The liquid marbles could further be destabilized by pH, isopropanol fumes, or successive laser ablation. As a proof-of-concept demonstration of targeted delivery, a single liquid marble was optically transported to a target location and disrupted to release the inner materials (Figure 26d).

Swimmers driven by optothermal Marangoni convection may face a challenge when the optothermal Marangoni convection is quenched due to the coexistence of the concentration-gradient-induced Marangoni convection.[371,379] To improve the robustness of optothermal Marangoni swimmers, additional operation modes can be added. For example, Xiong and co-workers developed dual-mode self-propelled swimmers.[380] At the low-laser-power intensity, the optothermal-paper-based swimmer moving at the water–air interface was powered by the optothermal Marangoni effect. With a higher-laser-power intensity, the swimmer could be fueled by the vapor due to the enhanced localized heating (Figure 26e). The moving direction could be well-controlled by the shape of the swimmer and the irradiation position of the laser beam on the swimmer (Figure 26f). Pan et al. developed multimode Marangoni swimmers composed of thermal-stimuli-responsive hydrogels and CuS nanoparticles. The Marangoni swimmers could switch among three working modes, including floating, self-propelling, and sinking, by simply adjusting the state of the incident laser beam (Figure 26g).[381] In brief, the floating was attributed to the optothermal buoyancy flow around the swimmer upon the laser heating, while the sinking stemmed from the

water absorption and resultant density gain of the thermal-responsive hydrogel due to the decreased temperature after the laser was turned off.

Opto-thermocapillary oscillators were demonstrated on a liquid-drop surface via the synergy of optothermal Marangoni propulsion and capillary repulsion (Figure 27a).[383] A millimeter-sized gel disc embedded with Au nanoparticles was placed atop a water droplet. Asymmetric thermal Marangoni forces were induced due to the nonuniformities of the disc that pushed the disc off the droplet apex. As the disc was propelled toward the droplet perimeter, the capillary force acted like a spring and restored the disc back to the apex, resulting in sustained oscillatory motion. This oscillation could be adjusted by the light intensity, droplet volume, and disc size (Figure 27b).

Several optothermal Marangoni rotors have been developed through engineering the optothermal response of the rotating objects.[256,384] For instance, Okawa et al. fabricated a millimetre-sized, cross-shaped Marangoni rotor where the light-absorbing film was attached to the clockwise face of each fin (Figure 28a).[377] The rotor could rotate at rates up to 70 rpm under the focused sunlight or NIR laser beam. Maggi et al. demonstrated that a microsized gear with an asymmetric shape could achieve a rotation rate of up to 300 rpm.[256] When the gear was uniformly irradiated by light, an asymmetric temperature field was built with the inner vertices being hotter than the outer ones (Figure 28b). Because the surface tension usually decreased with the rise of temperature, the gear rotated with the long teeth edge forward, i.e., clockwise (Figure 28c). Thermophoresis was excluded as a driving force for the gear because it would require a 10^5 larger power density to achieve a similar rotation rate as that for Marangoni convection.[385] Yang et al. demonstrated the controllable rotation of cross-shaped Marangoni rotors by dynamically changing the position of the focused light on the edges of the rotors (Figure 28d), whose rotation rate could reach up to 40 rpm.[380]

9.   OPTICAL MANIPULATION BASED ON ELECTROTHERMOPLASMONIC FLOW

Compared with the natural convective flow upon the same laser irradiation, an ETP flow possesses a notably higher velocity for the rapid delivery of particles. The ETP flow can be generated by the fluid's permittivity and conductivity gradients under external electric fields.[78,155,386–388] It has been exploited for fast particle transport in plasmonic trapping[155] and combined with the electro-osmotic flow for particle trapping[78] and assembly.[387]

By combining the ETP flow with plasmonic nanotweezers, Ndukaife et al. developed hybrid ETP nanotweezers for rapid transport and versatile manipulation of single nano-objects (Figure 29a).[155] The on/off states of the electric field and the laser beam enabled different manipulation modes of the nanotweezers. When both the ac field and the heating laser were on, individual suspended particles were rapidly delivered to the Au nanoantennas via the ETP flow and got trapped at the plasmonic hotspots within 2 s. It is worth noting that the radial velocity of an ETP flow can reach 11.8 μm s^{-1}, which is 150 times higher than the velocity (i.e., 75 nm s^{-1}) without applying the electric field. After a particle was trapped, the three following manipulation modes were available:

1. Trapping: Turn off the ac electric field and keep the laser beam on.

2. Releasing: Turn off both electric field and laser beam.

3. Immobilizing: Temporarily switch the ac field to the direct current (dc) field and then turn off both inputs (Figure 29c).

The same research group further utilized plasmonic nanohole arrays to achieve high-throughput ETP-flow-assisted assembly of the particle ensembles.[387] The interparticle spacing of the assembled particles could be reversibly tuned by the on/off state and frequency of the ac field. Moreover, Ndukaife and co-workers developed opto-thermo-electrohydrodynamic tweezers (OTET) to manipulate sub-10 nm biological objects based on the synergy of the ETP flow and the electro-osmotic flow (Figure 29b).[78] Bovine serum albumin protein with a hydrodynamic radius of 3.4 nm was trapped at several micrometers away from the laser illumination through the balance between the ETP flow and the ac electro-osmotic flow. The trapping of single proteins at a position away from the laser beam could effectively avoid photodamages and thermal damages. By translating the laser beam or the microscopic stage, the trapped protein could be dynamically manipulated to different positions around the Au nanohole arrays (Figure 29d). Because the intensity of the ETP flow and electro-osmotic flow could be tuned by the frequency of the ac field, the distance between the trapped object and the edge of the nanohole arrays as well as the trapping stability could be tuned via altering the ac field frequency, which could be used for sorting of nano-objects with different sizes.

10. OPTICAL MANIPULATION BASED ON OPTOTHERMAL DEFORMATION

Optical manipulation of objects can also be achieved by controlled optothermal deformation of the target objects or substrates. On the basis of the controlled optothermal deformation of the objects, researchers have developed a variety of artificial systems that can move in various ways under external stimuli, including crawling, walking, swimming, jumping, oscillating, and gripping. Many light-absorbing materials, including azobenzene,[67] AuNPs,[389] rGO,[63,390,391] CNTs,[64,392] graphene,[65] and PDA,[66] have been embedded into soft matrixes to achieve efficient optothermal shape deformation and thus light-driven active systems. The active systems are commonly at the macroscale and operated in both air and liquid. In the category of optothermal deformation of substrates, different polymer or surfactant films are utilized for the reconfigurable nudging and printing of various objects on solid substrates at nanoscale accuracy. In this section, we categorize and discuss the optical manipulation techniques exploiting optothermal deformation based on different working mechanisms.

10.1. Thermal Expansion

10.1.1. Thermal Expansion of Objects.—Optothermal actuators, motors, and robots based on thermal expansion[393,394] of the objects can be classified into two categories: (1) bimorph structures with two parts of different coefficients of thermal expansion (CTEs) and (2) hydrogels doped with nanosheets that possess thermally induced electrostatic repulsion. For the first type, the difference in the thermal-expansion mismatch can lead to different motions such as oscillating,[395] crawling,[396] and walking.[397] Polymers with large positive

CTEs such as PDMS,[398] polypropylene,[399,400] polyethylene,[401] and polycarbonate[402] are chosen as the expansion layers, while the counterparts are usually graphene, CNTs, and GO due to their negative CTEs and high coefficients of hygroscopic expansion, which can contract upon laser irradiation.[403] Zhang et al. fabricated an optothermal actuator by coating CNTs on polycarbonate membranes.[402] Assembly of the actuator membranes into a cylinder with CNTs facing outward led to a centimeter-sized motor, which would roll on a flat surface upon tilted light illumination. The tilted illumination on the motor caused the curvature of the cylinder to decrease on the light-facing side due to the thermal expansion, which caused a change to the center of mass of the motor and generated a torque that drove the motor away from light at a speed of ~6 cm s^{-1} (Figure 30a). Similarly, Hu et al. developed rolled rGO-CNT/PDMS bimorph soft actuators with a pseudoshape-memory feature.[404] Upon heating laser irradiation, the curled film would be flattened due to the thermal expansion of PMDS, which recovered to the rolled shape after the laser was turned off. This reversible shape change enabled tanklike crawling of the actuator. Wu and co-workers developed optothermal CNT/PDMS soft actuators with a curled shape for jumping[405] and oscillating motions.[395] The jumping behavior was attributed to the sudden release of the light-fueled elastic energy. The self-sustained oscillation was achieved under continuous illumination due to the self-shadowing effect and time delay in the optothermal response (Figure 30b). Deng et al. developed CNTs + paraffin wax/polyimide bimorph soft actuators where the aligned direction of CNTs could tune the phototropic or apheliotropic bending of the actuators. Such actuation was driven by the optothermally deformed paraffin wax that tended to expand perpendicularly to the orientation of the aligned CNTs.[406] Recently, Wang et al. reported a controllable and tunable optothermal actuation based on bimorph structure composed of 3D silk photonic crystals (PCs) doped with AuNPs and PDMS.[80] The optical bandgap energy of the PC film was designed to match the optical absorption energy of the AuNPs. With light irradiation from the PDMS side, the PC film reflected more light to the suspended AuNPs, inducing the much stronger light absorption and the resultant larger macroscopic deformation due to the thermal expansion (Figure 30c). Various deformation configurations were achieved by selectively patterning the PDMS layers with the PC films (Figure 30d).

Optically controlled thermal expansion coupled with electrostatic repulsion was also exploited for the actuation of soft robots. Aida and co-workers designed anisotropic poly(*N*-isopropylacrylamide) (PNIPAM) hydrogel actuators containing magnetically oriented titanate nanosheets and AuNPs.[396] The AuNPs enhanced optothermal conversion and thermal expansion of PNIPAM. Upon light illumination on the actuators, the anisotropic electrostatic repulsion between the titanate nanosheets in the hydrogel was synchronously modulated, causing reversible expansion and contraction of the hydrogel isovolumetrically along a direction orthogonal to the titanate nanosheets. When the irradiation spot was moved along the cylindrical actuator axis, the hydrogel held in a capillary underwent earthworm-like peristaltic crawling due to quick and sequential elongation/contraction events and moved oppositely toward the laser scanning direction (Figure 30e). Furthermore, Zhu et al. developed optothermal actuators based on an electrically oriented nanosheet/AuNP/PNIPAM hydrogel, which made progress toward robots undergoing swift locomotion in free space

without geometric constraints.[397] Isochoric-deformation-induced crawling and walking were achieved on a solid substrate by spatial light stimuli.

10.1.2.   Thermal Expansion of Solid Substrates.—Undesired capillary forces and Brownian motion can interfere with optical manipulation of objects in solutions, limiting precision in the object positioning and assembly. Additional processes are often required to immobilize the suspended objects being manipulated onto solid substrates to create functional structures for device applications. Optical manipulation of objects on solid substrates can be attractive for the precise and reconfigurable assembly of functional structures.[407–410] However, it is not straightforward for light to overcome the strong van der Waals interactions at the object–substrate interfaces to achieve versatile optical manipulation.[411] Recent years have witnessed success in the development of both in-plane and out-of-plane optothermal nudging for the optical manipulation on solid substrates.[412–414] Out-of-plane optothermal nudging of colloidal particles can be achieved by the thermal expansion of the solid substrate, which enables opto-thermomechanical nanoprinting with sub-100 nm accuracy (Figure 31a).[413,414] The target objects were first drop-casted and naturally dried on a donor substrate composed of a thin film with a large thermal expansion coefficient. For light-absorbing particles (e.g., AuNPs), a transparent donor substrate like PDMS can be used. If the particles are transparent to the laser beam, an absorptive substrate should be exploited as the donor substrate (e.g., indium-tin-oxide-coated polyethylene terephthalate). As shown in Figure 31b, when a AuNP was heated by a laser, the PDMS film was deformed to provide a strong thermal expansion force (F_{TE}). F_{TE} and optical axial force F_Z overcame the van der Waals force (F_V) to transport the AuNP from the PMDS film toward the receiver substrate (Figure 31c). A 10×10 array of AuNPs was fabricated via nudging the particles from the donor substrate onto the receiver substrate (Figure 31d). The scatter plot of the printing error indicates that 70% of the nanoparticles were printed in sub-100 nm accuracy (Figure 31e). Furthermore, the printing of nanoparticles into a complex "NANO" pattern was demonstrated (Figure 31f).

10.2.   Phase Transition

10.2.1.   Phase Transition of Objects.—Upon optical heating, some of the phase-transition materials such as liquid crystals (LCs)[415,416] and shape-memory polymers/alloys (SMPs/SMAs)[417,418] can undergo shape changes. They have been widely used in optothermally driven actuators and robots, representing another type of optical manipulation based on optothermal deformation. The elastic energy of LCs is related to the orientational order of the mesogenic monomers, which is highly relevant to the temperature. To enhance the optothermal response of the LCs, one can increase their light absorptivity by doping photosensitive components (e.g., azobenzene[419–423] and carbon nanotubes[392]) into the LCs. When the LCs are heated by light, the reduced molecular order leads to macroscopic deformation, which can be recovered by turning off the light to cool the LCs down. Both liquid-crystal elastomers (LCEs) and liquid-crystal networks (LCNs) have been used in soft robotics to achieve such motions as oscillating,[422,424,425] crawling,[419,421,423] walking,[426] and swimming.[257,426] Similarly, the SMAs/SMPs can undergo shape changes when optically heated above the critical temperature that have also been widely used for optothermal

robots.[427] For example, vanadium dioxide (VO_2) as a type of SMA can change its shape due to the optothermally induced lattice change from monoclinic to rutile structure.

For instance, millimeter-sized LCEs could be modified with azo dyes to achieve fast mechanical deformation (with a relaxation time of ~60 ms) under laser irradiation.[67] On the basis of the enhanced light-driven bending behaviors of the modified LCEs, a primary optical swimmer was demonstrated that operated on the controlled on/off states of the heating laser. To enhance control of the shape and mechanical motion, Palagi et al. induced local deformation of homogeneously azobenzene-doped LCEs by encoding the incident light spatially and temporally.[257] Upon visible laser irradiation, the strong light absorption of azobenzene promoted the fast phase transition and shape change of the LCEs. The modulated light irradiation enabled the flat-curving deformation of the LCEs for their directional swimming and rotation (Figures 32a and b). In a series of publications, Zeng and co-workers and Priimagi and co-workers studied the locomotion of LCE-/LCN-based optothermal soft robots.[419–423] As one example, they developed a millimeter-sized LCE-based soft robot that could walk on paper, glass, and human fingers when powered by temporally modulated incident light (Figure 32c).[421]

One can couple optothermal phase transitions with an optomechanical effect to achieve more sophisticated shape control and mechanical motion based on the LCs.[422] Priimagi and co-workers developed reconfigurable LCN soft robots by exploiting the synergy of optothermal and optomechanical effects of the doped azobenzene molecules in the LCN.[428] The optomechanical effect, which corresponded to azobenzene trans–cis isomerization, was triggered by ultraviolet (UV) light, while the heating by a red light led to the optothermal deformation of the doped LCN. Controlled motion of the LCN soft robot was powered by irradiating it with UV light of predesigned patterns for partial trans–cis isomerization and then illuminating it with red light to achieve selective macroscopic deformation. This spatial coding of deformation could be erased by irradiating the robot with blue–green light that induced the reversible cis–trans isomerization. To further enhance the optothermal response, Lu et al. fabricated LCNs doped with both Au nanorods and azobenzene molecules. For such doped LCNs, plasmon-enhanced optothermal deformation and optomechanical deformation could be activated via NIR and UV irradiation, respectively.[429] To achieve the optimum performance in the different working environments, the optothermal and optomechanical deformations of azobenzene-doped LCNs could be finely tuned by using different types of azobenzene molecules.[430] For example, monoacrylate azobenzene acts as side-chain chromophores for the optothermal deformation of LCNs, which is suitable for the actuation in nonliquid environments. Diacrylate azobenzene works as cross-linked chromophores for both optothermal and optomechanical deformation, which can be applied in both liquid and nonliquid environments.

Optothermal robots based on phase transition can also be achieved in an aqueous environment with diverse working modes, including crawling, jumping, and swimming.[426] The robots made of liquid-crystal gels (LCGs) were driven by the shape deformation and the storage of elastic energy, which microscopically stemmed from the decreased molecular alignment in the gels upon laser heating. Compared with LCEs and LCNs, LCGs had a lower and sharper phase-transition temperature with easier orientational

control due to the highly coupled thermomechanical response from their self-assembled nanoscale composites.[431] Crawling of millimeter-sized LCGs was achieved by either the self-shadowing effect of laser irradiation at a certain angle or scanning of the laser beam along the LCGs (Figure 32d). The walking of LCGs was realized on a ratchet surface upon periodic laser irradiation (Figure 32e). In brief, laser illumination led to the bending of LCGs with an anchoring point on the substrate. After the laser was turned off, the stored elastic energy was released to push the LCGs forward. Swimming of LCGs in the aqueous environment was achieved by triggering the undulatory bending of the LCG films.

Various SMPs/SMAs have been applied in optothermal actuators. For instance, Bai et al. fabricated metal-ion-doped poly(vinyl alcohol) polyacrylic acid that exhibited NIR-driven optothermal actuation.[432] Yang et al. designed a *cis*-1,4-polybutadiene–polyethylene semicrystalline copolymer that underwent optothermal bending, grasping, and walking.[433] Liu et al. achieved micron-sized optothermal actuators based on Cr/VO_2 bimorph structures.[427] Sepúlveda and co-workers demonstrated CNT/VO_2 bimorph structures exhibiting light-driven oscillation with amplitudes higher than those for VO_2-based actuators (Figure 32f).[434,435] This is because CNTs promoted the light absorption and heat generation. In addition, CNTs of different chiralities enabled wavelength-selective optothermal actuation.[434]

10.2.2. Phase Transition of Solid Substrates.—In-plane optothermal nudging of colloidal particles on solid substrates can be achieved by the synergy of heat-induced phase transition of thin films and optical scattering forces, which enables reconfigurable nanofabrication directly on the solid substrates. Fedoruk et al. demonstrated the optical nudging of single AuNPs inside a poly(vinyl alcohol) (PVA) film by the combination of laser heating and optical forces.[436] Upon laser irradiation, plasmonic heating of AuNPs resulted in rapid melting and thermal decomposition of the PVA film. Simultaneously, the irradiated AuNP was pushed by optical forces within the localized melting region. Note that this manipulation process was irreversible because the PVA along the AuNP traces was decomposed. Recently, Li et al. achieved noninvasive and reversible optical nanomanipulation of colloidal particles on solid substrates via optothermally gated photon nudging (OPN).[412] The key to OPN is to introduce a thin surfactant layer (e.g., CTAC) with a low phase-transition temperature between target particles and a substrate to modify the particle–substrate interactions (Figure 33a). Without laser heating, the surfactant layer maintained the solid form and immobilized particles by van der Waals forces. When a laser beam irradiated the particle with a strong optothermal response, abundant heat was generated to trigger a localized phase transition of the surfactant layer from the solid phase to a quasi-liquid structure around the particle. Thus, the van der Waals friction between the particle and the substrate was considerably reduced, and the particle could simultaneously be nudged away from the laser beam by optical scattering force (Figure 33b). By steering the laser beam or translating the substrate with a motorized stage, particles could be manipulated to any target position with nanoscale accuracy. The laser could be turned off to immobilize the particles on the substrate where the surfactant layer recovered to the solid form. OPN is applicable to manipulating particles with a wide range of materials (e.g., metals, semiconductors, and dielectrics), sizes, and shapes. As a demonstration,

reconfigurable patterning of metal–dielectric hybrid superstructures composed of one Au nanowire and two Si nanoparticles was achieved (Figure 33c). It is worth noting that the surfactant layer can be removed without destroying the patterned superstructure after the manipulation process is complete. Recently, Li et al. further exploited the OPN technique to assemble tunable dielectric chiral nanostructures with a movable Si nanoparticle and a static Si nanowire, which served as a platform for the study of light–matter interactions at the chiral nanostructures (Figure 33d).[437] In situ chiroptical spectroscopy revealed that the optical chirality stemmed from the handedness-dependent coupling between optical resonances of the Si nanoparticle and the Si nanowire, which could be altered in real time by manipulating the nanoparticle along the nanowire (Figure 33e).

10.3. Water Sorption and Desorption

Materials with considerable hydrophilic groups, including poly(*N*-isopropylacrylamide) (PNIPAM),[389,390,438–442] PDA,[443,444] elastin-like polypeptides,[391] polyacrylate,[445] and cellulose,[446] can change their shapes upon water sorption and desorption. They usually desorb water molecules above the critical solution temperature to undergo shape contraction and reabsorb water after getting cooled to experience shape contraction. Optothermally controlled water sorption and desorption have been exploited for the development of light-driven soft robots based on shape deformation.

By creating asymmetric shape deformation of the robots via engineering the compositions, structures, and light illumination, various operation modes such as oscillating,[439] gripping,[390] crawling,[443] and swimming[389] have been achieved. Mu et al. developed self-folding walking robots based on the optothermally induced water sorption and desorption of GO-PDA/rGO composited papers.[443] Upon laser irradiation, the composited papers could bend because GO-PDA experienced a larger shape deformation than rGO in response to the laser-heating-induced water desorption. The walking of the robots was achieved by selectively exposing the papers to the laser beam to facilitate asymmetrically regional bending (Figure 34a). Gripping and crawling were also achieved for the paper-based robots by modulating the on/off state of the heating laser (Figure 34b). Ma et al. reported a general strategy toward designing macroscopically anisotropic polymer hydrogels that consisted of patterned rGO in PNIPAM, which are promising for optothermally induced 3D complex deformation based on water sorption and desorption.[390] He and co-workers developed centimeter-sized phototactic swimmers based on the temperature-dependent water sorption and desorption of Au-nano-particle-embedded PNIPAM hydrogels.[389] The mechanism of the swimmer driven by a self-sustained hydrogel oscillator under constant light irradiation was based on the self-shadowing-enabled built-in feedback loop (Figure 34c). When the illuminated side of the hydrogel exceeded the lower critical solution temperature of PNIPAM (~32 °C), water desorption at this side led to the bending of the hydrogel to block the incident light. The resultant temperature cooldown led to water absorption by the hydrogel and its recovery to the original shape, allowing the light to heat the hydrogel again. This optothermally induced self-shadowing effect could activate the continuous oscillation of the hydrogel, enabling the swimming of the hydrogel robots under constant light irradiation (Figure 34d). The same research group utilized a similar hydrogel system to develop a synthetic phototropism, where the hydrogel could

achieve omnidirectional self-orientation toward the incident light like a sunflower for more efficient solar-energy harvesting.[63] Exploiting the optothermally induced water sorption and desorption of PNIPAM-coated AuNPs, Baumberg and co-workers developed light-driven nanotransducers,[438] nano-oscillators,[439] and motile artificial chromatophores.[447] In addition to polymers, other materials, including transition metal dichalcogenides,[448] nickel hydroxide–oxyhydroxide,[449] and π-stacked carbon nitride films,[450] were also applied for light-driven dynamic systems based on their optothermally induced water sorption and desorption.

To further enhance heat-mediated optical manipulation based on shape deformation, one can exploit the synergy of optothermal expansion and water adsorption/desorption in heterogeneous multilayer materials. For example, bimorph structures featuring both thermal expansion and water absorption/desorption were proposed to enhance the degree of deformation and the response time.[400] Tai et al. fabricated a CNT/poly(vinylidene fluoride) bilayer structure for fast-responsive soft actuators due to simultaneous water desorption from CNTs and thermal expansion from poly(vinylidene fluoride).[451] Yang and co-workers developed a bilayer soft robot composed of GO-PDA-AuNPs and PDMS. GO-PDAAuNPs could respond to optical heating via water absorption/desorption, while PDMS could undergo thermal expansion. The bending amplitude and response speed of the bilayer structure were improved up to 173% and 3.5-fold, respectively.[441] Li et al. fabricated optical actuators based on the three-layered structures composed of a carbon black slurry as the thermal expansion layer, a polyethylene terephthalate film as the passive layer, and a waterborne acrylic adhesive as the water absorption/desorption layer.[452] A shorter response time, a larger actuation amplitude, and a faster actuation speed at a smaller temperature change were obtained for the three-layered actuators compared with the counterpart bilayer actuators.

10.4. Heat-Induced Surface Acoustic Waves

Shape deformation caused by optothermally induced surface acoustic waves (SAWs) has been exploited for the directional motion of metal nanostructures on solid substrates.[453] For instance, Linghu et al. demonstrated the crawling of Au nanowires on a silica fiber (Figure 35a).[168] When a pulsed 1064 nm laser was channeled through the silica fiber, surface plasmon polaritons were excited on the Au nanowire, which generated abundant thermal energy at the front end of the nanowire. The optical heating further caused the lattice expansion of the nanowire and resulted in the formation of SAWs. This lattice expansion increased the friction between the nanowire and the microfiber due to the decrease in the interfacial gap. As the nanowire began to contract, the center of the nanowire would be pushed forward, leading to movement along the light-propagation direction. The calculated positioning resolution of single-pulse actuation was 0.56 nm (Figure 35b). As a demonstration, a Au nanowire was successfully transported on a C-shaped curved microfiber (Figure 35c). In contrast, a 532 nm pulsed laser triggered the crawling of the nanowire against the light-propagation direction. In this case, no SAWs were excited, but abundant heat was still generated due to the strong light absorption by the Au nanowire, which induced thermal expansion at the back end of the nanowire and pulled the nanowire toward the light source. Lu et al. demonstrated light-induced SAW-driven rotation of Au nanoplates

(thickness = 30 nm) around an optical fiber in a nonliquid environment based on the local thermo-elastic expansion (Figure 35d).[454] Upon pulsed laser irradiation, the local heating of the Au nanoplate induced thermal expansion and formation of SAWs or Lamb wave (Figure 35e). The resultant collective motion of the surface Au atoms triggered the rotation of the nanoplate at a rotation rate ranging from 10^{-2} to 10^2 rpm. Both clockwise and anticlockwise rotation could be achieved (Figure 35f).

11. CONCLUSIONS AND OUTLOOK

We have discussed a wide range of heat-mediated optical manipulation techniques where optical heating is harnessed to enable new manipulation capabilities or enhance the existing ones (Table 1). However, our coverage is not intended to be exhaustive. In a broader sense, there are many other interesting optothermal manipulation techniques with working mechanisms and functions beyond what we have discussed. These include laser cooling and trapping of atoms and molecules, an exciting research field where thermal energy is optically released from the target objects to enhance their trapping stability,[455–457] optothermal-assisted coating[458] or melting at nanoscale,[218,459] laser ablation,[460–463] and optothermal manipulation of micro/nanofluids[53] in such areas as optofluidics[464–468] and solar steam generation.[469,470] In the area of optical rotors, rather than powering the rotation, optical heating of particles was exploited to reduce the viscosity of the surrounding fluids to improve the rotation speed of the particle rotors.[471–474] In addition, thermal creep flow created at the inner wall of an optical fiber was exploited for the optical manipulation of particles and living cells.[475,476] Hot vapor jet flows generated by optical heating have enabled millimeter-sized swimmers at the liquid–air interface.[477,478] Luo and co-workers demonstrated ballistic optical pushing and pulling of Au core–shell nanoparticles in water based on optothermal nanobubbles.[479,480] The nanobubbles assisted the formation of the saddle singularity for negative momentum against the laser Poynting vector and created a virtually frictionless environment around the illuminated particle based on the Leidenfrost effect for the ultrafast movement (~336 000 μm s^{-1}).

Conversion of light into heat is just one of many approaches toward enriching or enhancing optical manipulation. A huge range of optical manipulation techniques based on different light-control and conversion methods or on light coupled with other fields has been developed. For example, plasmonic tweezers were proposed to overcome the diffraction limit of light in conventional optical tweezers. Plasmonic tweezers exploit the plasmon-enhanced concentration and enhancement of light at the plasmonic nanostructures to trap nanometer-sized objects with nanoscale accuracy.[481,482] However, because surface plasmons are confined within the vicinity of the nanostructures, it is usually difficult to trap objects away from the nanostructures and to achieve 3D dynamic manipulation. One of the approaches to improving the plasmonic trapping efficiency is to couple plasmonic tweezers with microfluidics, which has developed into a field known as plasmofluidics.[483–486] Using project light patterns to form virtual electrodes on a photosensitive substrate, optoelectronic tweezers manipulate micro- and nanoscale objects based on dielectrophoresis.[49,50,487,488] They combine the advantages of optical tweezers and electrode-based dielectrophoresis to achieve arbitrary manipulation of objects in 2D with simple and low-power optics. Photocatalytic motors are fueled by light-driven catalytic chemical reactions.[177,240] With

the capacity for organic pollutant degradation that could be driven by sunlight, these motors are promising for environmental remediation.[240] On the other hand, a majority of photocatalytic motors require toxic chemical fuels such as hydrogen peroxide with typical working wavelengths ranging from UV to visible light, limiting their biological applications.

Each of these optical manipulation techniques has its advantages and limits depending on the applications, which makes it challenging to fairly compare the different techniques in a comprehensive manner. Heat-mediated optical manipulation is versatile in enabling remote and noncontact manipulation of diverse objects with variable materials, shapes, and sizes using low-power and simple optics. By rationally controlling the temperature field and optothermo–matter coupling, one can achieve various manipulation modes, including trapping, nudging, rotating, pulling, oscillating, and walking, which remarkably extends the capabilities of conventional optical tweezers. For instance, it is challenging to trap metal nanoparticles with conventional optical tweezers due to the strong scattering force and heating effect. We have shown that opto-thermoelectric tweezers can trap and manipulate various metal nanoparticles with an ultralow optical power.[224] Optothermal tweezers can also overcome the challenge of optical tweezers in trapping objects with a low refractive index in contrast to the surrounding medium. It has been common for heat-mediated optical manipulation exploiting photophoresis,[287] Marangoni convection,[377] and shape deformation[402] to manipulate millimeter-sized or larger objects in various media, which is challenging for conventional optical tweezers. With the capability of rapidly transporting and assembling numerous objects, heat-mediated optical manipulation exploiting natural, Marangoni, and ETP convective flows features high throughput. Because of the entropically favorable light-to-heat conversion, heat-mediated optical manipulation techniques have less-stringent requirements on the optical power, beam profile, and polarization than conventional optical tweezers, opening a new window of opportunities for the applications.

Up to now, heat-mediated optical manipulation techniques have already shown promising applications in robotics, sensing, manufacturing, and biomedical engineering. We conclude this Review with our outlook for the future development of heat-mediated optical manipulation for more applications.

11.1. Light Source

Optical heating or cooling is the basis in heat-mediated optical manipulation. Many parameters of the light source, including working wavelength, continuity, beam shape, coherence, phase, and polarization, should be tailored to tune the temperature and its gradient at substrates or target objects to achieve the desired manipulations for the different applications.[24] For example, to operate noninvasive optothermal nudging in vivo, an NIR laser beam is preferable due to its maximum depth of penetration in tissue.[192] Compared with a continuous-wave laser, the use of a pulsed laser as the heating source can constrain both heat transfer and collective heating on the substrates, which can enhance the temperature gradient for optothermal trapping of small objects with higher stability and precision.[62] In the manipulation that relies on a synergy of the optical field and temperature field, rational design of the light sources would become more critical in facilitating the regulation of both optical forces and optothermal forces.[412]

11.2. Heat Management

Because of their high optothermal conversion efficiency and nanoscale heat management, plasmonic nanostructures such as AuNIs, Au nanorods, and Au nanohole arrays have been commonly employed as heating sources in heat-mediated optical manipulation.[57] There is still plenty of room for enhanced heat generation and management through substrate or object engineering. For example, plasmonic metasurfaces, with the capability of programmable control position of the electromagnetic hotspots to dynamically shape the temperature gradient, are promising as the substrates or stick-on labels for objects to improve the manipulation versatility. Mechanically flexible optothermal substrates would provide an additional degree of freedom for 3D manipulation. In addition, the potential use of nonmetallic materials such as silicon[489] as heating sources is promising for the development of multifunctional integrated systems with the capabilities of analyte concentrating, capturing, sorting, and sensing.[339,341,490]

11.3. Manipulated Objects

Properties of target objects such as shape, size, and optothermal response also play an essential role in heat-mediated optical manipulation. For instance, in the same critical binary mixture, a Janus particle composed of a silica sphere and a Au cap was nudged through laser heating,[242] while a silica microsphere with randomly distributed absorbing inclusions underwent an in-plane rotation.[255] Heat-mediated optical manipulation has already been applied to control objects of variable sizes, shapes, and compositions that range from molecules in living cells[491] to artificial motors at a centimeter scale.[477] In the future, we expect to witness research on more diverse objects in heat-mediated optical manipulation with the goals of improving the fundamental understanding of the optothermo–matter coupling and multiphysics and of broadening the functions and applications of the manipulation techniques.[492]

11.4. Additional Fields

Synergistic integrations of optical heating with other fields, including electric field,[155] chemical field,[493,494] acoustic field,[495] and fluid flow,[496] have been demonstrated to improve the functionality of optical manipulation. For instance, Wu et al. exploited optical heating to accelerate the kinetics of a chemical reaction at the catalytic microswimmers for faster motion at a low concentration of chemical fuels.[497] Xie et al. developed optoacoustic tweezers exploiting optothermally generated and acoustically activated surface bubbles for the manipulation of synthetic particles and living cells.[498] Along this line, future development of heat-mediated optical manipulation exploiting additional fields could also benefit from tremendous progress in magnetics and bioenergetics.[253,499–501] For instance, a switchable magnetic field can be coupled into heat-mediated optical manipulation through optical heating of ferromagnetic particles to their Curie point to induce the change of their magnetic property.[61] However, it should be noted that multifield coupling will also pose additional challenges to the design and implementation of the manipulation techniques.

11.5. Enhanced Capabilities

One should further improve the throughput and accuracy of the heat-mediated optical manipulation for some of the applications.[502,503] Two approaches have proved to be effective in improving the manipulation throughput: (1) optical generation of large-area temperature gradient fields[228] and (2) generation of multiple laser beams for parallel manipulation of multiple objects using a spatial light modulator,[504] a digital micromirror device,[221] or an acousto-optical deflector.[10] These devices can independently control multiple laser beams with programs and software such as LabVIEW, MATLAB, and C++ for versatile manipulation.[505,506] By further integrating in situ optical imaging and spectroscopy into the optical manipulation systems, one can develop feedback-control algorithms to automatically control multiple objects with high precision.[507] With the capability of decoding complex data and enabling rapid and accurate analysis of optical spectra and images, machine learning is expected to play an increasing role in improving the robustness, automation, accuracy, and throughput of heat-mediated optical manipulation.[508,509]

Another exciting development will be exploiting the multimode heat-mediated optical manipulation to accomplish more complex tasks. For instance, as an initial demonstration along this direction, one can switch between optothermal rotation and nudging of a Janus particle in the same manipulation system by simply changing the wavelength of the incident light, enabling a microswimmer with well-controlled directional movement for targeted delivery.[235] In addition, controlling mutual interactions and collective behaviors of active objects driven by heat-mediated optical manipulation is promising for swarm intelligence.[10,248,510]

11.6. Applications

Heat-mediated optical manipulation is promising for a wide range of applications. We discuss some of the applications in five categories.

1. Therapeutics. Driven by NIR light without any need for chemical fuels, optothermal micro- and nanomotors are well-suited for targeted drug delivery.[192] By harnessing optical trapping and optothermal nudging, Maier et al. demonstrated the light-controlled guiding and injection of plasmonic Janus nanopens into living cells, revealing the potential of the nanopens to work as nanocarriers for the spatially controlled injection of genetic materials into cells for gene therapy.[188] Photothermal cancer therapy can be achieved through transporting optothermal motors to the target sites where abundant heat is released for protein degradation and cancer cell apoptosis upon an increase of the laser power.[497] To push forward the therapeutic applications, more research is needed to improve the drug-load capacity, penetration depth, and delivery accuracy of the optothermal motors.

2. Untethered micro/nanometric probes. Heat-mediated optical manipulation of objects can be highly sensitive to a change in the local environments surrounding the objects. For example, any change of temperature, viscosity, or biomolecules in the solvent surrounding an optothermal rotary motor can impact its Brownian

dynamics. Monitoring of the Brownian dynamics of the untethered motor provides an effective way to probe the local environmental parameters at the micro/nanoscale.[250,511] Such untethered small probes are promising for in vivo biomedical applications, including early disease diagnostics, and lab-on-a-chip devices.

3. Nanomanufacturing. Some of the heat-mediated optical manipulation techniques such as opto-thermoelectric assembly and bubble printing proved powerful for bottom-up nanomanufacturing. With the capability of arranging and bonding colloidal particles with variable sizes, shapes, and compositions as building blocks, optothermal assembly techniques have been employed to construct various architected nanomaterials with low optical power and simple experimental setup.[224,230,412] For its practical applications, the optothermal bottom-up nanomanufacturing techniques need to make significant advancements in 3D assembly and throughput.[344]

4. Fundamental study. Heat-mediated optical manipulation can be developed into a versatile platform for fundamental studies in various fields such as physics, chemistry, and biology. For instance, reconfigurable chiral meta-molecules made by optothermal assembly were employed to explore optical chirality at the nanoscale and to better understand the origin of chirality in atomic and molecular systems.[225] An investigation on optothermally active microparticles revealed the interparticle interactions based on the information about other particle positions. A study of the information flows among the active particles that formed emerging structures could provide an insight into the emergence of collective animal behaviors such as crowds of people, flocks of birds, schools of fishes, and swarms of bacteria.[10] With the further development and applications of heat-mediated optical manipulation, in combination with progress in the in situ characterization tools,[512] we expect many more reports on exciting scientific discoveries.

5. Force spectroscopy. Conventional optical tweezers have been widely exploited for the quantitative force measurement in investigating different biological processes, such as cell adhesion, segregation of DNA, and characterization of motor proteins.[8] The development of novel force spectroscopy methods based on heat-mediated optical tweezers is promising due to the lower operational power, simpler optical setup, and less photodamage compared with optical tweezers. However, the introduction of heating into the system would pose additional challenges to the measurement of temperature-sensitive properties, such as enzymatic activity and fluidic viscosity.[8] In addition, the calibration of force models can be difficult in the presence of thermal fluctuation, thermophoresis, and convective flows. A potential direction is to integrate machine learning and other novel algorithms to establish well-calibrated force-measurement models to account for the thermal forces in heat-mediated optical tweezing techniques. Such an advancement will be promising to improve the applicability and resolution[513] of light-based force spectroscopy, exploiting sub-10 nm objects[78] or light-absorbing particles.[224]

ACKNOWLEDGMENTS

Biographies

Zhihan Chen is a Ph.D. student in Yuebing Zheng's group at The University of Texas at Austin. He received his B.Sc. in Materials Science and Engineering at the Shanghai Jiao Tong University in 2018.

Jingang Li is a Ph.D. candidate in Yuebing Zheng's group at The University of Texas at Austin. He received his B.Sc. in Applied Physics from the Special Class for the Gifted Young at the University of Science and Technology of China in 2017.

Yuebing Zheng is an associate professor of Mechanical Engineering and Materials Science & Engineering at The University of Texas at Austin. He also holds the Temple Foundation Endowed Teaching Fellowship in Engineering #2. He received his Ph.D. in Engineering Science and Mechanics from The Pennsylvania State University in 2010. He was a postdoctoral researcher at The University of California, Los Angeles, from 2010 to 2013. His research group (http://zheng.engr.utexas.edu) engages in interdisciplinary research involving optics, materials science, chemistry, biology, engineering, and machine learning to innovate optical manipulation and measurement for the nanoscale, biological, and extraterrestrial world. He has been awarded the NIH Director's New Innovator Award, the NASA Early Career Faculty Award, the ONR Young Investigator Award, and the Beckman Young Investigator Award.

REFERENCES

(1). Pauzauskie PJ; Radenovic A; Trepagnier E; Shroff H; Yang P; Liphardt J Optical Trapping and Integration of Semiconductor Nanowire Assemblies in Water. Nat. Mater 2006, 5, 97–101. [PubMed: 16429143]

(2). Snezhko A; Aranson IS Magnetic Manipulation of Self-Assembled Colloidal Asters. Nat. Mater 2011, 10, 698–703. [PubMed: 21822260]

(3). Guo F; Li P; French JB; Mao Z; Zhao H; Li S; Nama N; Fick JR; Benkovic SJ; Huang TJ Controlling Cell–Cell Interactions Using Surface Acoustic Waves. Proc. Natl. Acad. Sci. U. S. A 2015, 112, 43–48. [PubMed: 25535339]

(4). Xie H; Sun M; Fan X; Lin Z; Chen W; Wang L; Dong L; He Q Reconfigurable Magnetic Microrobot Swarm: Multimode Transformation, Locomotion, and Manipulation. Sci. Robot 2019, 4, No. eeav8006.

(5). Liang Z; Teal D; Fan D Light Programmable Micro/Nanomotors with Optically Tunable in-Phase Electric Polarization. Nat. Commun 2019, 10, 5275. [PubMed: 31754176]

(6). Geiselmann M; Juan ML; Renger J; Say JM; Brown LJ; De Abajo FJG; Koppens F; Quidant R Three-Dimensional Optical Manipulation of a Single Electron Spin. Nat. Nanotechnol 2013, 8, 175–179. [PubMed: 23396312]

(7). Nakayama Y; Pauzauskie PJ; Radenovic A; Onorato RM; Saykally RJ; Liphardt J; Yang P Tunable Nanowire Nonlinear Optical Probe. Nature 2007, 447, 1098–1101. [PubMed: 17597756]

(8). Neuman KC; Nagy A Single-Molecule Force Spectroscopy: Optical Tweezers, Magnetic Tweezers and Atomic Force Microscopy. Nat. Methods 2008, 5, 491–505. [PubMed: 18511917]

(9). Chang DE; Regal C; Papp S; Wilson D; Ye J; Painter O; Kimble HJ; Zoller P Cavity Opto-Mechanics Using an Optically Levitated Nanosphere. Proc. Natl. Acad. Sci. U. S. A 2010, 107, 1005–1010. [PubMed: 20080573]

(10). Khadka U; Holubec V; Yang H; Cichos F Active Particles Bound by Information Flows. Nat. Commun 2018, 9, 3864. [PubMed: 30242284]

(11). Ashkin A Acceleration and Trapping of Particles by Radiation Pressure. Phys. Rev. Lett 1970, 24, 156–159.

(12). Maragò OM; Jones PH; Gucciardi PG; Volpe G; Ferrari AC Optical Trapping and Manipulation of Nanostructures. Nat. Nanotechnol 2013, 8, 807–819. [PubMed: 24202536]

(13). He Y; Tsutsui M; Scheicher RH; Bai F; Taniguchi M; Kawai T Thermophoretic Manipulation of DNA Translocation through Nanopores. ACS Nano 2013, 7, 538–546. [PubMed: 23199225]

(14). Jiang H-R; Wada H; Yoshinaga N; Sano M Manipulation of Colloids by a Nonequilibrium Depletion Force in a Temperature Gradient. Phys. Rev. Lett 2009, 102, 208301. [PubMed: 19519079]

(15). Gascoyne PR; Vykoukal J Particle Separation by Dielectrophoresis. Electrophoresis 2002, 23, 1973–1983. [PubMed: 12210248]

(16). Barik A; Zhang Y; Grassi R; Nadappuram BP; Edel JB; Low T; Koester SJ; Oh S-H Graphene-Edge Dielectrophoretic Tweezers for Trapping of Biomolecules. Nat. Commun 2017, 8, 1867. [PubMed: 29192277]

(17). Voldman J Electrical Forces for Microscale Cell Manipulation. Annu. Rev. Biomed. Eng 2006, 8, 425–454. [PubMed: 16834563]

(18). Rikken RS; Nolte RJ; Maan JC; van Hest JC; Wilson DA; Christianen PC Manipulation of Micro-and Nanostructure Motion with Magnetic Fields. Soft Matter 2014, 10, 1295–1308. [PubMed: 24652392]

(19). Ozcelik A; Rufo J; Guo F; Gu Y; Li P; Lata J; Huang TJ Acoustic Tweezers for the Life Sciences. Nat. Methods 2018, 15, 1021–1028. [PubMed: 30478321]

(20). Tian Z; Yang S; Huang P-H; Wang Z; Zhang P; Gu Y; Bachman H; Chen C; Wu M; Xie Y; et al. Wave Number–Spiral Acoustic Tweezers for Dynamic and Reconfigurable Manipulation of Particles and Cells. Sci. Adv 2019, 5, No. eaau6062. [PubMed: 31172021]

(21). Asplund MC; Johnson JA; Patterson JE The 2018 Nobel Prize in Physics: Optical Tweezers and Chirped Pulse Amplification. Anal. Bioanal. Chem 2019, 411, 5001–5005. [PubMed: 31143967]

(22). Juan ML; Righini M; Quidant R Plasmon Nano-Optical Tweezers. Nat. Photonics 2011, 5, 349–356.

(23). Xin H; Li Y; Liu YC; Zhang Y; Xiao YF; Li B Optical Forces: From Fundamental to Biological Applications. Adv. Mater 2020, 32, 2001994.

(24). Zemánek P; Volpe G; Jonáš A; Brzobohatý O Perspective on Light-Induced Transport of Particles: From Optical Forces to Phoretic Motion. Adv. Opt. Photonics 2019, 11, 577–678.

(25). Yang Y; Ren Y; Chen M; Arita Y; Rosales-Guzmán C Optical Trapping with Structured Light: A Review. Advanced Photonics 2021, 3, 034001.

(26). O'neil A; MacVicar I; Allen L; Padgett M Intrinsic and Extrinsic Nature of the Orbital Angular Momentum of a Light Beam. Phys. Rev. Lett 2002, 88, 053601. [PubMed: 11863722]

(27). Simpson N; Dholakia K; Allen L; Padgett M Mechanical Equivalence of Spin and Orbital Angular Momentum of Light: An Optical Spanner. Opt. Lett 1997, 22, 52–54. [PubMed: 18183100]

(28). Padgett M; Bowman R Tweezers with a Twist. Nat. Photonics 2011, 5, 343–348.

(29). Brzobohatý O; Karásek V; Šiler M; Chvátal L; Čižmár T; Zemánek P Experimental Demonstration of Optical Transport, Sorting and Self-Arrangement Using a 'Tractor Beam'. Nat. Photonics 2013, 7, 123–127.

(30). Chen J; Ng J; Lin Z; Chan C Optical Pulling Force. Nat. Photonics 2011, 5, 531–534.

(31). Novitsky A; Qiu C-W; Wang H Single Gradientless Light Beam Drags Particles as Tractor Beams. Phys. Rev. Lett 2011, 107, 203601. [PubMed: 22181730]

(32). Burns MM; Fournier J-M; Golovchenko JA Optical Binding. Phys. Rev. Lett 1989, 63, 1233. [PubMed: 10040510]

(33). Bowman RW; Padgett MJ Optical Trapping and Binding. Rep. Prog. Phys 2013, 76, 026401. [PubMed: 23302540]

(34). Yan Z; Gray SK; Scherer NF Potential Energy Surfaces and Reaction Pathways for Light-Mediated Self-Organization of Metal Nanoparticle Clusters. Nat. Commun 2014, 5, 3751. [PubMed: 24786197]

(35). Parker J; Peterson CW; Yifat Y; Rice SA; Yan Z; Gray SK; Scherer NF Optical Matter Machines: Angular Momentum Conversion by Collective Modes in Optically Bound Nanoparticle Arrays. Optica 2020, 7, 1341–1348.

(36). Figliozzi P; Sule N; Yan Z; Bao Y; Burov S; Gray SK; Rice SA; Vaikuntanathan S; Scherer NF Driven Optical Matter: Dynamics of Electrodynamically Coupled Nanoparticles in an Optical Ring Vortex. Phys. Rev. E: Stat. Phys., Plasmas, Fluids, Relat. Interdiscip. Top 2017, 95, 022604.

(37). Yan Z; Scherer NF Optical Vortex Induced Rotation of Silver Nanowires. J. Phys. Chem. Lett 2013, 4, 2937–2942.

(38). Rodrigo JA; Angulo M; Alieva T All-Optical Motion Control of Metal Nanoparticles Powered by Propulsion Forces Tailored in 3D Trajectories. Photonics Res. 2021, 9, 1–12.

(39). Arlt J; Garcés-Chávez V; Sibbett W; Dholakia K Optical Micromanipulation Using a Bessel Light Beam. Opt. Commun 2001, 197, 239–245.

(40). Lee S-H; Roichman Y; Grier DG Optical Solenoid Beams. Opt. Express 2010, 18, 6988–6993. [PubMed: 20389718]

(41). Rodrigo JA; Angulo M; Alieva T Tailored Optical Propulsion Forces for Controlled Transport of Resonant Gold Nanoparticles and Associated Thermal Convective Fluid Flows. Light: Sci. Appl 2020, 9, 181. [PubMed: 33133521]

(42). Nan F; Han F; Scherer NF; Yan Z Dissipative Self-Assembly of Anisotropic Nanoparticle Chains with Combined Electrodynamic and Electrostatic Interactions. Adv. Mater 2018, 30, 1803238.

(43). Coursault D; Sule N; Parker J; Bao Y; Scherer NF Dynamics of the Optically Directed Assembly and Disassembly of Gold Nanoplatelet Arrays. Nano Lett. 2018, 18, 3391–3399. [PubMed: 29717877]

(44). Yan Z; Sajjan M; Scherer NF Fabrication of a Material Assembly of Silver Nanoparticles Using the Phase Gradients of Optical Tweezers. Phys. Rev. Lett 2015, 114, 143901. [PubMed: 25910124]

(45). Neuman KC; Chadd EH; Liou GF; Bergman K; Block SM Characterization of Photodamage to Escherichia Coli in Optical Traps. Biophys. J 1999, 77, 2856–2863. [PubMed: 10545383]

(46). Babynina A; Fedoruk M; Kühler P; Meledin A; Döblinger M; Lohmüller T Bending Gold Nanorods with Light. Nano Lett. 2016, 16, 6485–6490. [PubMed: 27598653]

(47). Pilát Z; Jonáš A; Ježek J; Zemánek P Effects of Infrared Optical Trapping on Saccharomyces Cerevisiae in a Microfluidic System. Sensors 2017, 17, 2640. [PubMed: 29144389]

(48). Manaresi N; Romani A; Medoro G; Altomare L; Leonardi A; Tartagni M; Guerrieri R A CMOS Chip for Individual Cell Manipulation and Detection. IEEE J. Solid-State Circuits 2003, 38, 2297–2305.

(49). Wu MC Optoelectronic Tweezers. Nat. Photonics 2011, 5, 322–324.

(50). Chiou PY; Ohta AT; Wu MC Massively Parallel Manipulation of Single Cells and Microparticles Using Optical Images. Nature 2005, 436, 370–372. [PubMed: 16034413]

(51). Fan X; White IM Optofluidic Microsystems for Chemical and Biological Analysis. Nat. Photonics 2011, 5, 591–597. [PubMed: 22059090]

(52). Schmidt H; Hawkins AR The Photonic Integration of Non-Solid Media Using Optofluidics. Nat. Photonics 2011, 5, 598–604.

(53). Chen J; Loo JF-C; Wang D; Zhang Y; Kong S-K; Ho H-P Thermal Optofluidics: Principles and Applications. Adv. Opt. Mater 2020, 8, 1900829.

(54). Ludwig C Diffusion between Unequally Heated Regions of Initially Uniform Solutions. Sitzber. Akad. Wiss. Wien 1856, 20, 539.

(55). Jovanovic O Photophoresis—Light Induced Motion of Particles Suspended in Gas. J. Quant. Spectrosc. Radiat. Transfer 2009, 110, 889–901.

(56). Baffou G; Cichos F; Quidant R Applications and Challenges of Thermoplasmonics. Nat. Mater 2020, 19, 946–958. [PubMed: 32807918]

(57). Jauffred L; Samadi A; Klingberg H; Bendix PM; Oddershede LB Plasmonic Heating of Nanostructures. Chem. Rev 2019, 119, 8087–8130. [PubMed: 31125213]

(58). Kuppe C; Rusimova KR; Ohnoutek L; Slavov D; Valev VK Hot" in Plasmonics: Temperature-Related Concepts and Applications of Metal Nanostructures. Adv. Opt. Mater 2020, 8, 1901166.

(59). Baffou G; Quidant R; García de Abajo FJ Nanoscale Control of Optical Heating in Complex Plasmonic Systems. ACS Nano 2010, 4, 709–716. [PubMed: 20055439]

(60). Li J; Lin L; Inoue Y; Zheng Y Opto-Thermophoretic Tweezers and Assembly. J. Micro Nano-Manuf 2018, 6, 040801.

(61). Lin L; Hill EH; Peng X; Zheng Y Optothermal Manipulations of Colloidal Particles and Living Cells. Acc. Chem. Res 2018, 51, 1465–1474. [PubMed: 29799720]

(62). Liu Y; Lin L; Bangalore Rajeeva B; Jarrett JW; Li X; Peng X; Kollipara P; Yao K; Akinwande D; Dunn AK; et al. Nanoradiator-Mediated Deterministic Opto-Thermoelectric Manipulation. ACS Nano 2018, 12, 10383–10392. [PubMed: 30226980]

(63). Qian X; Zhao Y; Alsaid Y; Wang X; Hua M; Galy T; Gopalakrishna H; Yang Y; Cui J; Liu N; et al. Artificial Phototropism for Omnidirectional Tracking and Harvesting of Light. Nat. Nanotechnol 2019, 14, 1048–1055. [PubMed: 31686005]

(64). Zhang X; Pint CL; Lee MH; Schubert BE; Jamshidi A; Takei K; Ko H; Gillies A; Bardhan R; Urban JJ; et al. Optically-and Thermally-Responsive Programmable Materials Based on Carbon Nanotube-Hydrogel Polymer Composites. Nano Lett. 2011, 11, 3239–3244. [PubMed: 21736337]

(65). Jiang W; Niu D; Liu H; Wang C; Zhao T; Yin L; Shi Y; Chen B; Ding Y; Lu B Photoresponsive Soft-Robotic Platform: Biomimetic Fabrication and Remote Actuation. Adv. Funct. Mater 2014, 24, 7598–7604.

(66). Tian H; Wang Z; Chen Y; Shao J; Gao T; Cai S Polydopamine-Coated Main-Chain Liquid Crystal Elastomer as Optically Driven Artificial Muscle. ACS Appl. Mater. Interfaces 2018, 10, 8307–8316. [PubMed: 29446620]

(67). Camacho-Lopez M; Finkelmann H; Palffy-Muhoray P; Shelley M Fast Liquid-Crystal Elastomer Swims into the Dark. Nat. Mater 2004, 3, 307–310. [PubMed: 15107840]

(68). Flores-Flores E; Torres-Hurtado S; Páez R; Ruiz U; Beltrán-Pérez G; Neale S; Ramirez-San-Juan J; Ramos-García R Trapping and Manipulation of Microparticles Using Laser-Induced Convection Currents and Photophoresis. Biomed. Opt. Express 2015, 6, 4079–4087. [PubMed: 26504655]

(69). Guo Y; Zhao X; Zhao F; Jiao Z; Zhou X; Yu G Tailoring Surface Wetting States for Ultrafast Solar-Driven Water Evaporation. Energy Environ. Sci 2020, 13, 2087–2095.

(70). Ilic O; Kaminer I; Lahini Y; Buljan H; Soljacic M Exploiting Optical Asymmetry for Controlled Guiding of Particles with Light. ACS Photonics 2016, 3, 197–202.

(71). Kavokine N; Zou S; Liu R; Nigués A; Zou B; Bocquet L Ultrafast Photomechanical Transduction through Thermophoretic Implosion. Nat. Commun 2020, 11, 50. [PubMed: 31898691]

(72). Liu Z; Lei J; Zhang Y; Tang X; Zhang Y; Zhao E; Yang J; Yuan L Light-Induced Thermal Convection for Size-Based Microparticle Sorting. J. Opt. Soc. Am. B 2016, 33, 1881–1887.

(73). Govorov AO; Zhang W; Skeini T; Richardson H; Lee J; Kotov NA Gold Nanoparticle Ensembles as Heaters and Actuators: Melting and Collective Plasmon Resonances. Nanoscale Res. Lett 2006, 1, 84.

(74). Baffou G; Quidant R; Girard C Heat Generation in Plasmonic Nanostructures: Influence of Morphology. Appl. Phys. Lett 2009, 94, 153109.

(75). Baffou G; Quidant R Thermo-Plasmonics: Using Metallic Nanostructures as Nano-Sources of Heat. LaserPhotonics Rev. 2013, 7, 171–187.

(76). Ghosh S; Biswas A; Roy B; Banerjee A Self-Assembly and Complex Manipulation of Colloidal Mesoscopic Particles by Active Thermocapillary Stress. Soft Matter 2019, 15, 4703–4713. [PubMed: 31119243]

(77). Kang Z; Chen J; Wu S-Y; Chen K; Kong S-K; Yong K-T; Ho H-P Trapping and Assembling of Particles and Live Cells on Large-Scale Random Gold Nano-Island Substrates. Sci. Rep 2015, 5, 9978. [PubMed: 25928045]

(78). Hong C; Yang S; Ndukaife JC Stand-Off Trapping and Manipulation of Sub-10 nm Objects and Biomolecules Using Opto-Thermo-Electrohydrodynamic Tweezers. Nat. Nanotechnol 2020, 15, 908–913. [PubMed: 32868919]

(79). Shoji T; Shibata M; Kitamura N; Nagasawa F; Takase M; Murakoshi K; Nobuhiro A; Mizumoto Y; Ishihara H; Tsuboi Y Reversible Photoinduced Formation and Manipulation of a Two-Dimensional Closely Packed Assembly of Polystyrene Nanospheres on a Metallic Nanostructure. J. Phys. Chem. C 2013, 117, 2500–2506.

(80). Wang Y; Li M; Chang J-K; Aurelio D; Li W; Kim BJ; Kim JH; Liscidini M; Rogers JA; Omenetto FG Light-Activated Shape Morphing and Light-Tracking Materials Using Biopolymer-Based Programmable Photonic Nanostructures. Nat. Commun 2021, 12, 1651. [PubMed: 33712607]

(81). Seletskiy DV; Epstein R; Sheik-Bahae M Laser Cooling in Solids: Advances and Prospects. Rep. Prog. Phys 2016, 79, 096401. [PubMed: 27484295]

(82). Sheik-Bahae M; Epstein RI Optical Refrigeration. Nat. Photonics 2007, 1, 693–699.

(83). Rayner A; Heckenberg NR; Rubinsztein-Dunlop H Condensed-Phase Optical Refrigeration. J. Opt. Soc. Am. B 2003, 20 (5), 1037–1053.

(84). Seletskiy DV; Epstein R; Sheik-Bahae M Laser Cooling in Solids: Advances and Prospects. Rep. Prog. Phys 2016, 79, 096401. [PubMed: 27484295]

(85). Seletskiy DV; Hehlen MP; Epstein RI; Sheik-Bahae M Cryogenic Optical Refrigeration. Adv. Opt. Photonics 2012, 4, 78–107.

(86). Pringsheim P Zwei Bemerkungen Über Den Unterschied Von Lumineszenz- Und Temperaturstrahlung. Eur. Phys. J. A 1929, 57, 739–746.

(87). Epstein RI; Buchwald MI; Edwards BC; Gosnell TR; Mungan CE Observation of Laser-Induced Fluorescent Cooling of a Solid. Nature 1995, 377, 500–503.

(88). Hehlen MP; Epstein RI; Inoue H Model of Laser Cooling in The Yb^{3+}-Doped Fluorozirconate Glass Zblan. Phys. Rev. B: Condens. Matter Mater. Phys 2007, 75, 144302.

(89). Seletskiy DV; Melgaard SD; Bigotta S; Di Lieto A; Tonelli M; Sheik-Bahae M Laser Cooling of Solids to Cryogenic Temperatures. Nat. Photonics 2010, 4, 161–164.

(90). Seletskiy DV; Melgaard SD; Epstein RI; Di Lieto A; Tonelli M; Sheik-Bahae M Local Laser Cooling of Yb:YLF to 110 K. Opt. Express 2011, 19, 18229–18236. [PubMed: 21935189]

(91). Melgaard SD; Seletskiy DV; Di Lieto A; Tonelli M; Sheik-Bahae M Optical Refrigeration to 119 K, Below National Institute of Standards and Technology Cryogenic Temperature. Opt. Lett 2013, 38, 1588–1590. [PubMed: 23632561]

(92). Rahman ATMA; Barker PF Laser Refrigeration, Alignment and Rotation of Levitated Yb^{3+}:YLF Nanocrystals. Nat. Photonics 2017, 11, 634–638.

(93). Melgaard SD; Albrecht AR; Hehlen MP; Sheik-Bahae M Solid-State Optical Refrigeration to Sub-100 K Regime. Sci. Rep 2016, 6, 20380. [PubMed: 26847703]

(94). Zhang J; Li D; Chen R; Xiong Q Laser Cooling of a Semiconductor by 40 K. Nature 2013, 493, 504–508. [PubMed: 23344360]

(95). Ha S-T; Shen C; Zhang J; Xiong Q Laser Cooling of Organic–Inorganic Lead Halide Perovskites. Nat. Photonics 2016, 10, 115–121.

(96). Roder PB; Smith BE; Zhou X; Crane MJ; Pauzauskie PJ Laser Refrigeration of Hydrothermal Nanocrystals in Physiological Media. Proc. Natl. Acad. Sci. U. S. A 2015, 112, 15024–15029. [PubMed: 26589813]

(97). Zhou X; Smith BE; Roder PB; Pauzauskie PJ Laser Refrigeration of Ytterbium-Doped Sodium–Yttrium–Fluoride Nanowires. Adv. Mater 2016, 28, 8658–8662. [PubMed: 27514650]

(98). Li J; Chen Z; Liu Y; Kollipara PS; Feng Y; Zhang Z; Zheng Y Opto-Refrigerative Tweezers. Sci. Adv 2021, 7, No. eabh1101. [PubMed: 34172454]

(99). Piazza R; Guarino A Soret Effect in Interacting Micellar Solutions. Phys. Rev. Lett 2002, 88, 208302. [PubMed: 12005610]

(100). Iacopini S; Piazza R Thermophoresis in Protein Solutions. Europhys. Lett 2003, 63, 247–253.

(101). Parola A; Piazza R Particle Thermophoresis in Liquids. Eur. Phys. J. E: Soft Matter Biol. Phys 2004, 15, 255–263.

(102). Piazza R; Parola A Thermophoresis in Colloidal Suspensions. J. Phys.: Condens. Matter 2008, 20, 153102.

(103). Anderson JL Colloid Transport by Interfacial Forces. Annu. Rev. Fluid Mech 1989, 21, 61–99.

(104). Piazza R Thermophoresis: Moving Particles with Thermal Gradients. Soft Matter 2008, 4, 1740–1744.

(105). Dhont JK Thermodiffusion of Interacting Colloids. I. A Statistical Thermodynamics Approach. J. Chem. Phys 2004, 120, 1632–1641. [PubMed: 15268291]

(106). Dhont JK Thermodiffusion of Interacting Colloids. Ii. A Microscopic Approach. J. Chem. Phys 2004, 120, 1642–1653. [PubMed: 15268292]

(107). Eslahian KA; Majee A; Maskos M; Würger A Specific Salt Effects on Thermophoresis of Charged Colloids. Soft Matter 2014, 10, 1931–1936. [PubMed: 24652409]

(108). Duhr S; Braun D Thermophoretic Depletion Follows Boltzmann Distribution. Phys. Rev. Lett 2006, 96, 168301. [PubMed: 16712279]

(109). Würger A Hydrodynamic Boundary Effects on Thermophoresis of Confined Colloids. Phys. Rev. Lett 2016, 116, 138302. [PubMed: 27082005]

(110). Helden L; Eichhorn R; Bechinger C Direct Measurement of Thermophoretic Forces. Soft Matter 2015, 11, 2379–2386. [PubMed: 25673057]

(111). Iacopini S; Rusconi R; Piazza R The "Macromolecular Tourist": Universal Temperature Dependence of Thermal Diffusion in Aqueous Colloidal Suspensions. Eur. Phys. J. E: Soft Matter Biol. Phys 2006, 19, 59–67.

(112). Putnam SA; Cahill DG Transport of Nanoscale Latex Spheres in a Temperature Gradient. Langmuir 2005, 21, 5317–5323. [PubMed: 15924455]

(113). Putnam SA; Cahill DG; Wong GCL Temperature Dependence of Thermodiffusion in Aqueous Suspensions of Charged Nanoparticles. Langmuir 2007, 23, 9221–9228. [PubMed: 17655335]

(114). Braibanti M; Vigolo D; Piazza R Does Thermophoretic Mobility Depend on Particle Size? Phys. Rev. Lett 2008, 100, 108303. [PubMed: 18352238]

(115). Duhr S; Braun D Why Molecules Move Along a Temperature Gradient. Proc. Natl. Acad. Sci. U. S. A 2006, 103, 19678–19682. [PubMed: 17164337]

(116). Ning H; Dhont JK; Wiegand S Thermal-Diffusive Behavior of a Dilute Solution of Charged Colloids. Langmuir 2008, 24, 2426–2432. [PubMed: 18254649]

(117). Würger A Transport in Charged Colloids Driven by Thermoelectricity. Phys. Rev. Lett 2008, 101, 108302. [PubMed: 18851262]

(118). Würger A Thermal Non-Equilibrium Transport in Colloids. Rep. Prog. Phys 2010, 73, 126601.

(119). Guthrie G Jr; Wilson JN; Schomaker V Theory of the Thermal Diffusion of Electrolytes in a Clusius Column. J. Chem. Phys 1949, 17, 310–313.

(120). Reichl M; Herzog M; Götz A; Braun D Why Charged Molecules Move across a Temperature Gradient: The Role of Electric Fields. Phys. Rev. Lett 2014, 112, 198101. [PubMed: 24877967]

(121). Majee A; Würger A Thermocharge of a Hot Spot in an Electrolyte Solution. Soft Matter 2013, 9, 2145–2153.

(122). Ruckenstein E Can Phoretic Motions Be Treated as Interfacial Tension Gradient Driven Phenomena? J. Colloid Interface Sci 1981, 83, 77–81.

(123). Bregulla AP; Würger A; Günther K; Mertig M; Cichos F Thermo-Osmotic Flow in Thin Films. Phys. Rev. Lett 2016, 116, 188303. [PubMed: 27203347]

(124). Das PK Effect of Thermodiffusion on Ph-Regulated Surface Charge Properties of Nanoparticle. Electrophoresis 2016, 37, 347–355. [PubMed: 26530465]

(125). Bresme F; Lervik A; Bedeaux D; Kjelstrup S Water Polarization under Thermal Gradients. Phys. Rev. Lett 2008, 101, 020602. [PubMed: 18764168]

(126). Di Lecce S; Bresme F Thermal Polarization of Water Influences the Thermoelectric Response of Aqueous Solutions. J. Phys. Chem. B 2018, 122, 1662–1668. [PubMed: 29293343]

(127). Armstrong J; Lervik A; Bresme F Enhancement of the Thermal Polarization of Water Via Heat Flux and Dipole Moment Dynamic Correlations. J. Phys. Chem. B 2013, 117, 14817–14826. [PubMed: 24168463]

(128). Würger A Temperature Dependence of the Soret Motion in Colloids. Langmuir 2009, 25, 6696–6701. [PubMed: 19320474]

(129). Sehnem A; Figueiredo Neto A; Aquino R; Campos A; Tourinho F; Depeyrot J Temperature Dependence of the Soret Coefficient of Ionic Colloids. Phys. Rev. E 2015, 92, 042311.

(130). Morthomas J; Würger A Thermoelectric Effect on Charged Colloids in the Hückel Limit. Eur. Phys. J. E: Soft Matter Biol. Phys 2008, 27, 425–434.

(131). Majee A; Würger A Collective Thermoelectrophoresis of Charged Colloids. Phys. Rev. E 2011, 83, 061403.

(132). Lüsebrink D; Ripoll M Collective Thermodiffusion of Colloidal Suspensions. J. Chem. Phys 2012, 137, 194904. [PubMed: 23181332]

(133). Chen Z; Kollipara PS; Ding H; Pughazhendi A; Zheng Y Liquid Optothermoelectrics: Fundamentals and Applications. Langmuir 2021, 37, 1315–1336. [PubMed: 33410698]

(134). Derjaguin B; Sidorenkov G; Zubashchenkov E; Kiseleva E Kinetic Phenomena in Boundary Films of Liquids. Kolloidn. Zh 1947, 9, 335–347.

(135). Prieve D; Anderson J; Ebel J; Lowell M Motion of a Particle Generated by Chemical Gradients. Part 2. Electrolytes. J. Fluid Mech 1984, 148, 247–269.

(136). Ebel J; Anderson JL; Prieve D Diffusiophoresis of Latex Particles in Electrolyte Gradients. Langmuir 1988, 4, 396–406.

(137). Anderson J; Lowell M; Prieve D Motion of a Particle Generated by Chemical Gradients. Part 1. Non-Electrolytes. J. Fluid Mech 1982, 117, 107–121.

(138). Staffeld PO; Quinn JA Diffusion-Induced Banding of Colloid Particles Via Diffusiophoresis: 1. Electrolytes. J. Colloid Interface Sci 1989, 130, 69–87.

(139). Sharifi-Mood N; Koplik J; Maldarelli C Diffusiophoretic Self-Propulsion of Colloids Driven by a Surface Reaction: The SubMicron Particle Regime for Exponential and Van Der Waals Interactions. Phys. Fluids 2013, 25, 012001.

(140). Sharifi-Mood N; Koplik J; Maldarelli C Molecular Dynamics Simulation of the Motion of Colloidal Nanoparticles in a Solute Concentration Gradient and a Comparison to the Continuum Limit. Phys. Rev. Lett 2013, 111, 184501. [PubMed: 24237522]

(141). Velegol D; Garg A; Guha R; Kar A; Kumar M Origins of Concentration Gradients for Diffusiophoresis. Soft Matter 2016, 12, 4686–4703. [PubMed: 27174044]

(142). Mao Y; Cates M; Lekkerkerker H Depletion Force in Colloidal Systems. Phys. A 1995, 222, 10–24.

(143). Edwards TD; Bevan MA Depletion-Mediated Potentials and Phase Behavior for Micelles, Macromolecules, Nanoparticles, and Hydrogel Particles. Langmuir 2012, 28, 13816–13823. [PubMed: 22950666]

(144). Deng H-D; Li G-C; Liu H-Y; Dai Q-F; Wu L-J; Lan S; Gopal AV; Trofimov VA; Lysak TM Assembling of Three-Dimensional Crystals by Optical Depletion Force Induced by a Single Focused Laser Beam. Opt. Express 2012, 20, 9616–9623. [PubMed: 22535053]

(145). Lin L; Peng X; Zheng Y Reconfigurable Opto-Thermoelectric Printing of Colloidal Particles. Chem. Commun 2017, 53, 7357–7360.

(146). Lin L; Kollipara PS; Kotnala A; Jiang T; Liu Y; Peng X; Korgel BA; Zheng Y Opto-Thermoelectric Pulling of Light-Absorbing Particles. Light: Sci. Appl 2020, 9, 34. [PubMed: 32194948]

(147). Gong Z; Pan Y-L; Videen G; Wang C Optical Trapping and Manipulation of Single Particles in Air: Principles, Technical Details, and Applications. J. Quant. Spectrosc. Radiat. Transfer 2018, 214, 94–119.

(148). Knudsen M Radiometer Pressure and Coefficient of Accommodation; AF Høst & Søn: 1930; Vol. 11, pp 1–75.

(149). Shvedov VG; Rode AV; Izdebskaya YV; Desyatnikov AS; Krolikowski W; Kivshar YS Giant Optical Manipulation. Phys. Rev. Lett 2010, 105, 118103. [PubMed: 20867612]

(150). Donner JS; Baffou G; McCloskey D; Quidant R Plasmon-Assisted Optofluidics. ACS Nano 2011, 5, 5457–5462. [PubMed: 21657203]

(151). Roxworthy BJ; Bhuiya AM; Vanka SP; Toussaint KC Understanding and Controlling Plasmon-Induced Convection. Nat. Commun 2014, 5, 3173. [PubMed: 24445431]

(152). Polezhaev V; Soboleva E Rayleigh-Bénard Convection in a near-Critical Fluid in the Neighborhood of the Stability Threshold. Fluid Dyn. 2005, 40 (2), 209–220.

(153). Scriven L; Sternling C The Marangoni Effects. Nature 1960, 187, 186–188.

(154). Quispe JE; Inga JC; Muñoz EM; Régnier S; Vela E In Single Particle Manipulation/Sorting through the Transient Response of Thermocapillary Convection Flows. 2016 International Conference on Manipulation, Automation and Robotics at Small Scales (MARSS), IEEE 2016, 1–6.

(155). Ndukaife JC; Kildishev AV; Nnanna AGA; Shalaev VM; Wereley ST; Boltasseva A Long-Range and Rapid Transport of Individual Nano-Objects by a Hybrid Electrothermoplasmonic Nanotweezer. Nat. Nanotechnol 2016, 11, 53–59. [PubMed: 26524398]

(156). Takashima Y; Hatanaka S; Otsubo M; Nakahata M; Kakuta T; Hashidzume A; Yamaguchi H; Harada A Expansion–Contraction of Photoresponsive Artificial Muscle Regulated by Host–Guest Interactions. Nat. Commun 2012, 3, 1270. [PubMed: 23232400]

(157). Koshima H; Nakaya H; Uchimoto H; Ojima N Photomechanical Motion of Furylfulgide Crystals. Chem. Lett 2012, 41, 107–109.

(158). Terao F; Morimoto M; Irie M Light-Driven Molecular-Crystal Actuators: Rapid and Reversible Bending of Rodlike Mixed Crystals of Diarylethene Derivatives. Angew. Chem., Int. Ed 2012, 51, 901–904.

(159). Gelebart AH; Jan Mulder D; Varga M; Konya A; Vantomme G; Meijer E; Selinger RL; Broer DJ Making Waves in a Photoactive Polymer Film. Nature 2017, 546, 632–636. [PubMed: 28658225]

(160). Wie JJ; Shankar MR; White TJ Photomotility of Polymers. Nat. Commun 2016, 7, 13260. [PubMed: 27830707]

(161). White TJ; Tabiryan NV; Serak SV; Hrozhyk UA; Tondiglia VP; Koerner H; Vaia RA; Bunning TJ A High Frequency Photodriven Polymer Oscillator. Soft Matter 2008, 4, 1796–1798.

(162). Huang C; Lv J.-a.; Tian X; Wang Y; Yu Y; Liu J Miniaturized Swimming Soft Robot with Complex Movement Actuated and Controlled by Remote Light Signals. Sci. Rep 2015, 5, 17414. [PubMed: 26633758]

(163). Wang H; Chen P; Wu Z; Zhao J; Sun J; Lu R Bending, Curling, Rolling, and Salient Behavior of Molecular Crystals Driven by [2 + 2] Cycloaddition of a Styrylbenzoxazole Derivative. Angew. Chem 2017, 129, 9591–9595.

(164). Yu Q; Yang X; Chen Y; Yu K; Gao J; Liu Z; Cheng P; Zhang Z; Aguila B; Ma S Fabrication of Light-Triggered Soft Artificial Muscles Via a Mixed-Matrix Membrane Strategy. Angew. Chem., Int. Ed 2018, 57, 10192–10196.

(165). Pilz da Cunha M; Debije MG; Schenning AP Bioinspired Light-Driven Soft Robots Based on Liquid Crystal Polymers. Chem. Soc. Rev 2020, 49, 6568–6578. [PubMed: 32779649]

(166). Han B; Zhang YL; Chen QD; Sun HB Carbon-Based Photothermal Actuators. Adv. Funct. Mater 2018, 28, 1802235.

(167). Li J; Zhou X; Liu Z Recent Advances in Photoactuators and Their Applications in Intelligent Bionic Movements. Adv. Opt. Mater 2020, 8, 2000886.

(168). Linghu S; Gu Z; Lu J; Fang W; Yang Z; Yu H; Li Z; Zhu R; Peng J; Zhan Q; et al. Plasmon-Driven Nanowire Actuators for on-Chip Manipulation. Nat. Commun 2021, 12, 385. [PubMed: 33452266]

(169). Ebbens SJ; Howse JR In Pursuit of Propulsion at the Nanoscale. Soft Matter 2010, 6, 726–738.

(170). Tu Y; Peng F; Wilson DA Motion Manipulation of Micro- and Nanomotors. Adv. Mater 2017, 29, 1701970.

(171). Xu T; Gao W; Xu L-P; Zhang X; Wang S Fuel-Free Synthetic Micro-/Nanomachines. Adv. Mater 2017, 29, 1603250.

(172). Wang J; Xiong Z; Zheng J; Zhan X; Tang J Light-Driven Micro/Nanomotor for Promising Biomedical Tools: Principle, Challenge, and Prospect. Acc. Chem. Res 2018, 51, 1957–1965. [PubMed: 30179455]

(173). Xu L; Mou F; Gong H; Luo M; Guan J Light-Driven Micro/Nanomotors: From Fundamentals to Applications. Chem. Soc. Rev 2017, 46, 6905–6926. [PubMed: 28949354]

(174). Sipova-Jungova H; Andren D; Jones S; Kall M Nanoscale Inorganic Motors Driven by Light: Principles, Realizations, and Opportunities. Chem. Rev 2020, 120, 269–287. [PubMed: 31869216]

(175). Wang J; Xiong Z; Tang J The Encoding of Light-Driven Micro/Nanorobots: From Single to Swarming Systems. Adv. Intell. Syst 2021, 3, 2000170.

(176). Chen H; Zhao Q; Du X Light-Powered Micro/Nanomotors. Micromachines 2018, 9, 41. [PubMed: 30393317]

(177). Villa K; Pumera M Fuel-Free Light-Driven Micro/Nanomachines: Artificial Active Matter Mimicking Nature. Chem. Soc. Rev 2019, 48, 4966–4978. [PubMed: 31368460]

(178). Jiang H-R; Yoshinaga N; Sano M Active Motion of a Janus Particle by Self-Thermophoresis in a Defocused Laser Beam. Phys. Rev. Lett 2010, 105, 268302. [PubMed: 21231718]

(179). Bregulla AP; Yang H; Cichos F Stochastic Localization of Microswimmers by Photon Nudging. ACS Nano 2014, 8, 6542–6550. [PubMed: 24861455]

(180). Wu Z; Si T; Gao W; Lin X; Wang J; He Q Superfast near-Infrared Light-Driven Polymer Multilayer Rockets. Small 2016, 12, 577–582. [PubMed: 26690728]

(181). Lozano C; ten Hagen B; Löwen H; Bechinger C Phototaxis of Synthetic Microswimmers in Optical Landscapes. Nat. Commun 2016, 7, 12828. [PubMed: 27687580]

(182). Yu N; Lou X; Chen K; Yang M Phototaxis of Active Colloids by Self-Thermophoresis. Soft Matter 2019, 15, 408–414. [PubMed: 30565640]

(183). Qian B; Montiel D; Bregulla A; Cichos F; Yang H Harnessing Thermal Fluctuations for Purposeful Activities: The Manipulation of Single Micro-Swimmers by Adaptive Photon Nudging. Chem. Sci 2013, 4, 1420–1429.

(184). Xuan M; Wu Z; Shao J; Dai L; Si T; He Q Near Infrared Light-Powered Janus Mesoporous Silica Nanoparticle Motors. J. Am. Chem. Soc 2016, 138, 6492–6497. [PubMed: 27152728]

(185). Wu Y; Si T; Shao J; Wu Z; He Q Near-Infrared Light-Driven Janus Capsule Motors: Fabrication, Propulsion, and Simulation. Nano Res. 2016, 9, 3747–3756.

(186). Herms A; Günther K; Sperling E; Heerwig A; Kick A; Cichos F; Mertig M Concept, Synthesis, and Structural Characterization of DNA Origami Based Self-Thermophoretic Nanoswimmers. Phys. Status Solidi A 2017, 214, 1600957.

(187). Heerwig A; Schubel M; Schirmer C; Herms A; Cichos F; Mertig M DNA Origami Ring Structures as Construction Element of Self-Thermophoretic Swimmers. Phys. Status Solidi A 2019, 216, 1800775.

(188). Maier CM; Huergo MA; Milosevic S; Pernpeintner C; Li M; Singh DP; Walker D; Fischer P; Feldmann J; Lohmüller T Optical and Thermophoretic Control of Janus Nanopen Injection into Living Cells. Nano Lett. 2018, 18, 7935–7941. [PubMed: 30468387]

(189). Volpe G; Gigan S; Volpe G Simulation of the Active Brownian Motion of a Microswimmer. Am. J. Phys 2014, 82, 659–664.

(190). Heidari M; Bregulla A; Landin SM; Cichos F; von Klitzing R Self-Propulsion of Janus Particles near a Brush-Functionalized Substrate. Langmuir 2020, 36, 7775–7780. [PubMed: 32544339]

(191). Ly A; Majee A; Würger A Nanoscale Seebeck Effect at Hot Metal Nanostructures. New J. Phys 2018, 20, 025001.

(192). Xuan M; Shao J; Gao C; Wang W; Dai L; He Q Self-Propelled Nanomotors for Thermomechanically Percolating Cell Membranes. Angew. Chem., Int. Ed 2018, 57, 12463–12467.

(193). Selmke M; Khadka U; Bregulla AP; Cichos F; Yang H Theory for Controlling Individual Self-Propelled Micro-Swimmers by Photon Nudging I: Directed Transport. Phys. Chem. Chem. Phys 2018, 20, 10502–10520. [PubMed: 29560993]

(194). Selmke M; Khadka U; Bregulla AP; Cichos F; Yang H Theory for Controlling Individual Self-Propelled Micro-Swimmers by Photon Nudging II: Confinement. Phys. Chem. Chem. Phys 2018, 20, 10521–10532. [PubMed: 29619451]

(195). Golestanian R Collective Behavior of Thermally Active Colloids. Phys. Rev. Lett 2012, 108, 038303. [PubMed: 22400792]

(196). Bickel T; Zecua G; Würger A Polarization of Active Janus Particles. Phys. Rev. E 2014, 89, 050303.

(197). Cohen JA; Golestanian R Emergent Cometlike Swarming of Optically Driven Thermally Active Colloids. Phys. Rev. Lett 2014, 112, 068302. [PubMed: 24580713]

(198). Rao Q; Si T; Wu Z; Xuan M; He Q A Light-Activated Explosive Micropropeller. Sci. Rep 2017, 7, 4621. [PubMed: 28676666]

(199). Kim JT; Choudhury U; Jeong HH; Fischer P Nanodiamonds That Swim. Adv. Mater 2017, 29, 1701024.

(200). Fränzl M; Muiños-Landin S; Holubec V; Cichos F Fully Steerable Symmetric Thermoplasmonic Microswimmers. ACS Nano 2021, 15, 3434–3440. [PubMed: 33556235]

(201). Muiños-Landin S; Fischer A; Holubec V; Cichos F Reinforcement Learning with Artificial Microswimmers. Sci. Robot 2021, 6, No. abd9285.

(202). Cichos F; Gustavsson K; Mehlig B; Volpe G Machine Learning for Active Matter. Nat. Mach. Intell 2020, 2, 94–103.

(203). Li D; Liu C; Yang Y; Wang L; Shen Y Micro-Rocket Robot with All-Optic Actuating and Tracking in Blood. Light Sci. Appl 2020, 9, 84. [PubMed: 32411369]

(204). Cui T; Wu S; Sun Y; Ren J; Qu X Self-Propelled Active Photothermal Nanoswimmer for Deep-Layered Elimination of Biofilm in Vivo. Nano Lett. 2020, 20, 7350–7358. [PubMed: 32856923]

(205). Yang PP; Zhai YG; Qi GB; Lin YX; Luo Q; Yang Y; Xu AP; Yang C; Li YS; Wang L; et al. NIR Light Propulsive Janus-Like Nanohybrids for Enhanced Photothermal Tumor Therapy. Small 2016, 12, 5423–5430. [PubMed: 27511451]

(206). Jiao X; Wang Z; Xiu J; Dai W; Zhao L; Xu T; Du X; Wen Y; Zhang X NIR Powered Janus Nanocarrier for Deep Tumor Penetration. Appl. Mater. Today 2020, 18, 100504.

(207). He W; Frueh J; Hu N; Liu L; Gai M; He Q Guidable Thermophoretic Janus Micromotors Containing Gold Nanocolorifiers for Infrared Laser Assisted Tissue Welding. Adv. Sci 2016, 3, 1600206.

(208). Braun M; Cichos F Optically Controlled Thermophoretic Trapping of Single Nano-Objects. ACS Nano 2013, 7, 11200–11208. [PubMed: 24215133]

(209). Braun M; Wurger A; Cichos F Trapping of Single Nano-Objects in Dynamic Temperature Fields. Phys. Chem. Chem. Phys 2014, 16, 15207–15213. [PubMed: 24939651]

(210). Braun M; Bregulla AP; Günther K; Mertig M; Cichos F Single Molecules Trapped by Dynamic Inhomogeneous Temperature Fields. Nano Lett. 2015, 15, 5499–5505. [PubMed: 26161841]

(211). Bespalova MI; Mahanta S; Krishnan M Single-Molecule Trapping and Measurement in Solution. Curr. Opin. Chem. Biol 2019, 51, 113–121. [PubMed: 31254807]

(212). Fränzl M; Thalheim T; Adler J; Huster D; Posseckardt J; Mertig M; Cichos F Thermophoretic Trap for Single Amyloid Fibril and Protein Aggregation Studies. Nat. Methods 2019, 16, 611–614. [PubMed: 31235884]

(213). Nedev S; Carretero-Palacios S; Kühler P; Lohmüller T; Urban AS; Anderson LJ; Feldmann J An Optically Controlled Microscale Elevator Using Plasmonic Janus Particles. ACS Photonics 2015, 2, 491–496. [PubMed: 25950013]

(214). Lin L; Peng X; Mao Z; Wei X; Xie C; Zheng Y Interfacial-Entropy-Driven Thermophoretic Tweezers. Lab Chip 2017, 17, 3061–3070. [PubMed: 28805878]

(215). Sharma V; Paul D; Chaubey SK; Tiwari S; Kumar GP Large-Scale Optothermal Assembly of Colloids Mediated by a Gold Microplate. J. Phys.: Condens. Matter 2020, 32, 324002. [PubMed: 32235046]

(216). Chen J; Cong H; Loo F-C; Kang Z; Tang M; Zhang H; Wu S-Y; Kong S-K; Ho H-P Thermal Gradient Induced Tweezers for the Manipulation of Particles and Cells. Sci. Rep 2016, 6, 35814. [PubMed: 27853191]

(217). Lin L; Peng X; Mao Z; Li W; Yogeesh MN; Rajeeva BB; Perillo EP; Dunn AK; Akinwande D; Zheng Y Bubble-Pen Lithography. Nano Lett. 2016, 16, 701–708. [PubMed: 26678845]

(218). Lin L; Li J; Li W; Yogeesh MN; Shi J; Peng X; Liu Y; Rajeeva BB; Becker MF; Liu Y; et al. Optothermoplasmonic Nanolithography for on-Demand Patterning of 2D Materials. Adv. Funct. Mater 2018, 28, 1803990.

(219). Kollipara PS; Li J; Zheng Y Optical Patterning of Two-Dimensional Materials. Research 2020, 2020, 6581250. [PubMed: 32043085]

(220). Peng X; Lin L; Hill EH; Kunal P; Humphrey SM; Zheng Y Optothermophoretic Manipulation of Colloidal Particles in Nonionic Liquids. J. Phys. Chem. C 2018, 122, 24226–24234.

(221). Lin L; Peng X; Wei X; Mao Z; Xie C; Zheng Y Thermophoretic Tweezers for Low-Power and Versatile Manipulation of Biological Cells. ACS Nano 2017, 11, 3147–3154. [PubMed: 28230355]

(222). Hill EH; Li J; Lin L; Liu Y; Zheng Y Opto-Thermophoretic Attraction, Trapping, and Dynamic Manipulation of Lipid Vesicles. Langmuir 2018, 34, 13252–13262. [PubMed: 30350700]

(223). Vigolo D; Buzzaccaro S; Piazza R Thermophoresis and Thermoelectricity in Surfactant Solutions. Langmuir 2010, 26, 7792–7801. [PubMed: 20146491]

(224). Lin L; Wang M; Peng X; Lissek EN; Mao Z; Scarabelli L; Adkins E; Coskun S; Unalan HE; Korgel BA; et al. Opto-Thermoelectric Nanotweezers. Nat. Photonics 2018, 12, 195–201. [PubMed: 29785202]

(225). Kollipara PS; Lin L; Zheng Y Thermo-Electro-Mechanics at Individual Particles in Complex Colloidal Systems. J. Phys. Chem. C 2019, 123, 21639–21644.

(226). Ding H; Kollipara PS; Lin L; Zheng Y Atomistic Modeling and Rational Design of Optothermal Tweezers for Targeted Applications. Nano Res. 2021, 14, 295–303. [PubMed: 35475031]

(227). Pughazhendi A; Chen Z; Wu Z; Li J; Zheng Y Opto-Thermoelectric Tweezers: Principles and Applications. Front. Phys 2020, 8, 468.

(228). Kotnala A; Kollipara PS; Zheng Y Opto-Thermoelectric Speckle Tweezers. Nanophotonics 2020, 9, 927–933. [PubMed: 34290954]

(229). Kotnala A; Zheng Y Opto-Thermophoretic Fiber Tweezers. Nanophotonics 2019, 8, 475–485. [PubMed: 34290953]

(230). Lin L; Zhang J; Peng X; Wu Z; Coughlan AC; Mao Z; Bevan MA; Zheng Y Opto-Thermophoretic Assembly of Colloidal Matter. Sci. Adv 2017, 3, No. e1700458. [PubMed: 28913423]

(231). Lin L; Peng X; Wang M; Scarabelli L; Mao Z; Liz-Marzán LM; Becker MF; Zheng Y Light-Directed Reversible Assembly of Plasmonic Nanoparticles Using Plasmon-Enhanced Thermophoresis. ACS Nano 2016, 10, 9659–9668. [PubMed: 27640212]

(232). Lin L; Lepeshov S; Krasnok A; Jiang T; Peng X; Korgel BA; Alù A; Zheng Y All-Optical Reconfigurable Chiral Meta-Molecules. Mater. Today 2019, 25, 10–20.

(233). Nechayev S; Barczyk R; Mick U; Banzer P Substrate-Induced Chirality in an Individual Nanostructure. ACS Photonics 2019, 6, 1876–1881.

(234). Peng X; Li J; Lin L; Liu Y; Zheng Y Opto-Thermophoretic Manipulation and Construction of Colloidal Superstructures in Photocurable Hydrogels. ACS Appl. Nano Mater 2018, 1, 3998–4004. [PubMed: 31106296]

(235). Peng X; Chen Z; Kollipara PS; Liu Y; Fang J; Lin L; Zheng Y Opto-Thermoelectric Microswimmers. Light: Sci. Appl 2020, 9, 141. [PubMed: 32864116]

(236). Maeda YT; Buguin A; Libchaber A Thermal Separation: Interplay between the Soret Effect and Entropic Force Gradient. Phys. Rev. Lett 2011, 107, 038301. [PubMed: 21838407]

(237). Maeda YT; Tlusty T; Libchaber A Effects of Long DNA Folding and Small Rna Stem–Loop in Thermophoresis. Proc. Natl. Acad. Sci. U. S. A 2012, 109, 17972–17977. [PubMed: 23071341]

(238). Maeda YT (2 + 1)-Dimensional Manipulation of Soft Biological Materials by Opto-Thermal Diffusiophoresis. Appl. Phys. Lett 2013, 103, 243704.

(239). Fukuyama T; Fuke A; Mochizuki M; Kamei K.-i.; Maeda YT Directing and Boosting of Cell Migration by the Entropic Force Gradient in Polymer Solution. Langmuir 2015, 31, 12567–12572. [PubMed: 26496637]

(240). Dong R; Cai Y; Yang Y; Gao W; Ren B Photocatalytic Micro/Nanomotors: From Construction to Applications. Acc. Chem. Res 2018, 51, 1940–1947. [PubMed: 30152999]

(241). Buttinoni I; Volpe G; Kümmel F; Volpe G; Bechinger C Active Brownian Motion Tunable by Light. J. Phys.: Condens. Matter 2012, 24, 284129. [PubMed: 22739052]

(242). Volpe G; Buttinoni I; Vogt D; Kümmerer H-J; Bechinger C Microswimmers in Patterned Environments. Soft Matter 2011, 7, 8810–8815.

(243). Würger A Self-Diffusiophoresis of Janus Particles in near-Critical Mixtures. Phys. Rev. Lett 2015, 115, 188304. [PubMed: 26565507]

(244). Lozano C; Bechinger C Diffusing Wave Paradox of Phototactic Particles in Traveling Light Pulses. Nat. Commun 2019, 10, 2495. [PubMed: 31175288]

(245). Ten Hagen B; Kümmel F; Wittkowski R; Takagi D; Löwen H; Bechinger C Gravitaxis of Asymmetric Self-Propelled Colloidal Particles. Nat. Commun 2014, 5, 4829. [PubMed: 25234416]

(246). Buttinoni I; Bialké J; Kümmel F; Löwen H; Bechinger C; Speck T Dynamical Clustering and Phase Separation in Suspensions of Self-Propelled Colloidal Particles. Phys. Rev. Lett 2013, 110, 238301. [PubMed: 25167534]

(247). Bäuerle T; Fischer A; Speck T; Bechinger C Self-Organization of Active Particles by Quorum Sensing Rules. Nat. Commun 2018, 9, 3232. [PubMed: 30104679]

(248). Lavergne FA; Wendehenne H; Bäuerle T; Bechinger C Group Formation and Cohesion of Active Particles with Visual Perception–Dependent Motility. Science 2019, 364, 70–74. [PubMed: 30948548]

(249). Bäuerle T; Löffler RC; Bechinger C Formation of Stable and Responsive Collective States in Suspensions of Active Colloids. Nat. Commun 2020, 11, 2547. [PubMed: 32439919]

(250). Shao L; Käll M Light-Driven Rotation of Plasmonic Nanomotors. Adv. Funct. Mater 2018, 28, 1706272.

(251). Balk AL; Mair LO; Mathai PP; Patrone PN; Wang W; Ahmed S; Mallouk TE; Liddle JA; Stavis SM Kilohertz Rotation of Nanorods Propelled by Ultrasound, Traced by Microvortex Advection of Nanoparticles. ACS Nano 2014, 8, 8300–8309. [PubMed: 25019966]

(252). Kim K; Xu X; Guo J; Fan DL Ultrahigh-Speed Rotating Nanoelectromechanical System Devices Assembled from Nanoscale Building Blocks. Nat. Commun 2014, 5, 3632. [PubMed: 24709694]

(253). Van den Heuvel MG; Dekker C Motor Proteins at Work for Nanotechnology. Science 2007, 317, 333–336. [PubMed: 17641191]

(254). Liu M; Zentgraf T; Liu Y; Bartal G; Zhang X Light-Driven Nanoscale Plasmonic Motors. Nat. Nanotechnol 2010, 5, 570–573. [PubMed: 20601945]

(255). Schmidt F; Magazzù A; Callegari A; Biancofiore L; Cichos F; Volpe G Microscopic Engine Powered by Critical Demixing. Phys. Rev. Lett 2018, 120, 068004. [PubMed: 29481280]

(256). Maggi C; Saglimbeni F; Dipalo M; De Angelis F; Di Leonardo R Micromotors with Asymmetric Shape That Efficiently Convert Light into Work by Thermocapillary Effects. Nat. Commun 2015, 6, 7855. [PubMed: 26220862]

(257). Palagi S; Mark AG; Reigh SY; Melde K; Qiu T; Zeng H; Parmeggiani C; Martella D; Sanchez-Castillo A; Kapernaum N; et al. Structured Light Enables Biomimetic Swimming and Versatile Locomotion of Photoresponsive Soft Microrobots. Nat. Mater 2016, 15, 647–653. [PubMed: 26878315]

(258). Soong RK; Bachand GD; Neves HP; Olkhovets AG; Craighead HG; Montemagno CD Powering an Inorganic Nanodevice with a Biomolecular Motor. Science 2000, 290, 1555–1558. [PubMed: 11090349]

(259). Di Leonardo R; Angelani L; Dell'Arciprete D; Ruocco G; Iebba V; Schippa S; Conte MP; Mecarini F; De Angelis F; Di Fabrizio E Bacterial Ratchet Motors. Proc. Natl. Acad. Sci. U. S. A 2010, 107, 9541–9545. [PubMed: 20457936]

(260). Nelson BJ; Kaliakatsos IK; Abbott JJ Microrobots for Minimally Invasive Medicine. Annu. Rev. Biomed. Eng 2010, 12, 55–85. [PubMed: 20415589]

(261). Padgett M; Di Leonardo R Holographic Optical Tweezers and Their Relevance to Lab on Chip Devices. Lab Chip 2011, 11, 1196–1205. [PubMed: 21327211]

(262). Kümmel F; ten Hagen B; Wittkowski R; Buttinoni I; Eichhorn R; Volpe G; Löwen H; Bechinger C Circular Motion of Asymmetric Self-Propelling Particles. Phys. Rev. Lett 2013, 110, 198302. [PubMed: 23705745]

(263). Shvedov VG; Desyatnikov AS; Rode AV; Krolikowski W; Kivshar YS Optical Guiding of Absorbing Nanoclusters in Air. Opt. Express 2009, 17, 5743–5757. [PubMed: 19333344]

(264). Porfirev A Optical Mill"—a Tool for the Massive Transfer of Airborne Light-Absorbing Particles. Appl. Phys. Lett 2019, 115, 201103.

(265). Pan Y-L; Hill SC; Coleman M Photophoretic Trapping of Absorbing Particles in Air and Measurement of Their Single-Particle Raman Spectra. Opt. Express 2012, 20, 5325–5334. [PubMed: 22418339]

(266). Wang C; Gong Z; Pan Y-L; Videen G Laser Pushing or Pulling of Absorbing Airborne Particles. Appl. Phys. Lett 2016, 109, 011905.

(267). Lin J; Hart AG; Li Y.-q. Optical Pulling of Airborne Absorbing Particles and Smut Spores over a Meter-Scale Distance with Negative Photophoretic Force. Appl. Phys. Lett 2015, 106, 171906.

(268). Cortes J; Stanczak C; Azadi M; Narula M; Nicaise SM; Hu H; Bargatin I Photophoretic Levitation of Macroscopic Nanocardboard Plates. Adv. Mater 2020, 32, 1906878.

(269). Pluchino AB Radiometric Levitation of Spherical Carbon Aerosol Particles Using a Nd: YAG Laser. Appl. Opt 1983, 22, 1861–1866. [PubMed: 18196047]

(270). Zhang Z; Cannan D; Liu J; Zhang P; Christodoulides DN; Chen Z Observation of Trapping and Transporting Air-Borne Absorbing Particles with a Single Optical Beam. Opt. Express 2012, 20, 16212–16217.

(271). Gong Z; Pan Y-L; Wang C Optical Configurations for Photophoretic Trap of Single Particles in Air. Rev. Sci. Instrum 2016, 87, 103104. [PubMed: 27802728]

(272). Shvedov VG; Hnatovsky C; Rode AV; Krolikowski W Robust Trapping and Manipulation of Airborne Particles with a Bottle Beam. Opt. Express 2011, 19, 17350–17356. [PubMed: 21935099]

(273). Zhang P; Zhang Z; Prakash J; Huang S; Hernandez D; Salazar M; Christodoulides DN; Chen Z Trapping and Transporting Aerosols with a Single Optical Bottle Beam Generated by Moiré Techniques. Opt. Lett 2011, 36, 1491–1493. [PubMed: 21499400]

(274). Alpmann C; Esseling M; Rose P; Denz C Holographic Optical Bottle Beams. Appl. Phys. Lett 2012, 100, 111101.

(275). Desyatnikov AS; Shvedov VG; Rode AV; Krolikowski W; Kivshar YS Photophoretic Manipulation of Absorbing Aerosol Particles with Vortex Beams: Theory Versus Experiment. Opt. Express 2009, 17, 8201–8211. [PubMed: 19434152]

(276). Shvedov V; Davoyan AR; Hnatovsky C; Engheta N; Krolikowski W A Long-Range Polarization-Controlled Optical Tractor Beam. Nat. Photonics 2014, 8, 846–850.

(277). Shvedov V; Rode AV; Izdebskaya YV; Leykam D; Desyatnikov AS; Krolikowski W; Kivshar YS Laser Speckle Field as a Multiple Particle Trap. J. Opt 2010, 12, 124003.

(278). Shvedov VG; Rode AV; Izdebskaya YV; Desyatnikov AS; Krolikowski W; Kivshar YS Selective Trapping of Multiple Particles by Volume Speckle Field. Opt. Express 2010, 18, 3137–3142. [PubMed: 20174149]

(279). Shvedov VG; Hnatovsky C; Shostka N; Rode AV; Krolikowski W Optical Manipulation of Particle Ensembles in Air. Opt. Lett 2012, 37, 1934–1936. [PubMed: 22660078]

(280). Lizana A; Zhang H; Turpin A; Van Eeckhout A; Torres-Ruiz FA; Vargas A; Ramirez C; Pi F; Campos J Generation of Reconfigurable Optical Traps for Microparticles Spatial Manipulation through Dynamic Split Lens Inspired Light Structures. Sci. Rep 2018, 8, 11263. [PubMed: 30050141]

(281). Smalley D; Nygaard E; Squire K; Van Wagoner J; Rasmussen J; Gneiting S; Qaderi K; Goodsell J; Rogers W; Lindsey M; et al. A Photophoretic-Trap Volumetric Display. Nature 2018, 553, 486–490. [PubMed: 29368704]

(282). Lu J; Yang H; Zhou L; Yang Y; Luo S; Li Q; Qiu M Light-Induced Pulling and Pushing by the Synergic Effect of Optical Force and Photophoretic Force. Phys. Rev. Lett 2017, 118, 043601. [PubMed: 28186804]

(283). Lin J; Li Y.-q. Optical Trapping and Rotation of Airborne Absorbing Particles with a Single Focused Laser Beam. Appl. Phys. Lett 2014, 104, 101909.

(284). Bera SK; Kumar A; Sil S; Saha TK; Saha T; Banerjee A Simultaneous Measurement of Mass and Rotation of Trapped Absorbing Particles in Air. Opt. Lett 2016, 41, 4356–4359. [PubMed: 27628396]

(285). Liu Z; Wu J; Zhang Y; Zhang Y; Tang X; Yang X; Zhang J; Yang J; Yuan L Optical Trapping and Axial Shifting for Strongly Absorbing Particle with Single Focused TEM00 Gaussian Beam. Appl. Phys. Lett 2018, 113, 091101.

(286). Zhang Y; Tang X; Zhang Y; Liu Z; Yang X; Zhang J; Yang J; Yuan L Optical Attraction of Strongly Absorbing Particles in Liquids. Opt. Express 2019, 27, 12414–12423. [PubMed: 31052781]

(287). Azadi M; Popov GA; Lu Z; Eskenazi AG; Bang AJW; Campbell MF; Hu H; Bargatin I Controlled Levitation of Nanostructured Thin Films for Sun-Powered near-Space Flight. Sci. Adv 2021, 7, No. eabe1127. [PubMed: 33579712]

(288). Brasiliense V; Berto P; Aubertin P; Maisonhaute E; Combellas C; Tessier G; Courty A; Kanoufi F Light Driven Design of Dynamical Thermosensitive Plasmonic Superstructures: A Bottom-up Approach Using Silver Supercrystals. ACS Nano 2018, 12, 10833–10842. [PubMed: 30346722]

(289). Liu Y; Poon AW Flow-Assisted Single-Beam Optothermal Manipulation of Microparticles. Opt. Express 2010, 18, 18483–18491. [PubMed: 20721243]

(290). Cong H; Loo F-C; Chen J; Wang Y; Kong S-K; Ho H-P Target Trapping and in Situ Single-Cell Genetic Marker Detection with a Focused Optical Beam. Biosens. Bioelectron 2019, 133, 236–242. [PubMed: 30953882]

(291). Kumar S; Gunaseelan M; Vaippully R; Kumar A; Ajith M; Vaidya G; Dutta S; Roy B Pitch-Rotational Manipulation of Single Cells and Particles Using Single-Beam Thermo-Optical Tweezers. Biomed. Opt. Express 2020, 11, 3555–3566. [PubMed: 33014551]

(292). Kotnala A; Kollipara PS; Li J; Zheng Y Overcoming Diffusion-Limited Trapping in Nanoaperture Tweezers Using Opto-Thermal-Induced Flow. Nano Lett. 2020, 20, 768–779. [PubMed: 31834809]

(293). Roxworthy BJ; Ko KD; Kumar A; Fung KH; Chow EK; Liu GL; Fang NX; Toussaint KC Jr Application of Plasmonic Bowtie Nanoantenna Arrays for Optical Trapping, Stacking, and Sorting. Nano Lett. 2012, 12, 796–801. [PubMed: 22208881]

(294). Braun D; Goddard NL; Libchaber A Exponential DNA Replication by Laminar Convection. Phys. Rev. Lett 2003, 91, 158103. [PubMed: 14611502]

(295). Jin CM; Lee W; Kim D; Kang T; Choi I Photothermal Convection Lithography for Rapid and Direct Assembly of Colloidal Plasmonic Nanoparticles on Generic Substrates. Small 2018, 14, 1803055.

(296). Lu F; Kuai Y; Chen J; Tang X; Xiang Y; Liu Y; Wang P; Lakowicz JR; Zhang D Switchable Assembly and Guidance of Colloidal Particles on an All-Dielectric One-Dimensional Photonic Crystal. Phys. Rev. Appl 2020, 13, 014020. [PubMed: 34113692]

(297). Garcés-Chávez V; Quidant R; Reece P; Badenes G; Torner L; Dholakia K Extended Organization of Colloidal Microparticles by Surface Plasmon Polariton Excitation. Phys. Rev. B: Condens. Matter Mater. Phys 2006, 73, 085417.

(298). Chen H; Gratton E; Digman MA Self-Assisted Optothermal Trapping of Gold Nanorods under Two-Photon Excitation. Methods Appl. Fluoresc 2016, 4, 035003. [PubMed: 28355163]

(299). Zhang Y; Lei J; Zhang Y; Liu Z; Zhang J; Yang X; Yang J; Yuan L Microparticles Controllable Accumulation, Arrangement, and Spatial Shaping Performed by Tapered-Fiber-Based Laser-Induced Convection Flow. Sci. Rep 2017, 7, 14378. [PubMed: 29085030]

(300). Dinh ND; Luo R; Christine MTA; Lin WN; Shih WC; Goh JCH; Chen CH Effective Light Directed Assembly of Building Blocks with Microscale Control. Small 2017, 13, 1700684.

(301). Qian Y; Neale SL; Marsh JH Microparticle Manipulation Using Laser-Induced Thermophoresis and Thermal Convection Flow. Sci. Rep 2020, 10, 19169. [PubMed: 33154506]

(302). Braun D; Libchaber A Trapping of DNA by Thermophoretic Depletion and Convection. Phys. Rev. Lett 2002, 89, 188103. [PubMed: 12398641]

(303). Kang CY; Li JJ; Wu LA; Wu CC; Chen YF Dynamic and Reversible Accumulation of Plasmonic Core-Satellite Nanostructures in a Light-Induced Temperature Gradient for in Situ Sers Detection. Part. Part. Syst. Charact 2018, 35, 1700405.

(304). Duhr S; Braun D Two-Dimensional Colloidal Crystals Formed by Thermophoresis and Convection. Appl. Phys. Lett 2005, 86, 131921.

(305). Weinert FM; Braun D An Optical Conveyor for Molecules. Nano Lett. 2009, 9, 4264–4267. [PubMed: 19807065]

(306). Wu C-L; Wang S-F; Kudo T; Yuyama K.-i.; Sugiyama T; Masuhara H Anomalously Large Assembly Formation of Polystyrene Nanoparticles by Optical Trapping at the Solution Surface. Langmuir 2020, 36, 14234–14242. [PubMed: 33197315]

(307). Chen J; Kang Z; Kong SK; Ho H-P Plasmonic Random Nanostructures on Fiber Tip for Trapping Live Cells and Colloidal Particles. Opt. Lett 2015, 40, 3926–3929. [PubMed: 26368677]

(308). Lv C; Varanakkottu SN; Baier T; Hardt S Controlling the Trajectories of Nano/Micro Particles Using Light-Actuated Marangoni Flow. Nano Lett. 2018, 18, 6924–6930. [PubMed: 30285458]

(309). Varanakkottu SN; Anyfantakis M; Morel M; Rudiuk S; Baigl D Light-Directed Particle Patterning by Evaporative Optical Marangoni Assembly. Nano Lett. 2016, 16, 644–650. [PubMed: 26630478]

(310). Varanakkottu SN; George SD; Baier T; Hardt S; Ewald M; Biesalski M Particle Manipulation Based on Optically Controlled Free Surface Hydrodynamics. Angew. Chem., Int. Ed 2013, 52, 7291–7295.

(311). Wang S; Jiang Z; Ouyang S; Dai Z; Wang T Internally/Externally Bubble-Propelled Photocatalytic Tubular Nanomotors for Efficient Water Cleaning. ACS Appl. Mater. Interfaces 2017, 9, 23974–23982. [PubMed: 28650608]

(312). Li Y; Mou F; Chen C; You M; Yin Y; Xu L; Guan J Light-Controlled Bubble Propulsion of Amorphous TiO2/Au Janus Micromotors. RSC Adv. 2016, 6, 10697–10703.

(313). Mou F; Li Y; Chen C; Li W; Yin Y; Ma H; Guan J Single-Component TiO2 Tubular Microengines with Motion Controlled by Light-Induced Bubbles. Small 2015, 11, 2564–2570. [PubMed: 25627213]

(314). Setoura K; Ito S; Miyasaka H Stationary Bubble Formation and Marangoni Convection Induced by CWLaser Heating of a Single Gold Nanoparticle. Nanoscale 2017, 9, 719–730. [PubMed: 27959376]

(315). Li X; Wang Y; Zaytsev ME; Lajoinie G; Le The H; Bomer JG; Eijkel JCT; Zandvliet HJW; Zhang X; Lohse D Plasmonic Bubble Nucleation and Growth in Water: Effect of Dissolved Air. J. Phys. Chem. C 2019, 123, 23586–23593.

(316). Wang Y; Zaytsev ME; Lajoinie G; The HL; Eijkel JCT; van den Berg A; Versluis M; Weckhuysen BM; Zhang X; Zandvliet HJW; et al. Explosive Plasmonic Bubbles by Delayed Nucleation. Proc. Natl. Acad. Sci. U. S. A 2018, 115, 7676–7681. [PubMed: 29997175]

(317). Hu W; Fan Q; Ohta AT An Opto-Thermocapillary Cell Micromanipulator. Lab Chip 2013, 13, 2285–2291. [PubMed: 23666050]

(318). Zhao C; Xie Y; Mao Z; Zhao Y; Rufo J; Yang S; Guo F; Mai JD; Huang TJ Theory and Experiment on Particle Trapping and Manipulation Via Optothermally Generated Bubbles. Lab Chip 2014, 14, 384–391. [PubMed: 24276624]

(319). Chikazawa J.-i.; Uwada T; Furube A; Hashimoto S Flow-Induced Transport Via Optical Heating of a Single Gold Nanoparticle. J. Phys. Chem. C 2019, 123, 4512–4522.

(320). Dai L; Ge Z; Jiao N; Liu L 2D to 3D Manipulation and Assembly of Microstructures Using Optothermally Generated Surface Bubble Microrobots. Small 2019, 15, 1902815.

(321). Dai L; Lin D; Wang X; Jiao N; Liu L Integrated Assembly and Flexible Movement of Microparts Using Multifunctional Bubble Microrobots. ACS Appl. Mater. Interfaces 2020, 12, 57587–57597. [PubMed: 33301292]

(322). Rahman MA; Cheng J; Wang Z; Ohta AT Cooperative Micromanipulation Using the Independent Actuation of Fifty Microrobots in Parallel. Sci. Rep 2017, 7, 3278. [PubMed: 28607359]

(323). Hu W; Ishii KS; Fan Q; Ohta AT Hydrogel Microrobots Actuated by Optically Generated Vapour Bubbles. Lab Chip 2012, 12, 3821–3826. [PubMed: 22899225]

(324). Villangca MJ; Palima D; Banas AR; Glückstad J Light-Driven Micro-Tool Equipped with a Syringe Function. Light: Sci. Appl 2016, 5, No. e16148. [PubMed: 30167189]

(325). Zheng Y; Liu H; Wang Y; Zhu C; Wang S; Cao J; Zhu S Accumulating Microparticles and Direct-Writing Micropatterns Using a Continuous-Wave Laser-Induced Vapor Bubble. Lab Chip 2011, 11, 3816–3820. [PubMed: 21956638]

(326). Namura K; Nakajima K; Kimura K; Suzuki M Photothermally Controlled Marangoni Flow around a Micro Bubble. Appl. Phys. Lett 2015, 106, 043101.

(327). Fujii S; Kanaizuka K; Toyabe S; Kobayashi K; Muneyuki E; Haga M.-a. Fabrication and Placement of a Ring Structure of Nanoparticles by a Laser-Induced Micronanobubble on a Gold Surface. Langmuir 2011, 27, 8605–8610. [PubMed: 21678969]

(328). Karim F; Vasquez ES; Sun Y; Zhao C Optothermal Microbubble Assisted Manufacturing of Nanogap-Rich Structures for Active Chemical Sensing. Nanoscale 2019, 11, 20589–20597. [PubMed: 31638631]

(329). Karim F; Vasquez ES; Zhao C Fabricated Nanogap-Rich Plasmonic Nanostructures through an Optothermal Surface Bubble in a Droplet. Opt. Lett 2018, 43, 334–336. [PubMed: 29328275]

(330). Kang Z; Chen J; Ho H-P Surface-Enhanced Raman Scattering Via Entrapment of Colloidal Plasmonic Nanocrystals by Laser Generated Microbubbles on Random Gold Nano-Islands. Nanoscale 2016, 8, 10266–10272. [PubMed: 27125956]

(331). Armon N; Greenberg E; Layani M; Rosen YS; Magdassi S; Shpaisman H Continuous Nanoparticle Assembly by a Modulated Photo-Induced Microbubble for Fabrication of Micrometric Conductive Patterns. ACS Appl. Mater. Interfaces 2017, 9, 44214–44221. [PubMed: 29172418]

(332). Fujii S; Kobayashi K; Kanaizuka K; Okamoto T; Toyabe S; Muneyuki E; Haga M.-a. Manipulation of Single DNA Using a Micronanobubble Formed by Local Laser Heating on a Au-Coated Surface. Chem. Lett 2010, 39, 92–93.

(333). Naka S; Shoji T; Fujii S; Ueno K; Wakisaka Y; Murakoshi K; Mizoguchi T; Tamiaki H; Tsuboi Y Thermo-Plasmonic Trapping of Living Cyanobacteria on a Gold Nanopyramidal Dimer Array: Implications for Plasmonic Biochips. ACS Appl. Nano Mater 2020, 3, 10067–10072.

(334). Tokonami S; Kurita S; Yoshikawa R; Sakurai K; Suehiro T; Yamamoto Y; Tamura M; Karthaus O; Iida T Light-Induced Assembly of Living Bacteria with Honeycomb Substrate. Sci. Adv 2020, 6, No. eaaz5757. [PubMed: 32158951]

(335). Yamamoto Y; Shimizu E; Nishimura Y; Iida T; Tokonami S Development of a Rapid Bacterial Counting Method Based on Photothermal Assembling. Opt. Mater. Express 2016, 6, 1280–1285.

(336). Uwada T; Fujii S; Sugiyama T; Usman A; Miura A; Masuhara H; Kanaizuka K; Haga M.-a. Glycine Crystallization in Solution by CW Laser-Induced Microbubble on Gold Thin Film Surface. ACS Appl. Mater. Interfaces 2012, 4, 1158–1163. [PubMed: 22339812]

(337). Vélez-Cordero JR; Hernández-Cordero J On the Motion of Carbon Nanotube Clusters near Optical Fiber Tips: Thermophoresis, Radiative Pressure, and Convection Effects. Langmuir 2015, 31, 10066–10075. [PubMed: 26309145]

(338). Yamamoto Y; Tokonami S; Iida T Surfactant-Controlled Photothermal Assembly of Nanoparticles and Microparticles for Rapid Concentration Measurement of Microbes. ACS Appl. Bio Mater 2019, 2, 1561–1568.

(339). Kim Y; Ding H; Zheng Y Enhancing Surface Capture and Sensing of Proteins with Low-Power Optothermal Bubbles in a Biphasic Liquid. Nano Lett. 2020, 20, 7020–7027. [PubMed: 32667815]

(340). Moon S; Zhang Q; Huang D; Senapati S; Chang HC; Lee E; Luo T Biocompatible Direct Deposition of Functionalized Nanoparticles Using Shrinking Surface Plasmonic Bubble. Adv. Mater. Interfaces 2020, 7, 2000597.

(341). Liu Y; Wu Z; Kollipara PS; Montellano R; Sharma K; Zheng Y Label-Free Ultrasensitive Detection of Abnormal Chiral Metabolites in Diabetes. ACS Nano 2021, 15, 6448–6456. [PubMed: 33760602]

(342). Lin L; Kollipara PS; Zheng Y Digital Manufacturing of Advanced Materials: Challenges and Perspective. Mater. Today 2019, 28, 49–62.

(343). Kotnala A; Zheng Y Digital Assembly of Colloidal Particles for Nanoscale Manufacturing. Part. Part. Syst. Charact 2019, 36, 1900152. [PubMed: 33041521]

(344). Li J; Hill EH; Lin L; Zheng Y Optical Nanoprinting of Colloidal Particles and Functional Structures. ACS Nano 2019, 13, 3783–3795. [PubMed: 30875190]

(345). Xie Y; Zhao C An Optothermally Generated Surface Bubble and Its Applications. Nanoscale 2017, 9, 6622–6631. [PubMed: 28485456]

(346). Roy B; Arya M; Thomas P; Jürgschat JK; Venkata Rao K; Banerjee A; Malla Reddy C; Roy S Self-Assembly of Mesoscopic Materials to Form Controlled and Continuous Patterns by Thermo-Optically Manipulated Laser Induced Microbubbles. Langmuir 2013, 29, 14733–14742. [PubMed: 24171640]

(347). Bangalore Rajeeva B; Lin L; Perillo EP; Peng X; Yu WW; Dunn AK; Zheng Y High-Resolution Bubble Printing of Quantum Dots. ACS Appl. Mater. Interfaces 2017, 9, 16725–16733. [PubMed: 28452214]

(348). Thomas P; Pei C; Roy B; Ghosh S; Das S; Banerjee A; Ben T; Qiu S; Roy S Site Specific Supramolecular Heterogeneous Catalysis by Optically Patterned Soft Oxometalate–Porous Organic Framework (SOM–POF) Hybrid on a Chip. J. Mater. Chem. A 2015, 3, 1431–1441.

(349). Wu Z; Kelp G; Yogeesh MN; Li W; McNicholas KM; Briggs A; Rajeeva BB; Akinwande D; Bank SR; Shvets G; et al. Dual-Band Moire Metasurface Patches for Multifunctional Biomedical Applications. Nanoscale 2016, 8, 18461–18468. [PubMed: 27778012]

(350). Sánchez-Solís A; Karim F; Alam MS; Zhan Q; López-Luke T; Zhao C Print Metallic Nanoparticles on a Fiber Probe for 1064-nm Surface-Enhanced Raman Scattering. Opt. Lett 2019, 44, 4997–5000. [PubMed: 31613262]

(351). Lukianova-Hleb E; Hu Y; Latterini L; Tarpani L; Lee S; Drezek RA; Hafner JH; Lapotko DO Plasmonic Nanobubbles as Transient Vapor Nanobubbles Generated around Plasmonic Nanoparticles. ACS Nano 2010, 4, 2109–2123. [PubMed: 20307085]

(352). Rajeeva BB; Alabandi MA; Lin L; Perillo EP; Dunn AK; Zheng Y Patterning and Fluorescence Tuning of Quantum Dots with Haptic-Interfaced Bubble Printing. J. Mater. Chem. C 2017, 5, 5693–5699.

(353). Rajeeva BB; Wu Z; Briggs A; Acharya PV; Walker SB; Peng X; Bahadur V; Bank SR; Zheng Y Point-and-Shoot" Synthesis of Metallic Ring Arrays and Surface-Enhanced Optical Spectroscopy. Adv. Opt. Mater 2018, 6, 1701213.

(354). Fujii S; Fukano R; Hayami Y; Ozawa H; Muneyuki E; Kitamura N; Haga M.-a. Simultaneous Formation and Spatial Patterning of ZnO on ITO Surfaces by Local Laser-Induced Generation of Microbubbles in Aqueous Solutions of $[Zn(NH_3)_4]^{2+}$. ACS Appl. Mater. Interfaces 2017, 9, 8413–8419. [PubMed: 28217991]

(355). Ghosh S; Das S; Paul S; Thomas P; Roy B; Mitra P; Roy S; Banerjee A In Situ Self-Assembly and Photopolymerization for Hetero-Phase Synthesis and Patterning of Conducting Materials Using Soft Oxometalates in Thermo-Optical Tweezers. J. Mater. Chem. C 2017, 5, 6718–6728.

(356). Edri E; Armon N; Greenberg E; Hadad E; Bockstaller MR; Shpaisman H Assembly of Conductive Polyaniline Microstructures by a Laser-Induced Microbubble. ACS Appl. Mater. Interfaces 2020, 12, 22278–22286. [PubMed: 32297505]

(357). Rajeeva BB; Kunal P; Kollipara PS; Acharya PV; Joe M; Ide MS; Jarvis K; Liu Y; Bahadur V; Humphrey SM; et al. Accumulation-Driven Unified Spatiotemporal Synthesis and Structuring of Immiscible Metallic Nanoalloys. Matter 2019, 1, 1606–1617.

(358). Greenberg E; Armon N; Kapon O; Ben-Ishai M; Shpaisman H Nanostructure and Mechanism of Metal Deposition by a Laser-Induced Photothermal Reaction. Adv. Mater. Interfaces 2019, 6, 1900541.

(359). Winterer F; Maier CM; Pernpeintner C; Lohmüller T Optofluidic Transport and Manipulation of Plasmonic Nanoparticles by Thermocapillary Convection. Soft Matter 2018, 14, 628–634. [PubMed: 29265159]

(360). Zhang X; Cao J; Yan J; Zhao J Surface Tension-Mediated Trapping and Propulsion of Small Objects at Liquid Interfaces by Using Line-Spot Lasers. Opt. Laser Technol 2021, 133, 106536.

(361). Zhang J; Wang Z; Wang Z; Zhang T; Wei L In-Fibre Particle Manipulation and Device Assembly Via Laser Induced Thermocapillary Convection. Nat. Commun 2019, 10, 5206. [PubMed: 31729394]

(362). Baigl D Photo-Actuation of Liquids for Light-Driven Microfluidics: State of the Art and Perspectives. Lab Chip 2012, 12, 3637–3653. [PubMed: 22864577]

(363). Hu W; Ohta AT Aqueous Droplet Manipulation by Optically Induced Marangoni Circulation. Microfluid. Nanofluid 2011, 11, 307–316.

(364). Verneuil E; Cordero M. a.; Gallaire F; Baroud CN Laser-Induced Force on a Microfluidic Drop: Origin and Magnitude. Langmuir 2009, 25, 5127–5134. [PubMed: 19358521]

(365). Won BJ; Lee W; Song S Estimation of the Thermocapillary Force and Its Applications to Precise Droplet Control on a Microfluidic Chip. Sci. Rep 2017, 7, 3062. [PubMed: 28596574]

(366). Nagelberg S; Totz JF; Mittasch M; Sresht V; Zeininger L; Swager TM; Kreysing M; Kolle M Actuation of Janus Emulsion Droplets Via Optothermally Induced Marangoni Forces. Phys. Rev. Lett 2021, 127, 144503. [PubMed: 34652186]

(367). Baroud CN; de Saint Vincent MR; Delville J-P An Optical Toolbox for Total Control of Droplet Microfluidics. LabChip 2007, 7, 1029–1033.

(368). Baroud CN; Delville J-P; Gallaire F; Wunenburger R Thermocapillary Valve for Droplet Production and Sorting. Phys. Rev. E 2007, 75, 046302.

(369). de Saint Vincent MR; Wunenburger R; Delville J-P Laser Switching and Sorting for High Speed Digital Microfluidics. Appl. Phys. Lett 2008, 92, 154105.

(370). Kotz K; Noble K; Faris G Optical Microfluidics. Appl. Phys. Lett 2004, 85, 2658–2660.

(371). Dietrich K; Jaensson N; Buttinoni I; Volpe G; Isa L Microscale Marangoni Surfers. Phys. Rev. Lett 2020, 125, 098001. [PubMed: 32915612]

(372). Yang R-L; Zhu Y-J; Chen F-F; Qin D-D; Xiong Z-C Superhydrophobic Photothermal Paper Based on Ultralong Hydrox-yapatite Nanowires for Controllable Light-Driven Self-Propelled Motion. ACS Sustainable Chem. Eng 2019, 7, 13226–13235.

(373). Liao M; Sun H; Tao X; Xu X; Li Z; Fu X; Xie S; Ye L; Zhang Y; Wang B; et al. Alignment of Thermally Conducting Nanotubes Making High-Performance Light-Driving Motors. ACS Appl. Mater. Interfaces 2018, 10, 26765–26771. [PubMed: 29999307]

(374). Ito M; Mayama H; Asaumi Y; Nakamura Y; Fujii S Light-Driven Locomotion of Bubbles. Langmuir 2020, 36, 7021–7031. [PubMed: 31859517]

(375). Kawashima H; Paven M; Mayama H; Butt H.-J. r.; Nakamura Y; Fujii S Transfer of Materials from Water to Solid Surfaces Using Liquid Marbles. ACS Appl. Mater. Interfaces 2017, 9, 33351–33359. [PubMed: 28879765]

(376). Paven M; Mayama H; Sekido T; Butt HJ; Nakamura Y; Fujii S Light-Driven Delivery and Release of Materials Using Liquid Marbles. Adv. Funct. Mater 2016, 26, 3199–3206.

(377). Okawa D; Pastine SJ; Zettl A; Fréchet JMJ Surface Tension Mediated Conversion of Light to Work. J. Am. Chem. Soc 2009, 131, 5396–5398. [PubMed: 20560635]

(378). Wang W; Liu YQ; Liu Y; Han B; Wang H; Han DD; Wang JN; Zhang YL; Sun HB Direct Laser Writing of Superhydrophobic Pdms Elastomers for Controllable Manipulation Via Marangoni Effect. Adv. Funct. Mater 2017, 27, 1702946.

(379). Würger A Thermally Driven Marangoni Surfers. J. Fluid Mech 2014, 752, 589–601.

(380). Yang R-L; Zhu Y-J; Qin D-D; Xiong Z-C Light-Operated Dual-Mode Propulsion at the Liquid/Air Interface Using Flexible, Superhydrophobic, and Thermally Stable Photothermal Paper. ACS Appl. Mater. Interfaces 2020, 12, 1339–1347. [PubMed: 31880902]

(381). Pan D; Wu D; Li PJ; Ji SY; Nie X; Fan SY; Chen GY; Zhang CC; Xin C; Xu B; et al. Transparent Light-Driven Hydrogel Actuator Based on Photothermal Marangoni Effect and Buoyancy Flow for Three-Dimensional Motion. Adv. Funct. Mater 2021, 31, 2009386.

(382). Wang W; Han B; Zhang Y; Li Q; Zhang YL; Han DD; Sun HB Laser-Induced Graphene Tapes as Origami and Stick-on Labels for Photothermal Manipulation Via Marangoni Effect. Adv. Funct. Mater 2021, 31, 2006179.

(383). Hauser AW; Sundaram S; Hayward RC Photo-thermocapillary Oscillators. Phys. Rev. Lett 2018, 121, 158001. [PubMed: 30362782]

(384). Lucchetta DE; Castagna R; Simoni F Light-Actuated Contactless Macro Motors Exploiting Bénard–Marangoni Convection. Opt. Express 2019, 27, 13574–13580. [PubMed: 31163819]

(385). Yang M; Ripoll M A Self-Propelled Thermophoretic Microgear. Soft Matter 2014, 10, 1006–1011. [PubMed: 24983112]

(386). Ndukaife JC; Mishra A; Guler U; Nnanna AGA; Wereley ST; Boltasseva A Photothermal Heating Enabled by Plasmonic Nanostructures for Electrokinetic Manipulation and Sorting of Particles. ACS Nano 2014, 8, 9035–9043. [PubMed: 25144369]

(387). Ndukaife JC; Xuan Y; Nnanna AGA; Kildishev AV; Shalaev VM; Wereley ST; Boltasseva A High-Resolution Large-Ensemble Nanoparticle Trapping with Multifunctional Thermoplasmonic Nanohole Metasurface. ACS Nano 2018, 12, 5376–5384. [PubMed: 29847087]

(388). Garcia-Guirado J; Rica RA; Ortega J; Medina J; Sanz V; Ruiz-Reina E; Quidant R Overcoming Diffusion-Limited Biosensing by Electrothermoplasmonics. ACS Photonics 2018, 5, 3673–3679.

(389). Zhao Y; Xuan C; Qian X; Alsaid Y; Hua M; Jin L; He X Soft Phototactic Swimmer Based on Self-Sustained Hydrogel Oscillator. Sci. Robot 2019, 4, No. eaax7112. [PubMed: 33137784]

(390). Ma C; Le X; Tang X; He J; Xiao P; Zheng J; Xiao H; Lu W; Zhang J; Huang Y; Chen T A Multiresponsive Anisotropic Hydrogel with Macroscopic 3D Complex Deformations. Adv. Funct. Mater 2016, 26 (47), 8670–8676.

(391). Wang E; Desai MS; Lee S-W Light-Controlled Graphene-Elastin Composite Hydrogel Actuators. Nano Lett. 2013, 13, 2826–2830. [PubMed: 23647361]

(392). Ahn C; Liang X; Cai S Bioinspired Design of Light-Powered Crawling, Squeezing, and Jumping Untethered Soft Robot. Adv. Mater. Technol 2019, 4, 1900185.

(393). Ho CY; Taylor RE Thermal Expansion of Solids; ASM International: 1998; Vol. 4, pp 1–108.

(394). Wunderlich B Thermal Analysis of Polymeric Materials; Springer Science & Business Media: 2005; pp 591–766.

(395). Yang L; Chang L; Hu Y; Huang M; Ji Q; Lu P; Liu J; Chen W; Wu Y An Autonomous Soft Actuator with Light-Driven Self-Sustained Wavelike Oscillation for Phototactic Self-Locomotion and Power Generation. Adv. Funct. Mater 2020, 30, 1908842.

(396). Sun Z; Yamauchi Y; Araoka F; Kim YS; Bergueiro J; Ishida Y; Ebina Y; Sasaki T; Hikima T; Aida T An Anisotropic Hydrogel Actuator Enabling Earthworm-Like Directed Peristaltic Crawling. Angew. Chem., Int. Ed 2018, 57, 15772–15776.

(397). Zhu QL; Du C; Dai Y; Daab M; Matejdes M; Breu J; Hong W; Zheng Q; Wu ZL Light-Steered Locomotion of Muscle-Like Hydrogel by Self-Coordinated Shape Change and Friction Modulation. Nat. Commun 2020, 11, 5166. [PubMed: 33056999]

(398). Wang W; Xiang C; Zhu Q; Zhong W; Li M; Yan K; Wang D Multistimulus Responsive Actuator with GO and Carbon Nanotube/PDMS Bilayer Structure for Flexible and Smart Devices. ACS Appl. Mater. Interfaces 2018, 10, 27215–27223. [PubMed: 30036482]

(399). Chen L; Weng M; Zhou P; Huang F; Liu C; Fan S; Zhang W Graphene-Based Actuator with Integrated-Sensing Function. Adv. Funct. Mater 2019, 29, 1806057.

(400). Weng M; Zhou P; Chen L; Zhang L; Zhang W; Huang Z; Liu C; Fan S Multiresponsive Bidirectional Bending Actuators Fabricated by a Pencil-on-Paper Method. Adv. Funct. Mater 2016, 26, 7244–7253.

(401). Li L; Meng J; Hou C; Zhang Q; Li Y; Yu H; Wang H Dual-Mechanism and Multimotion Soft Actuators Based on Commercial Plastic Film. ACS Appl. Mater. Interfaces 2018, 10, 15122–15128. [PubMed: 29658270]

(402). Zhang X; Yu Z; Wang C; Zarrouk D; Seo J-WT; Cheng JC; Buchan AD; Takei K; Zhao Y; Ager JW; et al. Photoactuators and Motors Based on Carbon Nanotubes with Selective Chirality Distributions. Nat. Commun 2014, 5, 2983. [PubMed: 24394587]

(403). Yu X; Cheng H; Zhang M; Zhao Y; Qu L; Shi G Graphene-Based Smart Materials. Nat. Rev. Mater 2017, 2, 17046.

(404). Hu Y; Wu G; Lan T; Zhao J; Liu Y; Chen W A Graphene-Based Bimorph Structure for Design of High Performance Photo-actuators. Adv. Mater 2015, 27, 7867–7873. [PubMed: 26498737]

(405). Hu Y; Liu J; Chang L; Yang L; Xu A; Qi K; Lu P; Wu G; Chen W; Wu Y Electrically and Sunlight-Driven Actuator with Versatile Biomimetic Motions Based on Rolled Carbon Nanotube Bilayer Composite. Adv. Funct. Mater 2017, 27, 1704388.

(406). Deng J; Li J; Chen P; Fang X; Sun X; Jiang Y; Weng W; Wang B; Peng H Tunable Photothermal Actuators Based on a Pre-Programmed Aligned Nanostructure. J. Am. Chem. Soc 2016, 138, 225–230. [PubMed: 26678012]

(407). Chini SF; Amirfazli A Understanding Pattern Collapse in Photolithography Process Due to Capillary Forces. Langmuir 2010, 26, 13707–13714. [PubMed: 20695624]

(408). Jones S; Andrén D; Karpinski P; Käll M Photothermal Heating of Plasmonic Nanoantennas: Influence on Trapped Particle Dynamics and Colloid Distribution. ACS Photonics 2018, 5, 2878–2887.

(409). Hidai H; Matsushita M; Matsusaka S; Chiba A; Morita N Moving Force of Metal Particle Migration Induced by Laser Irradiation in Borosilicate Glass. Opt. Express 2013, 21, 18955–18962. [PubMed: 23938809]

(410). Hidai H; Wada J; Iwamoto T; Matsusaka S; Chiba A; Kishi T; Morita N Experimental and Theoretical Study on the Driving Force and Glass Flow by Laser-Induced Metal Sphere Migration in Glass. Sci. Rep 2016, 6, 38545. [PubMed: 27934897]

(411). Nosonovsky M Model for Solid-Liquid and Solid-Solid Friction of Rough Surfaces with Adhesion Hysteresis. J. Chem. Phys 2007, 126, 224701. [PubMed: 17581074]

(412). Li J; Liu Y; Lin L; Wang M; Jiang T; Guo J; Ding H; Kollipara PS; Inoue Y; Fan D; et al. Optical Nanomanipulation on Solid Substrates Via Optothermally-Gated Photon Nudging. Nat. Commun 2019, 10, 5672. [PubMed: 31831746]

(413). Alam MS; Zhao C Nondestructive Approach for Additive Nanomanufacturing of Metallic Nanostructures in the Air. ACS Omega 2018, 3, 1213–1219. [PubMed: 31457963]

(414). Alam MS; Zhan Q; Zhao C Additive Opto-Thermomechanical Nanoprinting and Nanorepairing under Ambient Conditions. Nano Lett. 2020, 20, 5057–5064. [PubMed: 32502352]

(415). Ube T; Ikeda T Photomobile Polymer Materials with Crosslinked Liquid-Crystalline Structures: Molecular Design, Fabrication, and Functions. Angew. Chem., Int. Ed 2014, 53, 10290–10299.

(416). Warner M; Terentjev EM Liquid Crystal Elastomers; Oxford University Press: 2007; Vol. 120, pp 1–8.

(417). Leng J; Lan X; Liu Y; Du S Shape-Memory Polymers and Their Composites: Stimulus Methods and Applications. Prog. Mater. Sci 2011, 56, 1077–1135.

(418). Yang H; Leow WR; Wang T; Wang J; Yu J; He K; Qi D; Wan C; Chen X 3D Printed Photoresponsive Devices Based on Shape Memory Composites. Adv. Mater 2017, 29, 1701627.

(419). Zeng H; Wasylczyk P; Parmeggiani C; Martella D; Burresi M; Wiersma DS Light-Fueled Microscopic Walkers. Adv. Mater 2015, 27, 3883–3887. [PubMed: 26033690]

(420). Zeng H; Wani OM; Wasylczyk P; Kaczmarek R; Priimagi A Self-Regulating Iris Based on Light-Actuated Liquid Crystal Elastomer. Adv. Mater 2017, 29, 1701814.

(421). Zeng H; Wani OM; Wasylczyk P; Priimagi A Light-Driven, Caterpillar-Inspired Miniature Inching Robot. Macromol. Rapid Commun 2018, 39, 1700224.

(422). Zeng H; Lahikainen M; Liu L; Ahmed Z; Wani OM; Wang M; Yang H; Priimagi A Light-Fuelled Freestyle Self-Oscillators. Nat. Commun 2019, 10, 5057. [PubMed: 31700006]

(423). Rogó M; Zeng H; Xuan C; Wiersma DS; Wasylczyk P Light-Driven Soft Robot Mimics Caterpillar Locomotion in Natural Scale. Adv. Opt. Mater 2016, 4, 1689–1694.

(424). Gelebart AH; Vantomme G; Meijer E; Broer DJ Mastering the Photothermal Effect in Liquid Crystal Networks: A General Approach for Self-Sustained Mechanical Oscillators. Adv. Mater 2017, 29, 1606712.

(425). Wei W; Zhang Z; Wei J; Li X; Guo J Phototriggered Selective Actuation and Self-Oscillating in Dual-Phase Liquid Crystal Photonic Actuators. Adv. Opt. Mater 2018, 6, 1800131.

(426). Shahsavan H; Aghakhani A; Zeng H; Guo Y; Davidson ZS; Priimagi A; Sitti M Bioinspired Underwater Locomotion of Light-Driven Liquid Crystal Gels. Proc. Natl. Acad. Sci. U. S. A 2020, 117, 5125–5133. [PubMed: 32094173]

(427). Liu K; Cheng C; Cheng Z; Wang K; Ramesh R; Wu J Giant-Amplitude, High-Work Density Microactuators with Phase Transition Activated Nanolayer Bimorphs. Nano Lett. 2012, 12, 6302–6308. [PubMed: 23157372]

(428). Lahikainen M; Zeng H; Priimagi A Reconfigurable Photoactuator through Synergistic Use of Photochemical and Photothermal Effects. Nat. Commun 2018, 9, 4148. [PubMed: 30297774]

(429). Lu X; Zhang H; Fei G; Yu B; Tong X; Xia H; Zhao Y Liquid-Crystalline Dynamic Networks Doped with Gold Nanorods Showing Enhanced Photocontrol of Actuation. Adv. Mater 2018, 30, 1706597.

(430). Pilz da Cunha M; van Thoor EA; Debije MG; Broer DJ; Schenning AP Unravelling the Photothermal and Photomechanical Contributions to Actuation of Azobenzene-Doped Liquid Crystal Polymers in Air and Water. J. Mater. Chem. C 2019, 7, 13502–13509.

(431). Hikmet R Anisotropic Gels and Plasticized Networks Formed by Liquid Crystal Molecules. Liq. Cryst 1991, 9, 405–416.

(432). Bai Y; Zhang J; Wen D; Yuan B; Gong P; Liu J; Chen X Fabrication of Remote Controllable Devices with Multistage Responsiveness Based on a Nir Light-Induced Shape Memory Ionomer Containing Various Bridge Ions. J. Mater. Chem. A 2019, 7, 20723–20732.

(433). Yang Q; Peng C; Ren J; Zhao W; Zheng W; Zhang C; Hu Y; Zhang X A near-Infrared Photoactuator Based on Shape Memory Semicrystalline Polymers toward Light-Fueled Crane, Grasper, and Walker. Adv. Opt. Mater 2019, 7, 1900784.

(434). Wang T; Torres D; Fernández FE; Wang C; Sepúlveda N Maximizing the Performance of Photothermal Actuators by Combining Smart Materials with Supplementary Advantages. Sci. Adv 2017, 3, No. e1602697. [PubMed: 28439553]

(435). Wang T; Torres D; Fernández FE; Green AJ; Wang C; Sepúlveda N Increasing Efficiency, Speed, and Responsivity of Vanadium Dioxide Based Photothermally Driven Actuators Using Single-Wall Carbon Nanotube Thin-Films. ACS Nano 2015, 9, 4371–4378. [PubMed: 25853931]

(436). Fedoruk M; Lutich AA; Feldmann J Subdiffraction-Limited Milling by an Optically Driven Single Gold Nanoparticle. ACS Nano 2011, 5, 7377–7382. [PubMed: 21812459]

(437). Li J; Wang M; Wu Z; Li H; Hu G; Jiang T; Guo J; Liu Y; Yao K; Chen Z; et al. Tunable Chiral Optics in All-Solid-Phase Reconfigurable Dielectric Nanostructures. Nano Lett. 2021, 21, 973–979. [PubMed: 33372805]

(438). Ding T; Valev VK; Salmon AR; Forman CJ; Smoukov SK; Scherman OA; Frenkel D; Baumberg JJ Light-Induced Actuating Nanotransducers. Proc. Natl. Acad. Sci. U. S. A 2016, 113, 5503–5507. [PubMed: 27140648]

(439). Cormier S; Ding T; Turek V; Baumberg JJ Actuating Single Nano-Oscillators with Light. Adv. Opt. Mater 2018, 6, 1701281.

(440). Kim D; Lee HS; Yoon J Highly Bendable Bilayer-Type Photo-Actuators Comprising of Reduced Graphene Oxide Dispersed in Hydrogels. Sci. Rep 2016, 6, 20921. [PubMed: 26865239]

(441). Zheng C; Jin F; Zhao Y; Zheng M; Liu J; Dong X; Xiong Z; Xia Y; Duan X Light-Driven Micron-Scale 3D Hydrogel Actuator Produced by Two-Photon Polymerization Microfabrication. Sens. Actuators, B 2020, 304, 127345.

(442). Luo R; Wu J; Dinh ND; Chen CH Gradient Porous Elastic Hydrogels with Shape-Memory Property and Anisotropic Responses for Programmable Locomotion. Adv. Funct. Mater 2015, 25, 7272–7279.

(443). Mu J; Hou C; Wang H; Li Y; Zhang Q; Zhu M Origami-Inspired Active Graphene-Based Paper for Programmable Instant Self-Folding Walking Devices. Sci. Adv 2015, 1, No. e1500533. [PubMed: 26601135]

(444). Ji M; Jiang N; Chang J; Sun J Near-Infrared Light-Driven, Highly Efficient Bilayer Actuators Based on Polydopamine-Modified Reduced Graphene Oxide. Adv. Funct. Mater 2014, 24, 5412–5419.

(445). Shi Q; Li J; Hou C; Shao Y; Zhang Q; Li Y; Wang H A Remote Controllable Fiber-Type near-Infrared Light-Responsive Actuator. Chem. Commun 2017, 53, 11118–11121.

(446). Cai G; Ciou J-H; Liu Y; Jiang Y; Lee PS Leaf-Inspired Multiresponsive Mxene-Based Actuator for Programmable Smart Devices. Sci. Adv 2019, 5, No. eaaw7956. [PubMed: 31309158]

(447). Salmon AR; Cormier S; Wang W; Abell C; Baumberg JJ Motile Artificial Chromatophores: Light-Triggered Nanoparticles for Microdroplet Locomotion and Color Change. Adv. Opt. Mater 2019, 7, 1900951.

(448). Zong L; Li M; Li C Bioinspired Coupling of Inorganic Layered Nanomaterials with Marine Polysaccharides for Efficient Aqueous Exfoliation and Smart Actuating Hybrids. Adv. Mater 2017, 29, 1604691.

(449). Kwan K; Li S; Hau N; Li W-D; Feng S; Ngan AH Light-Stimulated Actuators Based on Nickel Hydroxide-Oxyhydroxide. Sci. Robot 2018, 3, No. eaat4051. [PubMed: 33141705]

(450). Arazoe H; Miyajima D; Akaike K; Araoka F; Sato E; Hikima T; Kawamoto M; Aida T An Autonomous Actuator Driven by Fluctuations in Ambient Humidity. Nat. Mater 2016, 15, 1084–1089. [PubMed: 27429210]

(451). Tai Y; Lubineau G; Yang Z Light-Activated Rapid-Response Polyvinylidene-Fluoride-Based Flexible Films. Adv. Mater 2016, 28, 4665–4670. [PubMed: 27061392]

(452). Li J; Zhang R; Mou L; Jung de Andrade M; Hu X; Yu K; Sun J; Jia T; Dou Y; Chen H; et al. Photothermal Bimorph Actuators with in-Built Cooler for Light Mills, Frequency Switches, and Soft Robots. Adv. Funct. Mater 2019, 29, 1808995.

(453). Li F; Pei C; Jiang L; Jin S Detaching and Moving of Adhered Particles with a Photoacoustic Micro-Resonator. Appl. Phys. Lett 2019, 114, 081905.

(454). Lu J; Li Q; Qiu C-W; Hong Y; Ghosh P; Qiu M Nanoscale Lamb Wave–Driven Motors in Nonliquid Environments. Sci. Adv 2019, 5, No. eaau8271. [PubMed: 30873431]

(455). Phillips WD Nobel Lecture: Laser Cooling and Trapping of Neutral Atoms. Rev. Mod. Phys 1998, 70, 721.

(456). Ashkin A History of Optical Trapping and Manipulation of Small-Neutral Particle, Atoms, and Molecules. IEEE J. Sel. Top. Quantum Electron 2000, 6, 841–856.

(457). Shuman ES; Barry JF; DeMille D Laser Cooling of a Diatomic Molecule. Nature 2010, 467, 820–823. [PubMed: 20852614]

(458). Enders M; Mukai S; Uwada T; Hashimoto S Plasmonic Nanofabrication through Optical Heating. J. Phys. Chem. C 2016, 120, 6723–6732.

(459). Osaka Y; Sugano S; Hashimoto S Plasmonic-Heating-Induced Nanofabrication on Glass Substrates. Nanoscale 2016, 8, 18187–18196. [PubMed: 27752691]

(460). Ravi-Kumar S; Lies B; Zhang X; Lyu H; Qin H Laser Ablation of Polymers: A Review. Polym. Int 2019, 68, 1391–1401.

(461). Morales AM; Lieber CM A Laser Ablation Method for the Synthesis of Crystalline Semiconductor Nanowires. Science 1998, 279 (5348), 208–211. [PubMed: 9422689]

(462). Vogel A; Venugopalan V Mechanisms of Pulsed Laser Ablation of Biological Tissues. Chem. Rev 2003, 103, 577–644. [PubMed: 12580643]

(463). Zeng H; Du XW; Singh SC; Kulinich SA; Yang S; He J; Cai W Nanomaterials Via Laser Ablation/Irradiation in Liquid: A Review. Adv. Funct. Mater 2012, 22, 1333–1353.

(464). Ciraulo B; Garcia-Guirado J; de Miguel I; Ortega Arroyo J; Quidant R Long-Range Optofluidic Control with Plasmon Heating. Nat. Commun 2021, 12, 2001. [PubMed: 33790293]

(465). Zheng J; Xing X; Yang J; Shi K; He S Hybrid Optofluidics and Three-Dimensional Manipulation Based on Hybrid Photothermal Waveguides. NPG Asia Mater. 2018, 10, 340–351.

(466). Chen J; Kang Z; Wang G; Loo JFC; Kong SK; Ho H-P Optofluidic Guiding, Valving, Switching and Mixing Based on Plasmonic Heating in a Random Gold Nanoisland Substrate. Lab Chip 2015, 15, 2504–2512. [PubMed: 25963226]

(467). Yan W; Zhao C; Luo W; Zhang W; Li X; Liu D Optically Guided Pyroelectric Manipulation of Water Droplet on a Superhydrophobic Surface. ACS Appl. Mater. Interfaces 2021, 13, 23181–23190. [PubMed: 33945247]

(468). Ma C; Yu P; Wang W; Zhu Y; Lin F; Wang J; Jing Z; Kong X-T; Li P; Govorov AO Chiral Optofluidics with a Plasmonic Metasurface Using the Photothermal Effect. ACS Nano 2021, 15, 16357. [PubMed: 34546029]

(469). Ghasemi H; Ni G; Marconnet AM; Loomis J; Yerci S; Miljkovic N; Chen G Solar Steam Generation by Heat Localization. Nat. Commun 2014, 5, 4449. [PubMed: 25043613]

(470). Chen C; Li Y; Song J; Yang Z; Kuang Y; Hitz E; Jia C; Gong A; Jiang F; Zhu J; et al. Highly Flexible and Efficient Solar Steam Generation Device. Adv. Mater 2017, 29, 1701756.

(471). Lehmuskero A; Ogier R; Gschneidtner T; Johansson P; Käll M Ultrafast Spinning of Gold Nanoparticles in Water Using Circularly Polarized Light. Nano Lett. 2013, 13, 3129–3134. [PubMed: 23777484]

(472). Arita Y; Richards JM; Mazilu M; Spalding GC; Skelton Spesyvtseva SE; Craig D; Dholakia K Rotational Dynamics and Heating of Trapped Nanovaterite Particles. ACS Nano 2016, 10, 11505–11510. [PubMed: 27966892]

(473). Lehmuskero A; Li Y; Johansson P; Käll M Plasmonic Particles Set into Fast Orbital Motion by an Optical Vortex Beam. Opt. Express 2014, 22, 4349–4356. [PubMed: 24663758]

(474). Rodriguez-Sevilla P; Lee T; Liang L; Haro-González P; Lifante G; Liu X; Jaque D Light-Activated Upconverting Spinners. Adv. Opt. Mater 2018, 6, 1800161.

(475). Unterkofler S; Garbos MK; Euser TG; Russell PSJ Long-Distance Laser Propulsion and Deformation- Monitoring of Cells in Optofluidic Photonic Crystal Fiber. J. Biophoton 2013, 6, 743–752.

(476). Schmidt OA; Garbos MK; Euser TG; Russell PSJ Reconfigurable Optothermal Microparticle Trap in Air-Filled Hollow-Core Photonic Crystal Fiber. Phys. Rev. Lett 2012, 109, 024502. [PubMed: 23030165]

(477). Meng F; Hao W; Yu S; Feng R; Liu Y; Yu F; Tao P; Shang W; Wu J; Song C; et al. Vapor-Enabled Propulsion for Plasmonic Photothermal Motor at the Liquid/Air Interface. J. Am. Chem. Soc 2017, 139, 12362–12365. [PubMed: 28837327]

(478). Luan T; Meng F; Tao P; Shang W; Wu J; Song C; Deng T Bubble-Enabled Underwater Motion of a Light-Driven Motor. Small 2019, 15, 1804959.

(479). Lee E; Huang D; Luo T Ballistic Supercavitating Nanoparticles Driven by Single Gaussian Beam Optical Pushing and Pulling Forces. Nat. Commun 2020, 11, 2404. [PubMed: 32415076]

(480). Lee E; Luo T Long-Distance Optical Pulling of Nanoparticle in a Low Index Cavity Using a Single Plane Wave. Sci. Adv 2020, 6, No. eaaz3646. [PubMed: 32671206]

(481). Zhang Y; Min C; Dou X; Wang X; Urbach HP; Somekh MG; Yuan X Plasmonic Tweezers: For Nanoscale Optical Trapping and Beyond. Light: Sci. Appl 2021, 10, 59. [PubMed: 33731693]

(482). Tan H; Hu H; Huang L; Qian K Plasmonic Tweezers for Optical Manipulation and Biomedical Applications. Analyst 2020, 145, 5699–5712. [PubMed: 32692343]

(483). Wang M; Zhao C; Miao X; Zhao Y; Rufo J; Liu YJ; Huang TJ; Zheng Y Plasmofluidics: Merging Light and Fluids at the Micro-/Nanoscale. Small 2015, 11, 4423–4444. [PubMed: 26140612]

(484). Peng X; Kotnala A; Rajeeva BB; Wang M; Yao K; Bhatt N; Penley D; Zheng Y Plasmonic Nanotweezers and Nanosensors for Point-of-Care Applications. Adv. Opt. Mater 2021, 9, 2100050. [PubMed: 34434691]

(485). Patra PP; Chikkaraddy R; Tripathi RPN; Dasgupta A; Kumar GVP Plasmofluidic Single-Molecule Surface-Enhanced Raman Scattering from Dynamic Assembly of Plasmonic Nanoparticles. Nat. Commun 2014, 5, 4357. [PubMed: 25000476]

(486). Patra PP; Chikkaraddy R; Thampi S; Tripathi RPN; Kumar GVP Large-Scale Dynamic Assembly of Metal Nanostructures in Plasmofluidic Field. Faraday Discuss. 2016, 186, 95–106. [PubMed: 26765282]

(487). Liang W; Liu L; Wang J; Yang X; Wang Y; Li WJ; Yang W A Review on Optoelectrokinetics-Based Manipulation and Fabrication of Micro/Nanomaterials. Micromachines 2020, 11, 78. [PubMed: 31936694]

(488). Zhang X; Mugisha ER; Mi Y; Liu X; Wang M; Gao Z; Gao K; Shi L; Chen H; Yan W Photovoltaic Cycling to-and-Fro Actuation of a Water-Microdroplet for Automatic Repeatable

Solute Acquisition on Oil-Infused Hydrophobic LN:Fe Surface. ACS Photonics 2021, 8, 639–647.

(489). Vella A; Shinde D; Houard J; Silaeva E; Arnoldi L; Blum I; Rigutti L; Pertreux E; Maioli P; Crut A; et al. Optothermal Response of a Single Silicon Nanotip. Phys. Rev. B: Condens. Matter Mater. Phys 2018, 97, 075409.

(490). Cui Y; Lieber CM Functional Nanoscale Electronic Devices Assembled Using Silicon Nanowire Building Blocks. Science 2001, 291, 851–853. [PubMed: 11157160]

(491). Reichl MR; Braun D Thermophoretic Manipulation of Molecules inside Living Cells. J. Am. Chem. Soc 2014, 136, 15955–15960. [PubMed: 25171388]

(492). Simoncelli S; Johnson S; Kriegel F; Lipfert J; Feldmann J Stretching and Heating Single Dna Molecules with Optically Trapped Gold–Silica Janus Particles. ACS Photonics 2017, 4, 2843–2851.

(493). Sanchez S; Ananth AN; Fomin VM; Viehrig M; Schmidt OG Superfast Motion of Catalytic Microjet Engines at Physiological Temperature. J. Am. Chem. Soc 2011, 133, 14860–14863. [PubMed: 21848337]

(494). Masuhara H; Yuyama K.-i. Optical Force-Induced Chemistry at Solution Surfaces. Annu. Rev. Phys. Chem 2021, 72, 565–589. [PubMed: 33567878]

(495). Shin JH; Seo J; Hong J; Chung SK Hybrid Optothermal and Acoustic Manipulations of Microbubbles for Precise and on-Demand Handling of Micro-Objects. Sens. Actuators, B 2017, 246, 415–420.

(496). Duhr S; Braun D Optothermal Molecule Trapping by Opposing Fluid Flow with Thermophoretic Drift. Phys. Rev. Lett 2006, 97, 038103. [PubMed: 16907547]

(497). Wu Z; Lin X; Wu Y; Si T; Sun J; He Q Near-Infrared Light-Triggered "on/Off" Motion of Polymer Multilayer Rockets. ACS Nano 2014, 8, 6097–6105. [PubMed: 24806430]

(498). Xie Y; Zhao C; Zhao Y; Li S; Rufo J; Yang S; Guo F; Huang TJ Optoacoustic Tweezers: A Programmable, Localized Cell Concentrator Based on Opto-Thermally Generated, Acoustically Activated, Surface Bubbles. Lab Chip 2013, 13, 1772–1779. [PubMed: 23511348]

(499). Guix M; Mayorga-Martinez CC; Merkoçi A Nano/Micromotors in (Bio) Chemical Science Applications. Chem. Rev 2014, 114, 6285–6322. [PubMed: 24827167]

(500). Wu K; Su D; Liu J; Saha R; Wang J-P Magnetic Nanoparticles in Nanomedicine: A Review of Recent Advances. Nanotechnology 2019, 30, 502003. [PubMed: 31491782]

(501). Dutz S; Hergt R Magnetic Particle Hyperthermia—a Promising Tumour Therapy? Nanotechnology 2014, 25, 452001. [PubMed: 25337919]

(502). Li J; Zheng Y Optothermally Assembled Nanostructures. Acc. Mater. Res 2021, 2, 352–363. [PubMed: 34396151]

(503). Palagi S; Singh DP; Fischer P Light-Controlled Micromotors and Soft Microrobots. Adv. Opt. Mater 2019, 7, 1900370.

(504). Daria VR; Eriksen RL; Glückstad J Dynamic Optical Manipulation of Colloidal Systems Using a Spatial Light Modulator. J. Mod. Opt 2003, 50, 1601–1614.

(505). Bowman RW; Gibson GM; Linnenberger A; Phillips DB; Grieve JA; Carberry DM; Serati S; Miles MJ; Padgett MJ Red Tweezers": Fast, Customisable Hologram Generation for Optical Tweezers. Comput. Phys. Commun 2014, 185, 268–273.

(506). Tanaka Y; Kawada H; Hirano K; Ishikawa M; Kitajima H Automated Manipulation of Non-Spherical Micro-Objects Using Optical Tweezers Combined with Image Processing Techniques. Opt. Express 2008, 16, 15115–15122. [PubMed: 18795050]

(507). Butaite UG; Gibson GM; Ho Y-LD; Taverne M; Taylor JM; Phillips DB Indirect Optical Trapping Using Light Driven Micro-Rotors for Reconfigurable Hydrodynamic Manipulation. Nat. Commun 2019, 10, 1215. [PubMed: 30872572]

(508). Yao K; Unni R; Zheng Y Intelligent Nanophotonics: Merging Photonics and Artificial Intelligence at the Nanoscale. Nanophotonics 2019, 8, 339–366. [PubMed: 34290952]

(509). Fang J; Swain A; Unni R; Zheng Y Decoding Optical Data with Machine Learning. Laser Photonics Rev. 2021, 15, 2000422.

(510). Wang H; Pumera M Coordinated Behaviors of Artificial Micro/Nanomachines: From Mutual Interactions to Interactions with the Environment. Chem. Soc. Rev 2020, 49, 3211–3230. [PubMed: 32307471]

(511). Šípová H; Shao L; Odebo Länk N; Andrén D; Käll M Photothermal DNA Release from Laser-Tweezed Individual Gold Nanomotors Driven by Photon Angular Momentum. ACS Photonics 2018, 5, 2168–2175.

(512). Bialkowski SE; Astrath NG; Proskurnin MA Photothermal Spectroscopy Methods; John Wiley & Sons: 2019; pp 1–56.

(513). Bustamante CJ; Chemla YR; Liu S; Wang MD Optical Tweezers in Single-Molecule Biophysics. Nat. Rev. Methods Primers 2021, 1, 25. [PubMed: 34849486]
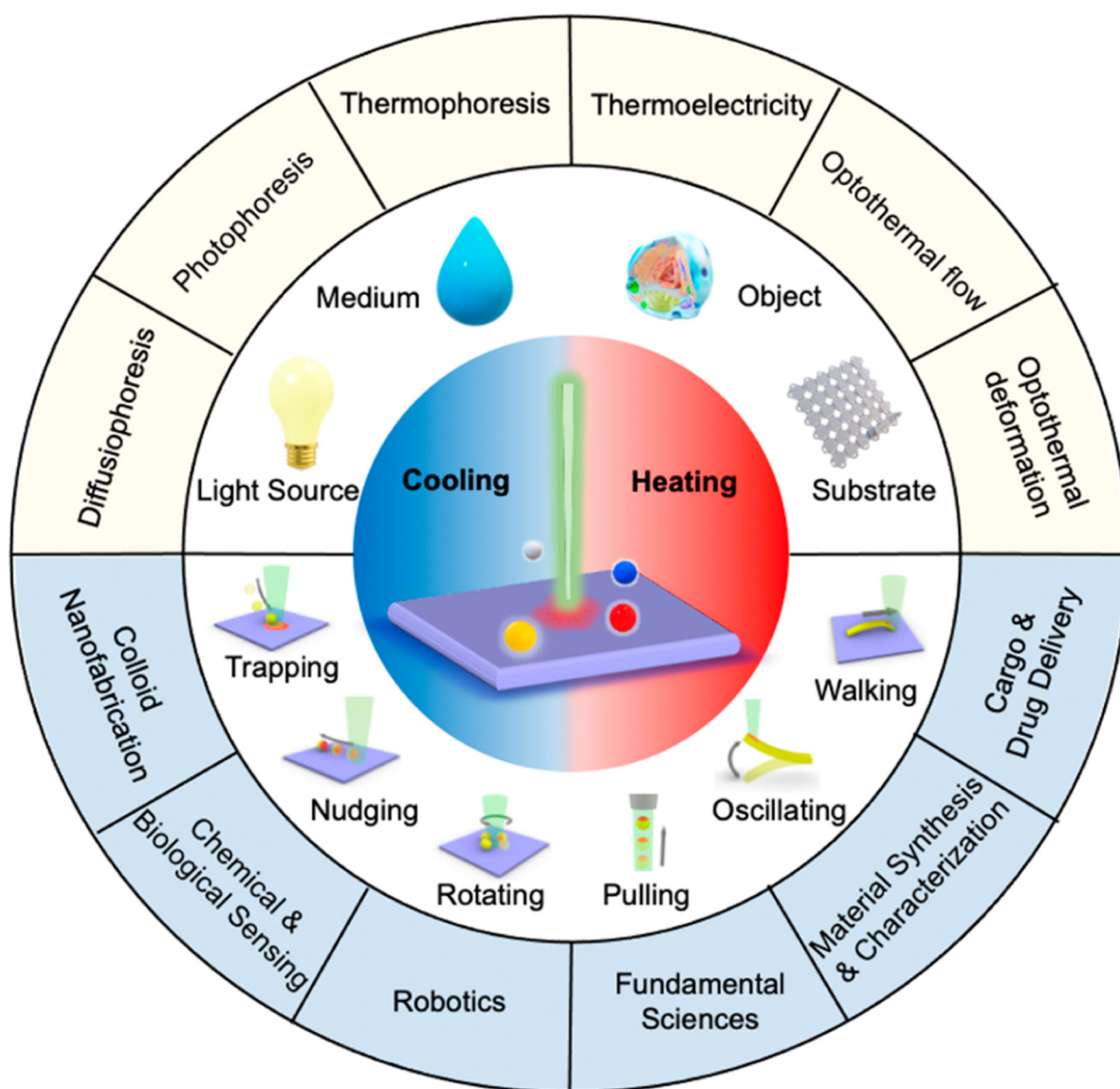
Figure 1.
Overview of heat-mediated optical manipulation. Efficient photothermal conversion leading to optical cooling or heating and diverse optothermo–matter coupling depending on the light source, medium, object, and substrate underpinning the versatile heat-mediated optical manipulation (e.g., trapping, nudging, rotating, pulling, oscillating, and walking). A variety of working mechanisms, including diffusiophoresis, photophoresis, thermophoresis, thermoelectricity, optothermal flows, and optothermal deformation, have been proposed for heat-mediated optical manipulation, leading to its applications in various fields such as colloid nanofabrication, chemical and biological sensing, material synthesis and characterization, robotics, fundamental sciences, and cargo and drug delivery.
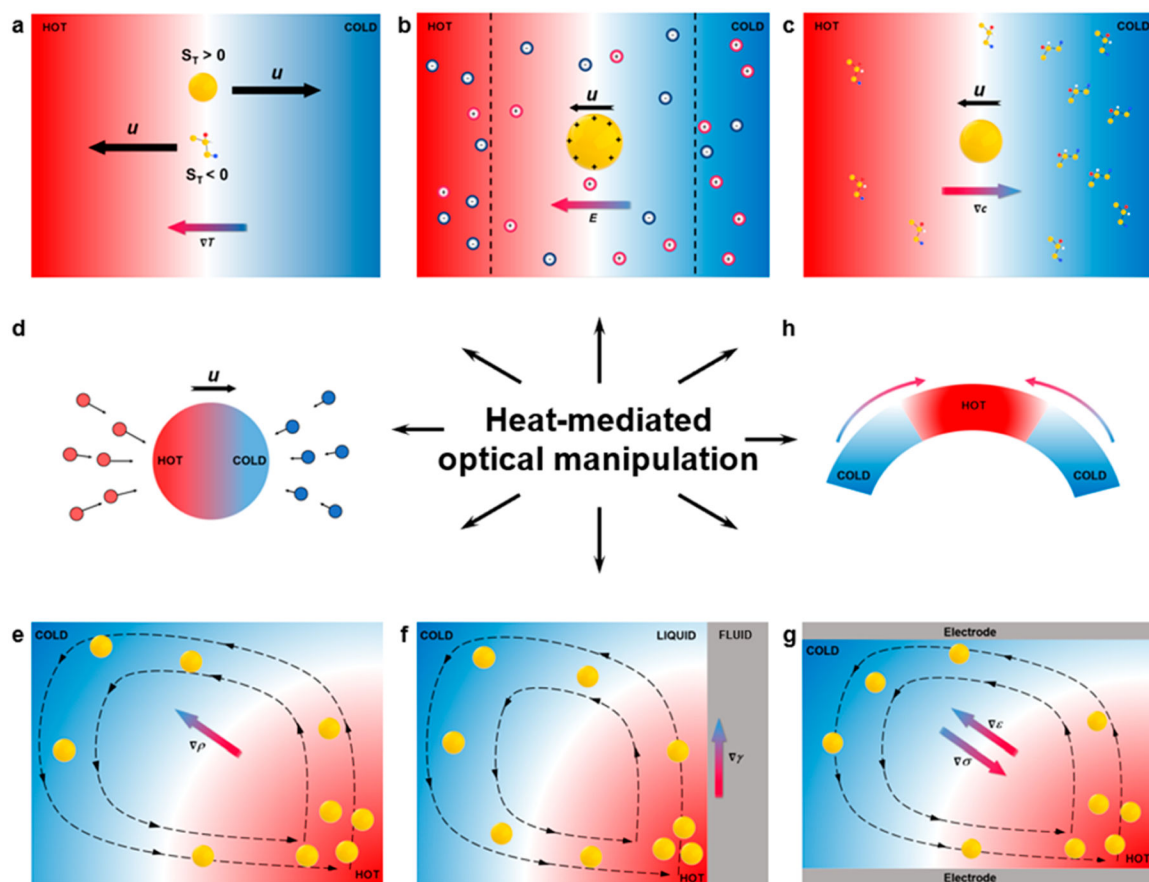
Figure 2.
Schematics of physical mechanisms for heat-mediated optical manipulation: (a) thermophoresis, (b) thermoelectricity, (c) heat-mediated diffusiophoresis, (d) photophoresis (ΔT force), (e) natural convection, (f) heat-mediated Marangoni convection, (g) electrothermoplasmonic flow, and (h) optothermal shape deformation.
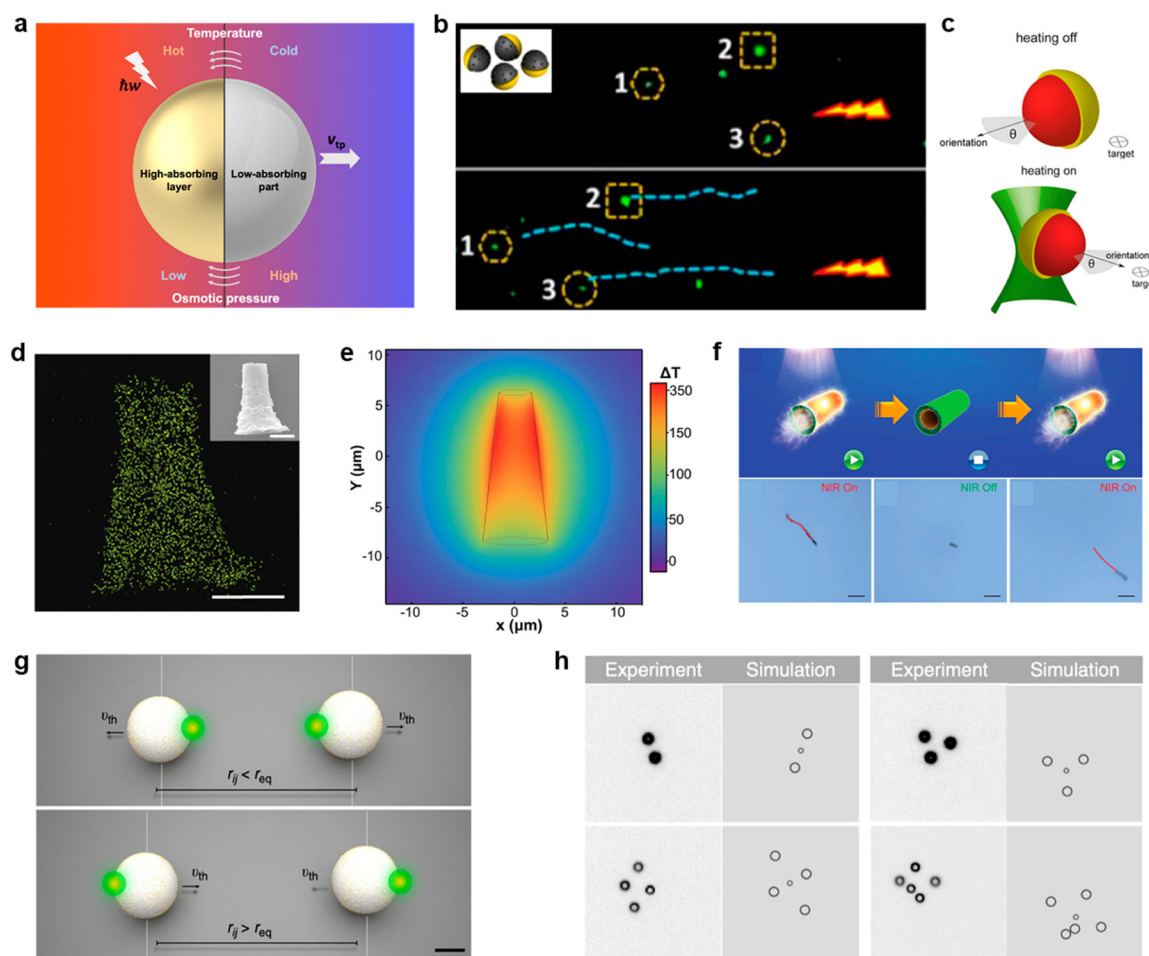
Figure 3.
Optothermophoretic swimmers. (a) Schematic showing the working mechanism of optothermophoretic swimmers based on self-thermophoresis. v_{tp} is the thermophoretic velocity of the swimmer. (b) Time-revolved optical images of 80 nm Janus swimmers triggered by the NIR laser. The inset shows the schematic of the Janus swimmers. Adapted with permission from ref 184. Copyright 2016 American Chemical Society. (c) Schematic showing the working principle of directional control of self-thermophoretic swimmers. θ is the acceptance angle for directional target delivery. Adapted with permission from ref 179. Copyright 2014 American Chemical Society. (d) Energy-dispersive X-ray spectroscopy (EDX) mapping of the tubular rocket with Au nanoshells. The inset shows the corresponding scanning electron micrograph. Scale bars: 2 μm. (e) Simulated steady-state temperature distribution of the rocket under laser illumination. (f) Schematic (top) and time-lapsed optical images showing the thermophoretic motions of the rocket. Scale bars: 20 μm. Adapted with permission from ref 180. Copyright 2016 Wiley-VCH. (g) Schematic of the pair interaction rule used to keep active particles (i.e., swimmers) at a constant interparticle distance. r_{ij} and r_{eq} represent the real-time distance and prescribed separation distance between two particles, respectively. Scale bar: 7 μm. (h) Simulations and experimental demonstrations of different structures arising from the interacting active particles based on

the pair interaction rule. Adapted with permission from ref 10. Copyright 2018 Springer Nature.
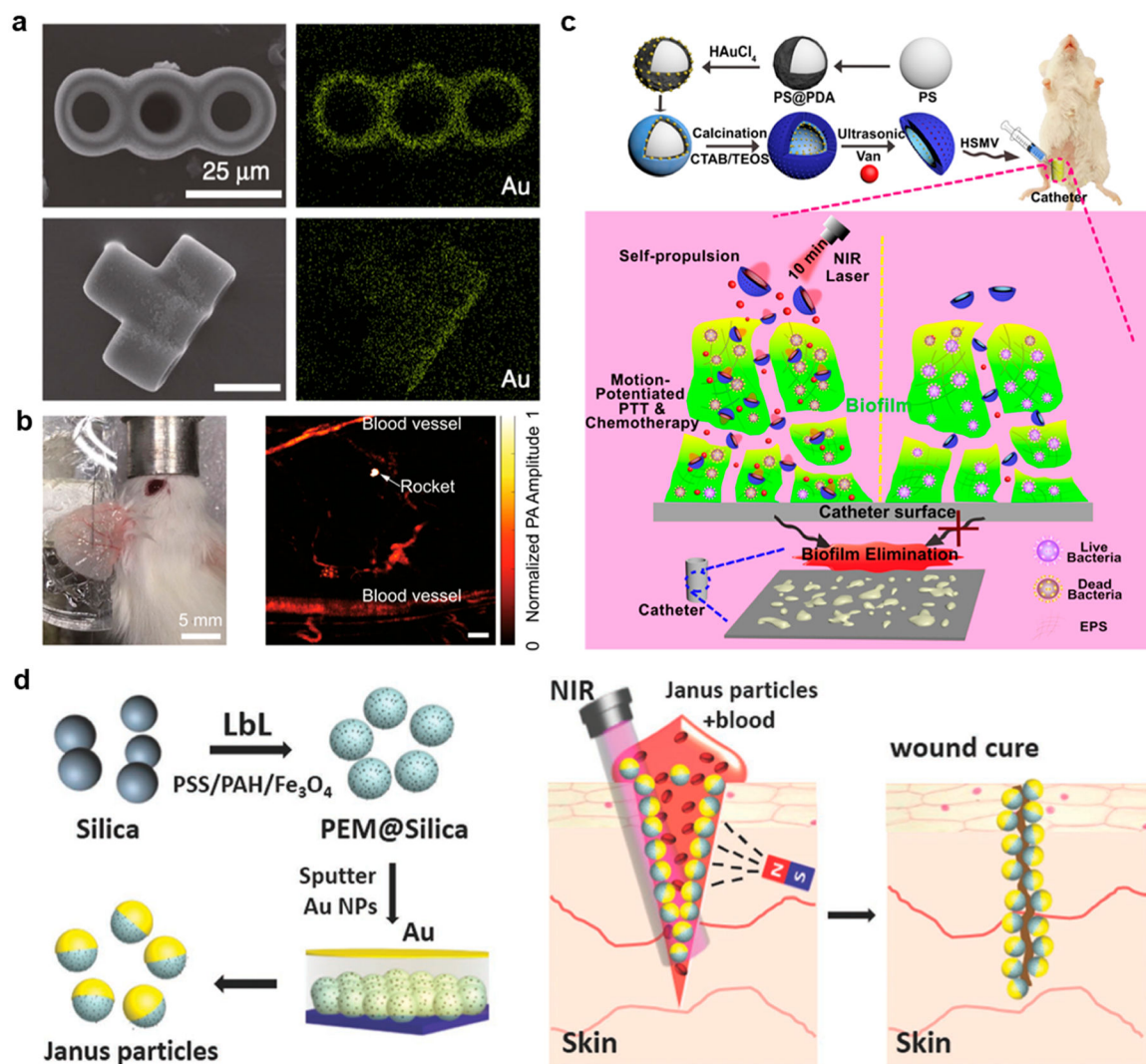
Figure 4.
Optothermophoretic swimmers for biological applications. (a) Top and side views of the EDX mapping of the Au-coated microrockets. (b) Optical image (left) and corresponding photoacoustic image (right) showing the tracking of the microrocket beneath a mouse ear. Adapted with permission from ref 203. Copyright 2020 Springer Nature. (c) Schematic showing the working principle of combined photothermal therapy and chemotherapy with the help of mesoporous Au-silica half-shell swimmers. HSMV and PTT represent half-shell motors and photothermal therapy, respectively. Adapted with permission from ref 204. Copyright 2020 American Chemical Society. (d) Schematic showing the swimming particle synthesis (left) and tissue welding process (right) assisted by NIR laser and magnetic fields. LbL, layer-by-layer assembly. Adapted with permission from ref 207. Copyright 2016 Wiley-VCH.
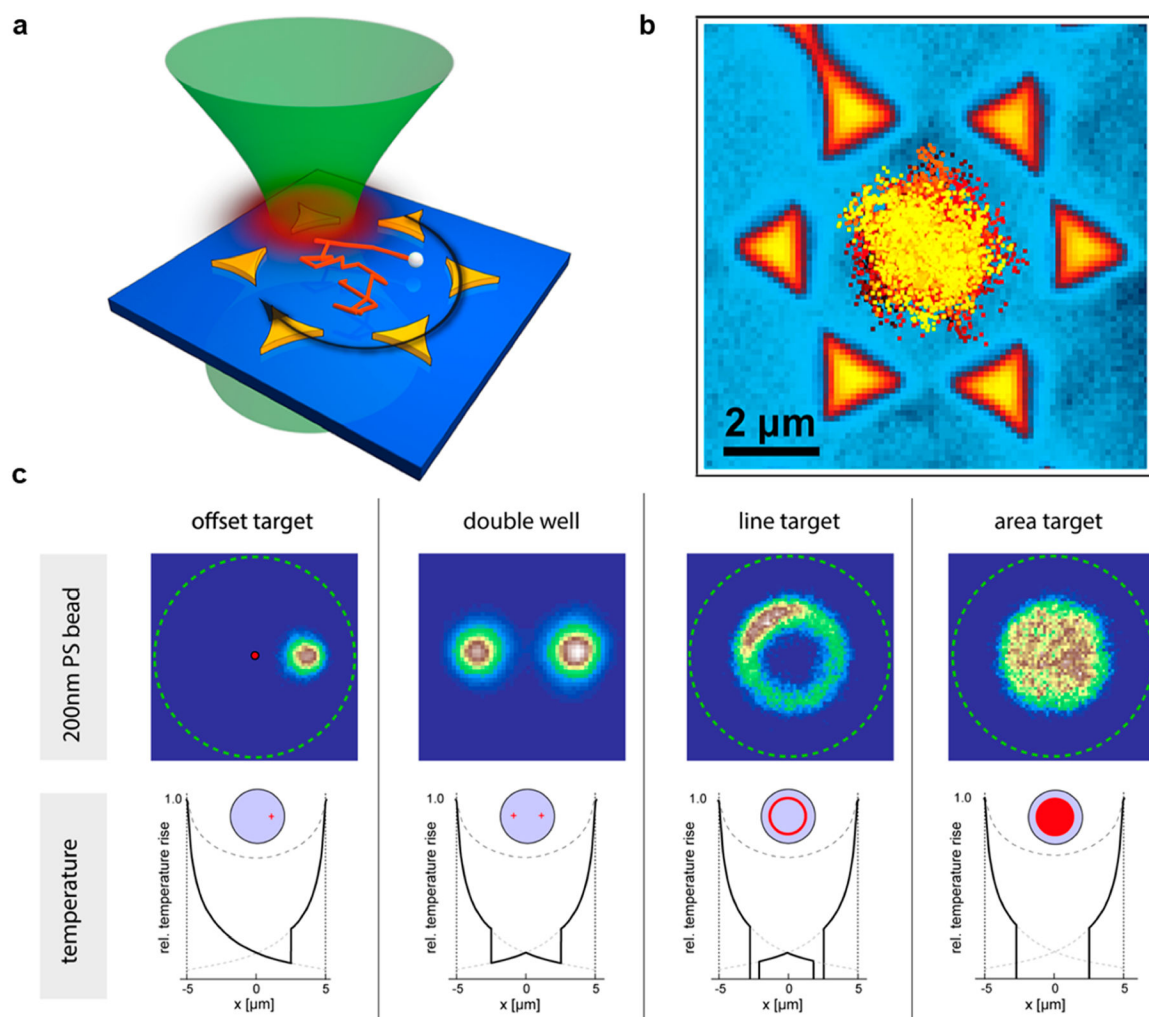
Figure 5.
Optothermophoretic trapping of thermophobic objects. (a) Schematic and (b) trajectory points showing the thermophoretic trapping of a 200 nm PS bead under a rotating laser beam. Adapted with permission from ref 208. Copyright 2013 American Chemical Society. (c) Different trapping modes based on different feedback-control rules of the heating laser. The top row represents the probability density distribution of trapped particles, and the bottom one shows the corresponding temperature rise. Adapted with permission from ref 210. Copyright 2015 American Chemical Society.
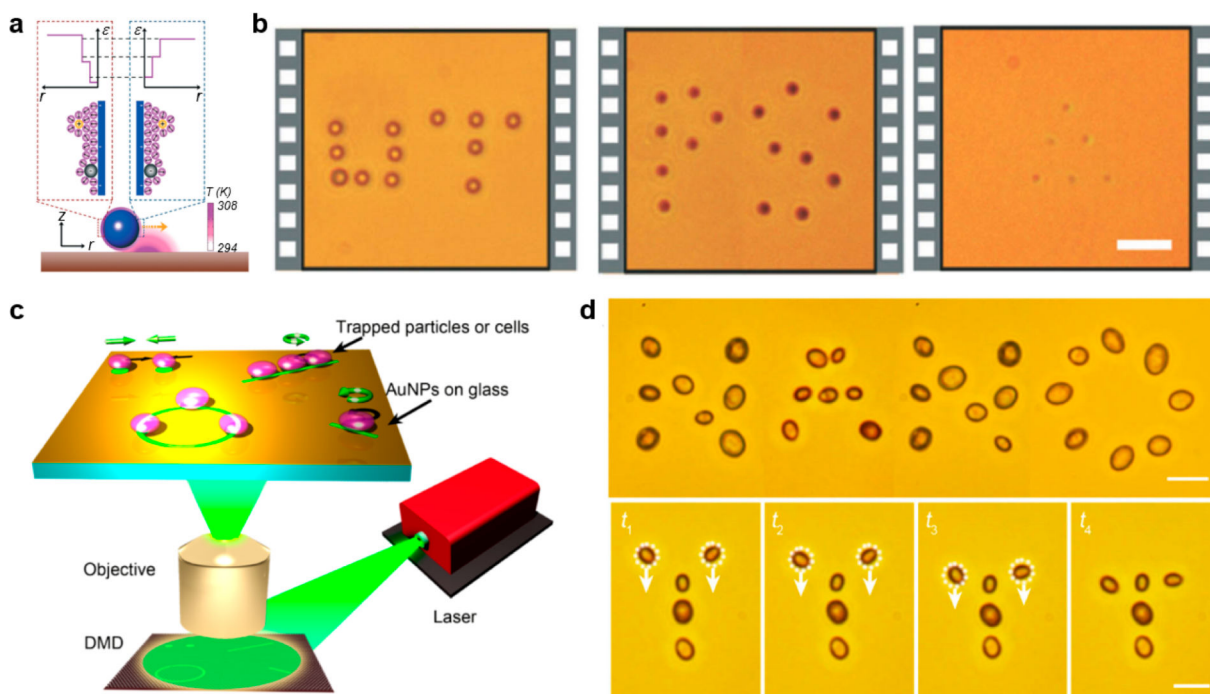
Figure 6.
Optothermophoretic tweezers. (a) Schematic showing the working principle of entropy-driven optothermophoretic tweezers. (b) Optical images of parallel trapping of PS beads with different sizes. Scale bar: 10 μm. Adapted with permission from ref 214. Copyright 2017 The Royal Society of Chemistry. (c) Optical setup integrated with a DMD for the versatile manipulation of colloidal particles or biological cells. (d) Parallel trapping and dynamic manipulation of yeast cells. Scale bar: 10 μm. Adapted with permission from ref 221. Copyright 2017 American Chemical Society.
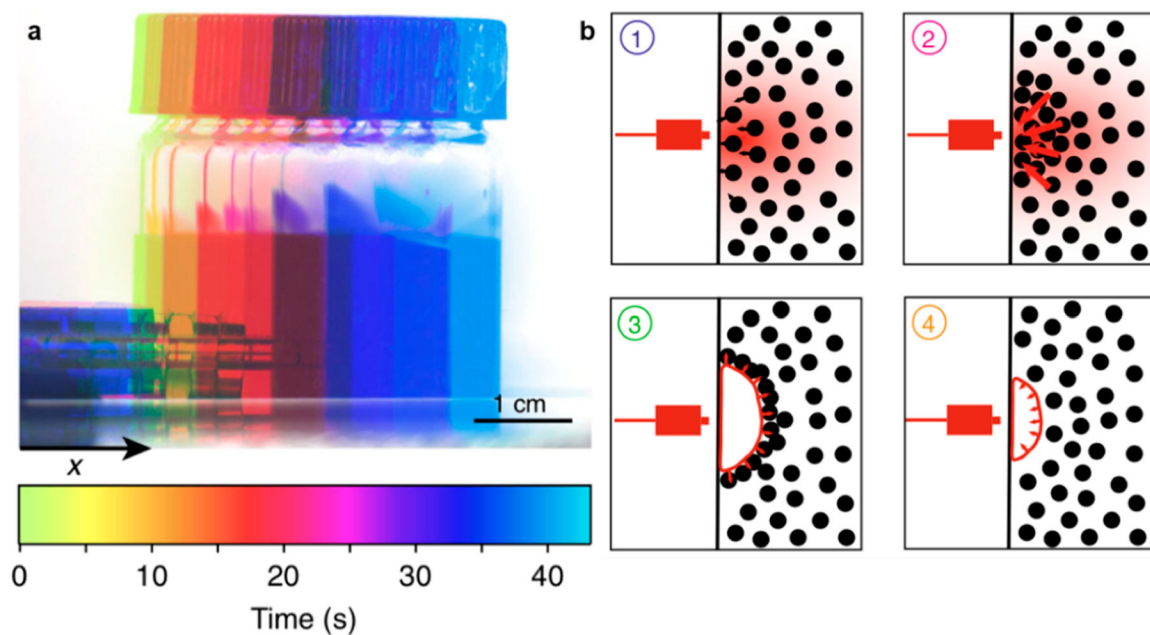
Figure 7.
Optothermophoretic manipulation at the macroscopic scale. (a) Time-elapsed optical images showing the macroscopic motion of a vial that contains a concentrated solution of lead sulfide nanoparticles in cyclohexane. The image is a superposition of 10 snapshots of the vial position, in which different colors represent different photographing moments. (b) Schematic showing the optothermophoretic mechanism underlying the vial's motion. Adapted with permission from ref 71. Copyright 2020 Springer Nature.
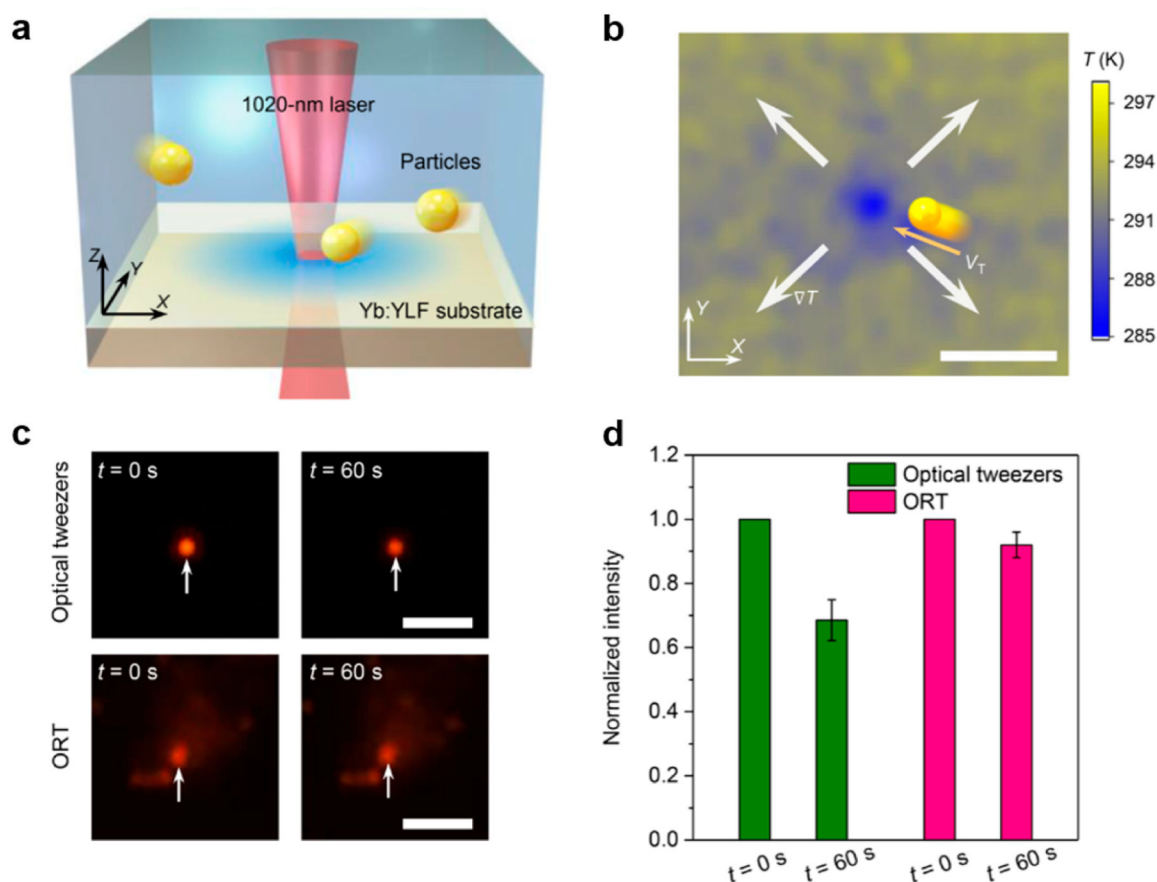
Figure 8.

Opto-refrigerative tweezers. (a) Schematic of the localized laser cooling of the Yb-doped YLiF$_4$ substrate and the thermophoretic trapping of particles at the cold spot. (b) Measured in-plane temperature distribution at the solution–substrate interface under laser cooling with an optical intensity of 25.8 mW μm^{-2}. Scale bar: 10 μm (c) Optical images and (d) normalized fluorescence intensity of a single 200 nm PS nanoparticle before and after being trapped by optical tweezers and ORT for 1 min. Scale bar: 5 μm. Adapted with permission from ref 98. Copyright 2021 American Association for the Advancement of Science.
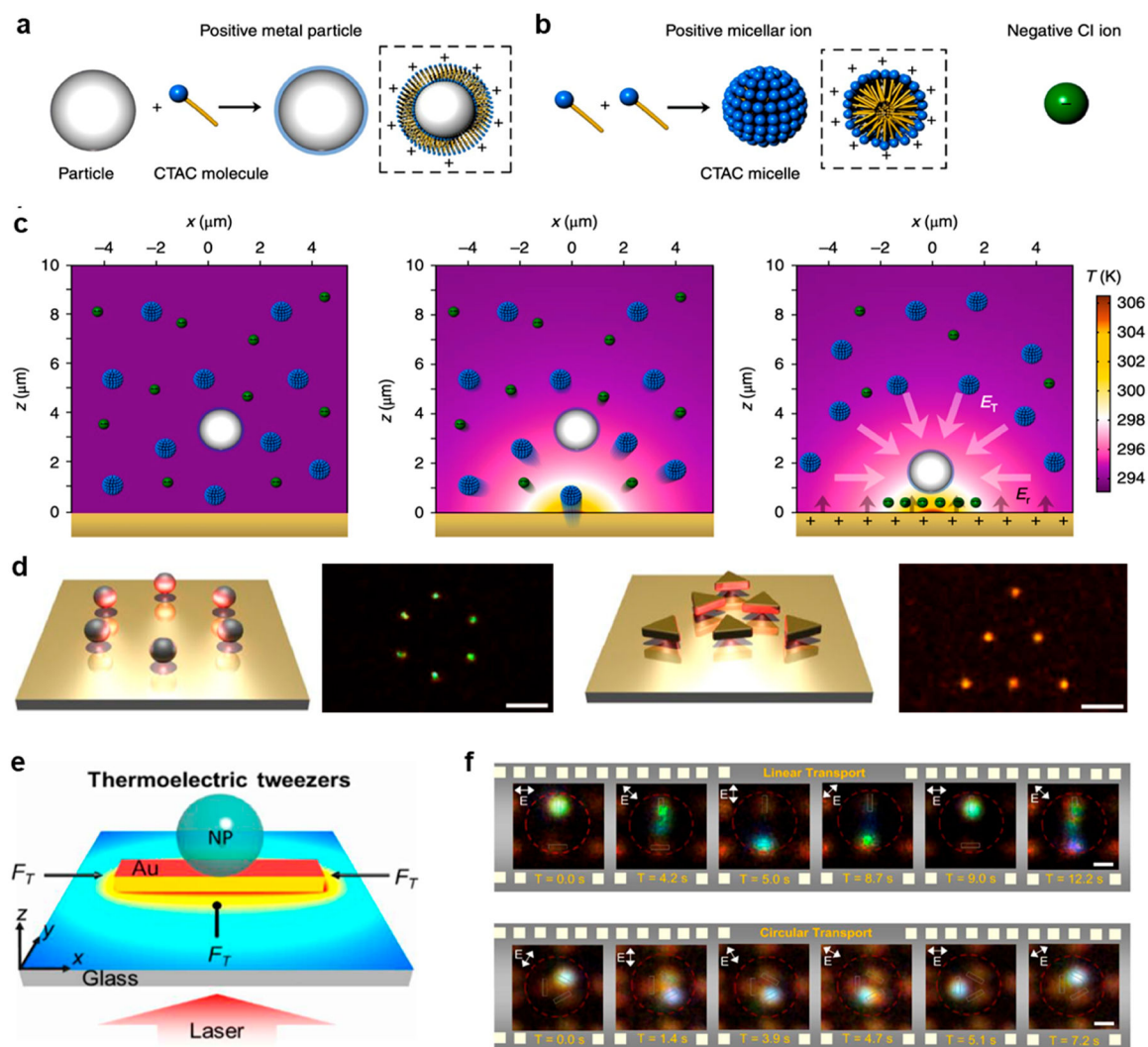
Figure 9.
Opto-thermoelectric tweezers. (a) Schematic showing the surface modification of particles by CTAC. (b) Schematic of CTAC micelles and Cl⁻ ions. (c) Schematic showing the working principle of OTENT. (d) Parallel trapping of six 100 nm silver nanospheres into a circular pattern (top) and six 140 nm gold nanotriangles into a triangular pattern (bottom). Scale bars: 5 μm. Adapted with permission from ref 224. Copyright 2018 Springer Nature. (e) Schematic of OTENT based on Au nanoantennas to trap a single nanoparticle (NP). (f) Successive dark-field optical images showing the polarization-controlled linear transport and circular transport of metal nanoparticles on Au nanorod arrays. Scale bar: 500 nm. Adapted with permission from ref 62. Copyright 2018 American Chemical Society.
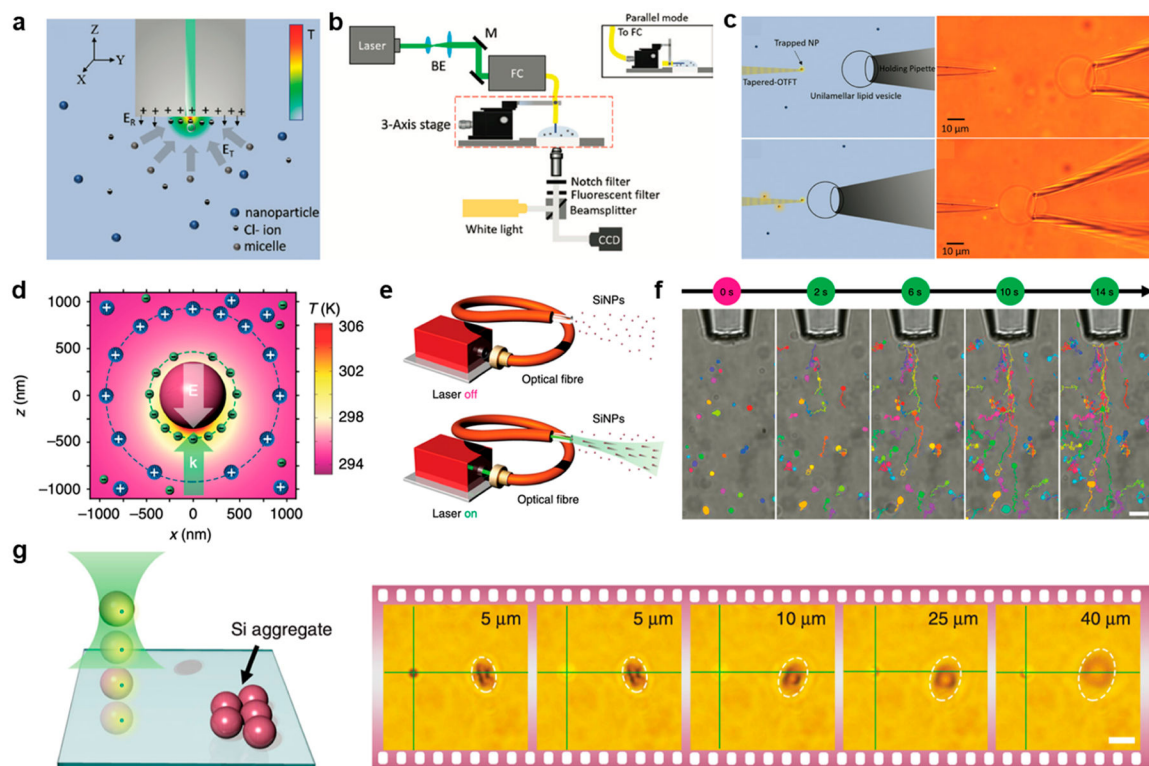
Figure 10.
3D opto-thermoelectric trapping and manipulation. (a) Schematic illustration of the working principle and (b) optical setup of opto-thermoelectric fiber tweezers (OTFT). BE, beam expander; M, mirror; FC, fiber coupler; CCD, charge-coupled device. (c) Schematics and optical images showing the single-particle delivery to a lipid vesicle. Adapted with permission from ref 229. Copyright 2019 De Gruyter. (d) Schematic of the ionic distribution, temperature field, and corresponding thermoelectric field E on a SiNP. k indicates the wave vector of the incident light. (e) Schematic of the experimental setup for opto-thermoelectric pulling. (f) Sequential optical images showing opto-thermoelectric pulling of 500 nm SiNPs. (g) Schematic and optical images showing the out-of-plane transport of a fluorescence PS bead using a single Si particle as a shuttle. Scale bar: 5 μm. Adapted with permission from ref 146. Copyright 2020 Springer Nature.
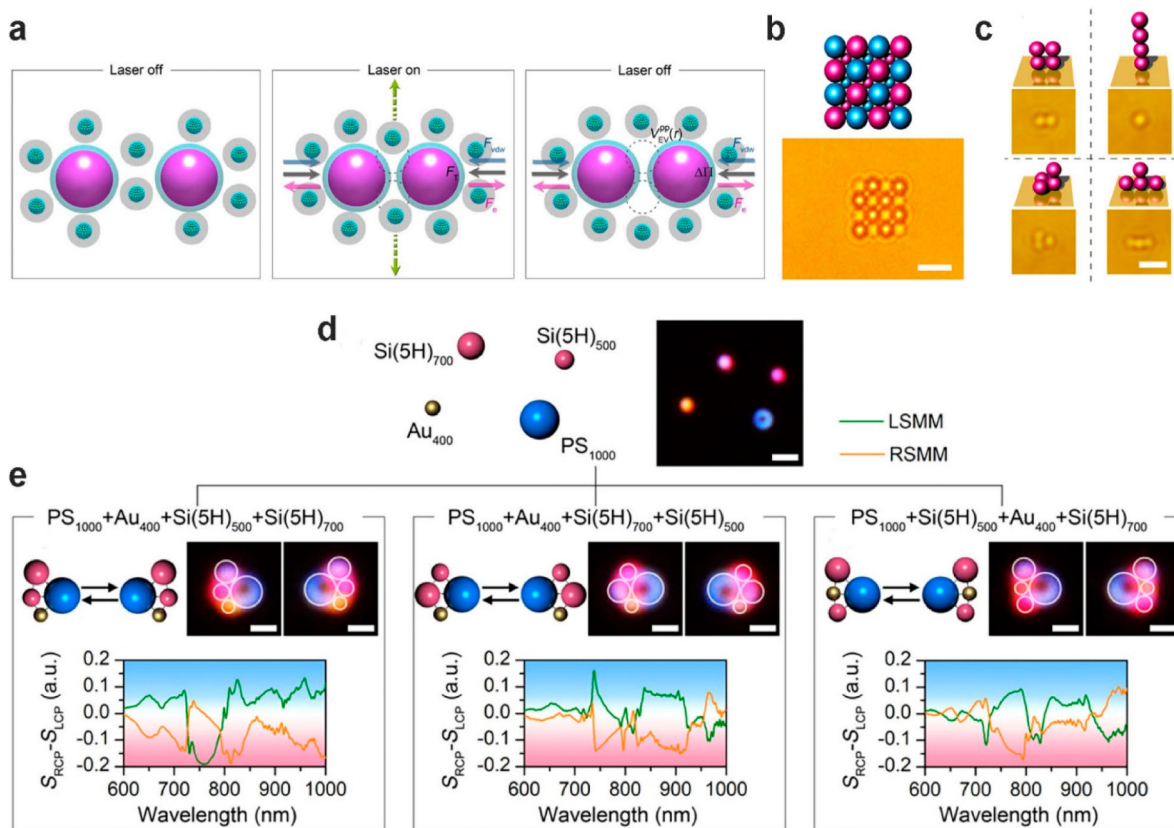
Figure 11.
Opto-thermoelectric assembly of colloidal matter. (a) Schematic of the working principle of optothermal assembly. (b) 2D hybrid superlattice of silica and PS beads with various sizes. Scale bar: 5 μm. (c) 3D assembly of PS beads. Scale bar: 2 μm. Adapted with permission from ref 230. Copyright 2017 American Association for the Advancement of Science. (d) Schematic and optical images of dispersed particles as the meta-atoms to build chiral meta-molecules. (e) Schematic, optical images, and differential scattering spectra of three sets of reconfigurable chiral meta-molecules with different configurations. LSMM/RSMM indicate left-handed/right-handed meta-molecules. S_{RCP} and S_{LCP} are the scattering spectra of meta-molecules under right-handed and left-handed circularly polarized light illumination, respectively. Adapted with permission from ref 232. Copyright 2019 Elsevier.
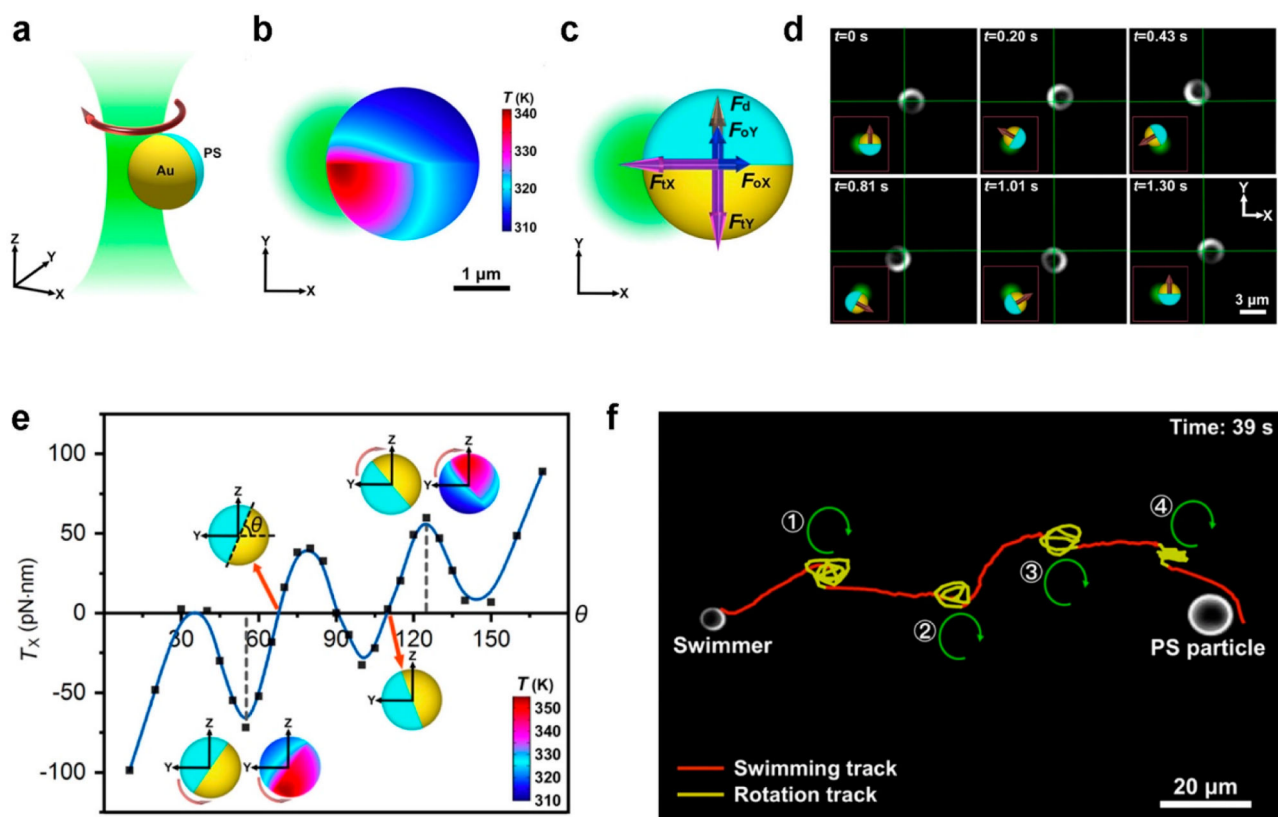
Figure 12.
Opto-thermoelectric swimmers. (a) Schematic of the rotation of a PS/Au Janus particle under a focused laser beam. (b) Simulated temperature profile of the Janus particle. (c) Schematic of force analysis. (d) Time-resolved dark-field images showing the rotation of a Janus particle. (e) Calculated thermoelectric torques as a function of angle θ, which is defined as the angle between the PS/Au interface relative to the substrate. (f) Trajectory of a Janus particle transported to a predesigned target. Adapted with permission from ref 235. Copyright 2020 Springer Nature.
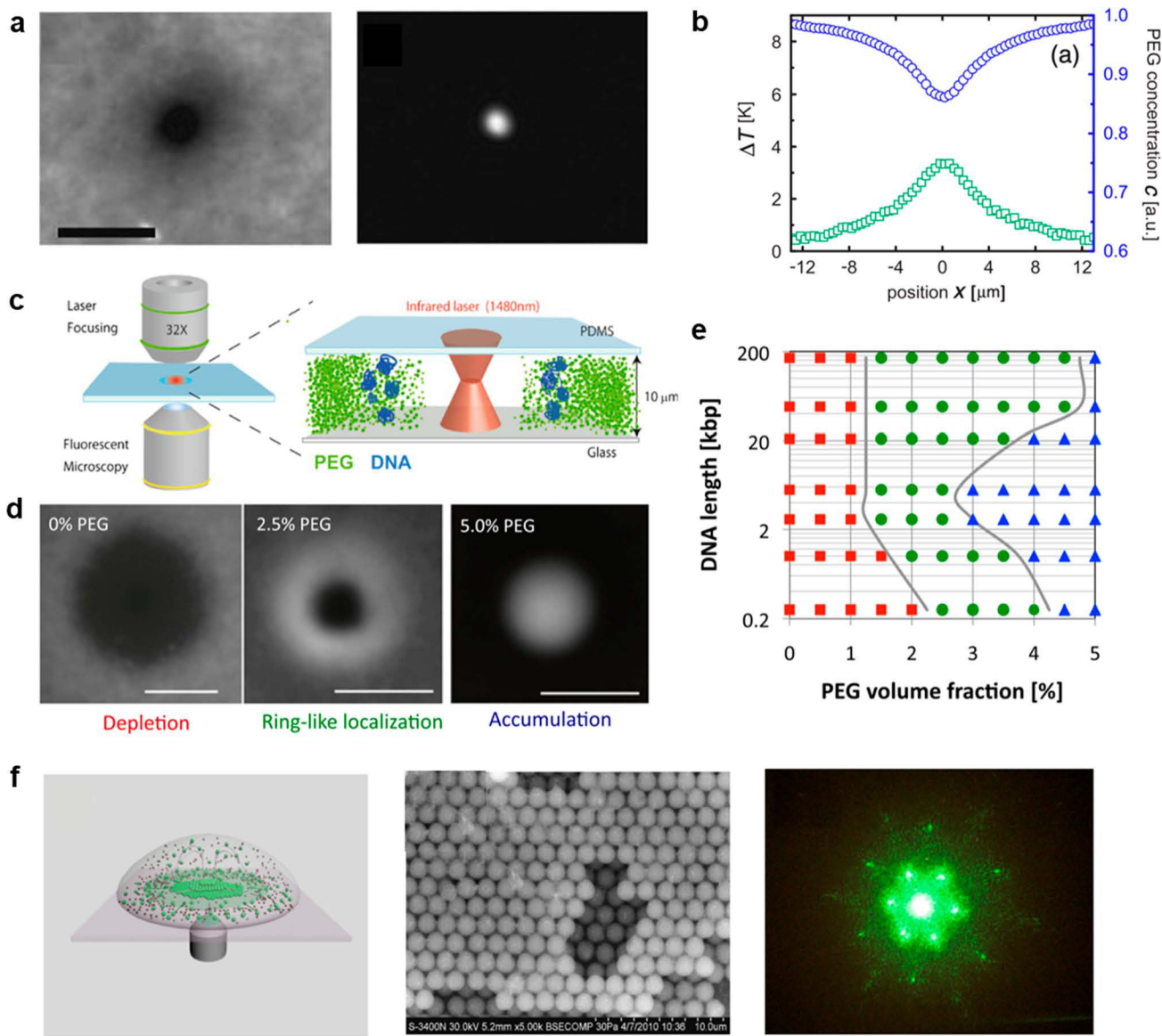
Figure 13.
Concentration and assembly of objects based on optothermally induced depletion force. (a) Fluorescence intensity of 100 nm PS beads under laser heating in a solution with 0% PEG (left) or 5% PEG (right). Scale bar: 10 μm. (b) Temperature (green) and density (blue) of PEG as a function of the distance from the laser beam center. Adapted with permission from ref 14. Copyright 2009 American Physical Society. (c) Schematic showing the optical setup and working principle of DNA accumulation assisted by the concentration gradient of PEG molecules upon laser heating. (d) Optical images showing the distribution of DNA (bright part) in 0%, 2.5%, and 5.0% PEG solutions, respectively. Scale bar: 35 μm. (e) Phase diagram of depletion (red), ringlike localization (green), and accumulation (blue) of DNA molecules as a function of the DNA length and PEG volume fraction. Adapted with permission from ref 237. Copyright 2012 National Academy of Sciences. (f) Schematic (left), scanning electron micrograph (middle), and optical diffraction pattern (right) of the

3D colloidal photonic crystals formed in a mixture of 1.6 μm silica beads and 12 nm magnetic nanoparticles under local laser illumination. Adapted with permission from ref 144. Copyright 2012 The Optical Society.
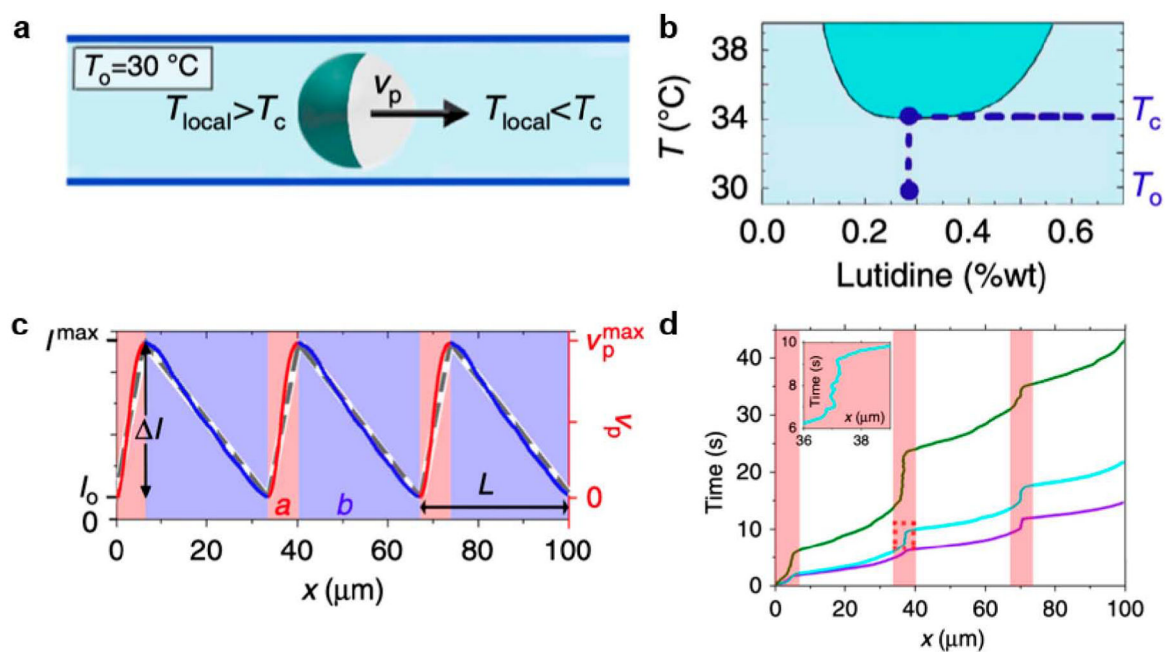
Figure 14.

Optothermal diffusiophoretic microswimmers in binary critical mixtures. (a) Schematic of the working mechanism of optothermal diffusiophoretic microswimmers. (b) Phase diagram of the binary critical mixture of water–2,6-lutidine. The dark-colored region indicates the demixing region of binary mixtures. (c) Experimental (solid line) and numerical (dashed line) intensity profiles. a and b represent the lengths of positive and negative ∇I, respectively. v_p represents the velocity of the illuminated particle. (j) Particle trajectories under different ∇I. The inset shows the back-and-forth motion of a particle of the framed region. Adapted with permission from ref 181. Copyright 2016 Springer Nature.
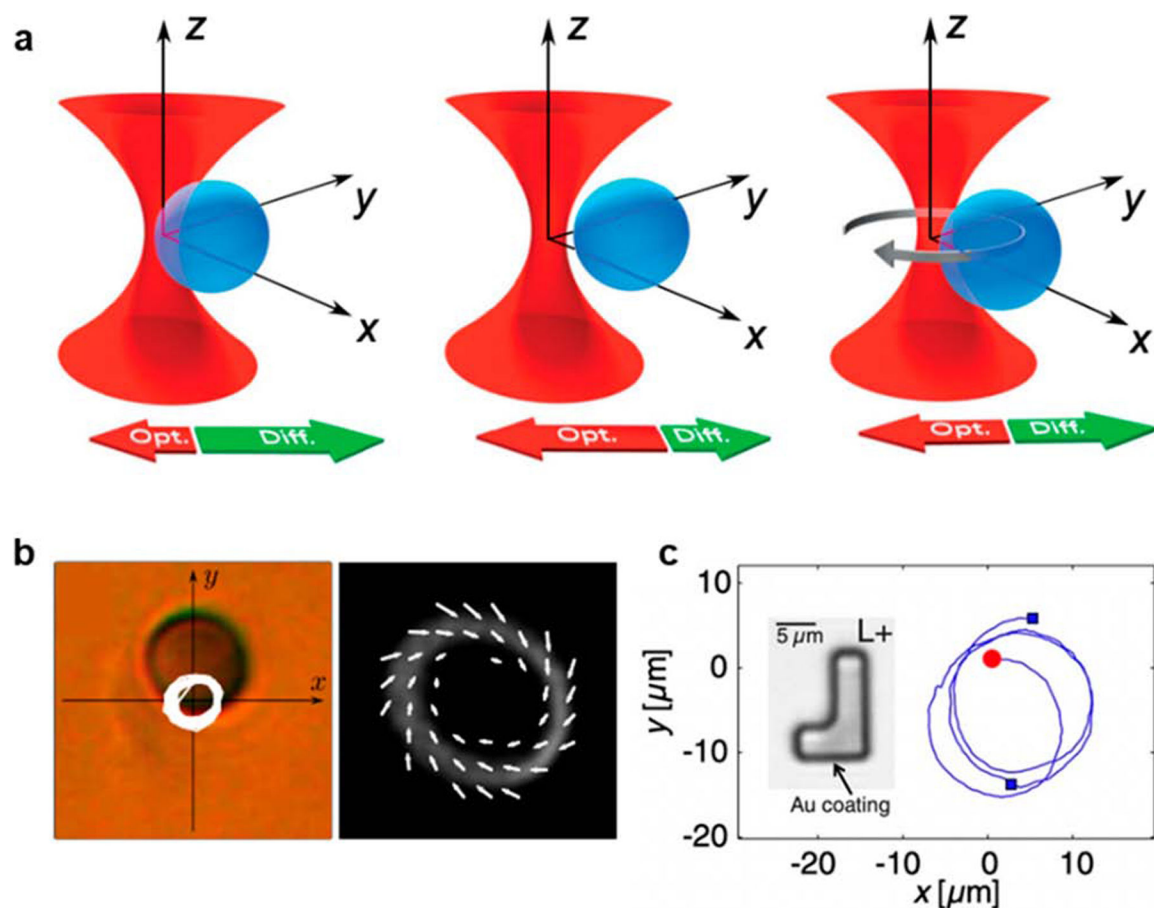
Figure 15.
Optothermal diffusiophoretic rotors. (a) Schematic showing the balance between optical force (red arrows) and diffusiophoretic force (green arrows) on an optically trapped microsphere as a rotor in a critical mixture. (b) Bright-field image of the trajectories of the microsphere within 0.6 s (left) and velocity drift fields (white arrows) with particle position probability distributions (the brighter color indicates the higher probability density) (right). Adapted with permission from ref 255. Copyright 2018 American Physical Society. (c) Trajectories of an L-shaped rotor with an asymmetric gold coating. The inset is the optical image of the rotor. The red circle and blue squares indicate the initial particle position and the positions after rotation for 1 min, respectively. Adapted with permission from ref 262. Copyright 2013 American Physical Society.
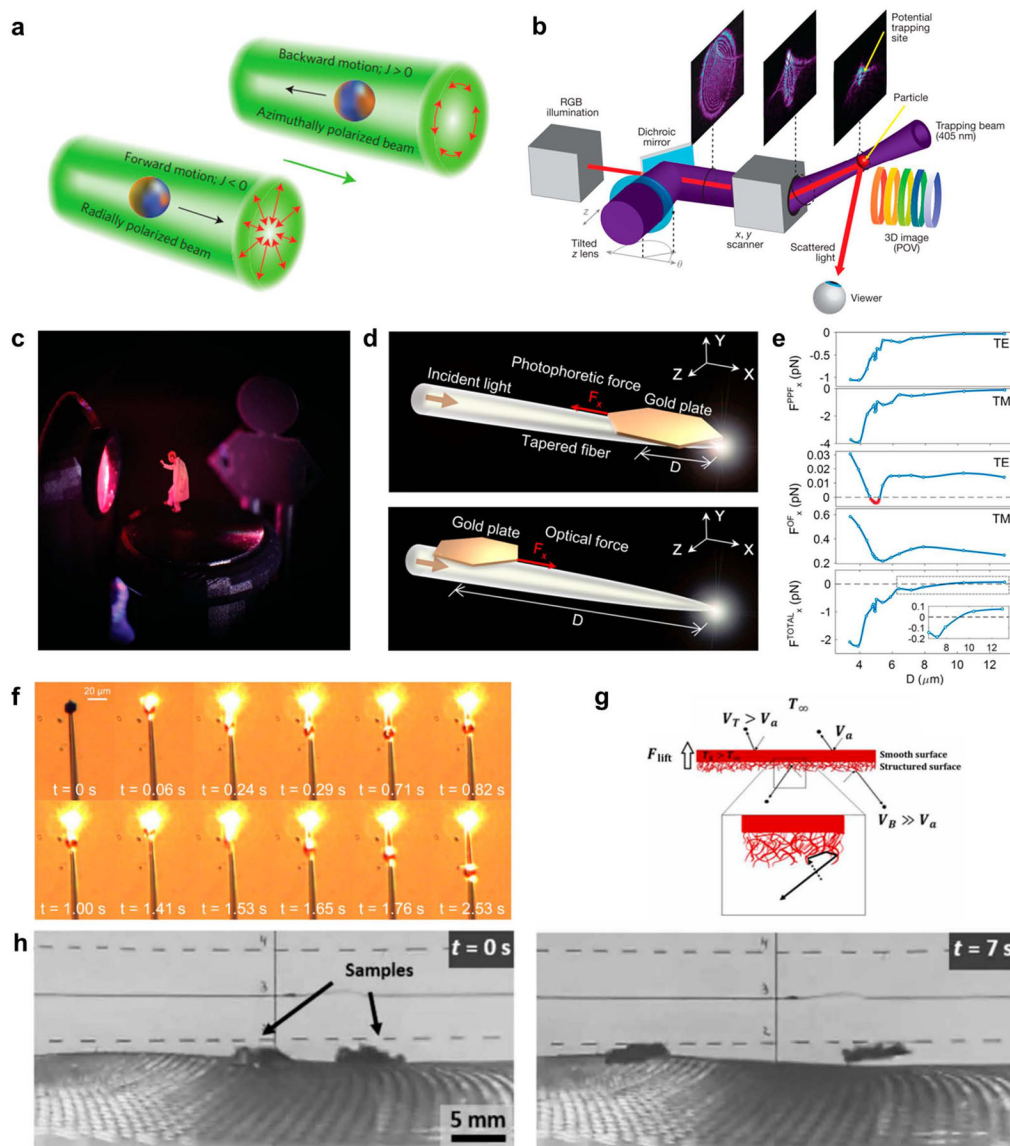
Figure 16.
Photophoretic manipulation. (a) Schematic showing the positive/negative photophoretic transportation controlled by the polarization state of an incident laser beam. J is an asymmetric parameter. Adapted with permission from ref 276. Copyright 2014 Springer Nature. (b) Schematic showing the working principle of the volumetric display based on photophoretic trapping of single particles. (c) Optical image demonstrating the projected image of a human configuration created by the volumetric display. Adapted with permission from ref 281. Copyright 2018 Springer Nature. (d) Schematic showing photophoretic pulling (top) and pushing (bottom) of a hexagonal gold plate on a tapered fiber in ambient air. (e) Calculated photophoretic force, optical force, and total light-induced force as a function of the distance along with the tapered fiber. (f) Optical images of a back-and-forth moving gold plate on a tapered fiber in ambient air. Adapted with permission from ref 282. Copyright 2017 American Physical Society. (g) Schematic and (h) optical images showing

the photophoretic levitation of a millimeter-sized plate. Adapted with permission from ref 287. Copyright 2021 American Association for the Advancement of Science.
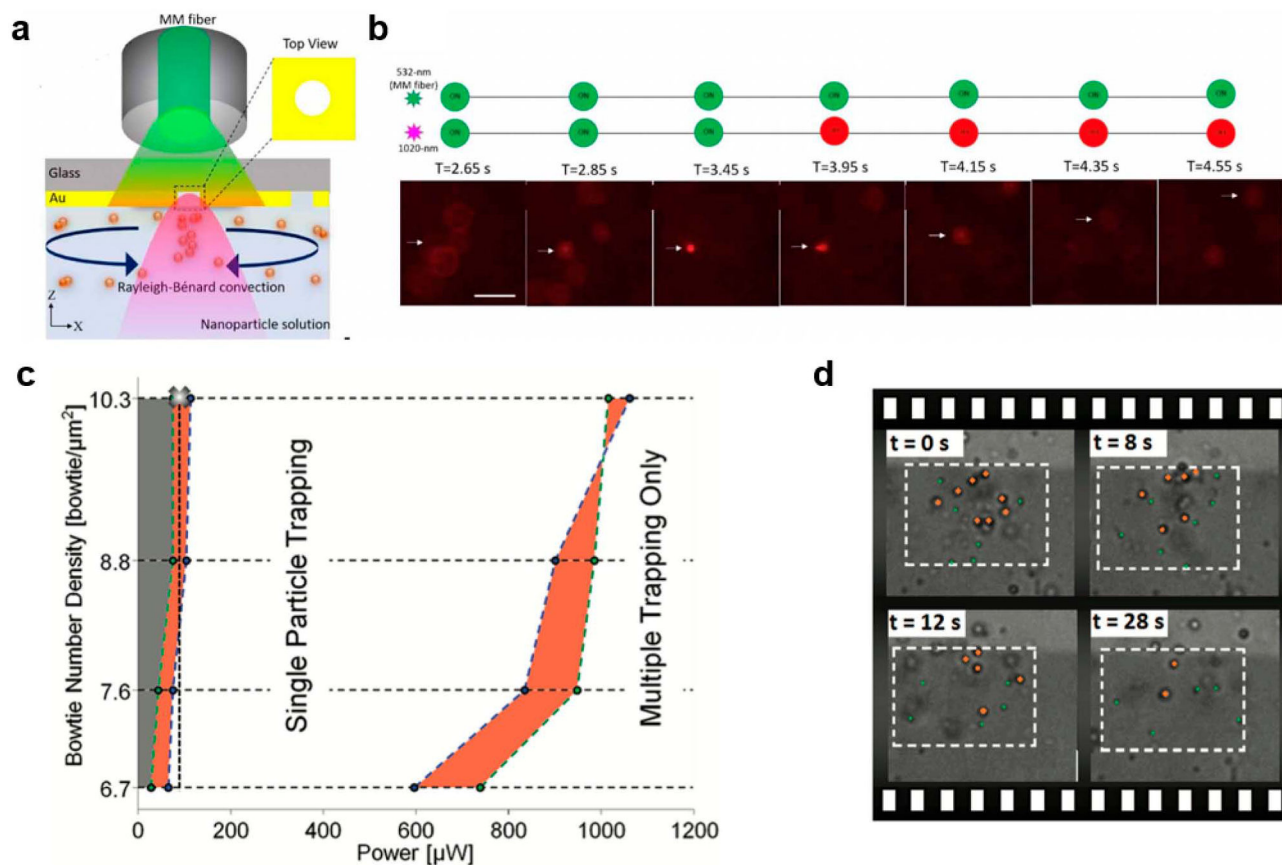
Figure 17.
Optical trapping assisted by natural convection. (a) Schematic of the natural-convection-assisted plasmonic nanoaperture tweezers. (b) Optical images demonstrating the trap and release of a 200 nm fluorescent PS particle assisted by the natural convection flow. Scale bar: 25 μm. Adapted with permission from ref 292. Copyright 2020 American Chemical Society. (c) Hybrid phase diagram of trapping 0.5 and 1.0 μm PS particles on Au bowtie nanoantenna arrays. (d) Optical images showing the trapping of 0.5 μm PS particles and the rejection of 1.0 μm PS particles. The green points indicate 0.5 μm PS particles (trapped), and the orange points indicate 1.0 μm PS particles, which were repelled due to the strong thermal convection. Adapted with permission from ref 293. Copyright 2012 American Chemical Society.
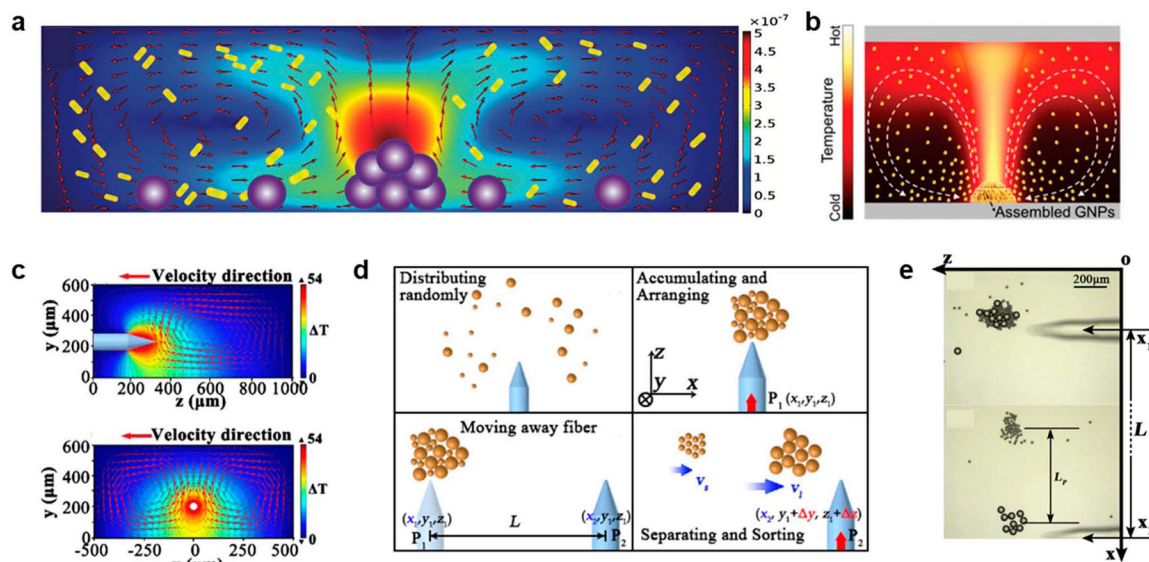
Figure 18.
Optothermal assembly and sorting based on natural convection. (a) Schematic showing the natural convection flows (with a unit of m s^{-1}) due to the light absorption of suspended Au nanorods. The convective flow concentrated hydrogel microparticles at the center of the laser spot. Adapted with permission from ref 300. Copyright 2017 Wiley-VCH. (b) Schematic showing the directed assembly and patterning of Au nanoparticles on generic substrates based on natural convection. Au nanoparticles serve as the light-absorbing medium for the optothermal generation of natural convection. Adapted with permission from ref 295. Copyright 2018 Wiley-VCH. (c) Two cross-sectional views of simulated velocity field induced by light absorption of water solution and the resultant optical heating. (d) Schematic showing the sorting process based on the thermal convection. (e) Optical images show the sorting of PS particles of different sizes. L is the displacement of the fiber tip. L_P represents the separation after the sorting. Adapted with permission from ref 72. Copyright 2016 The Optical Society.
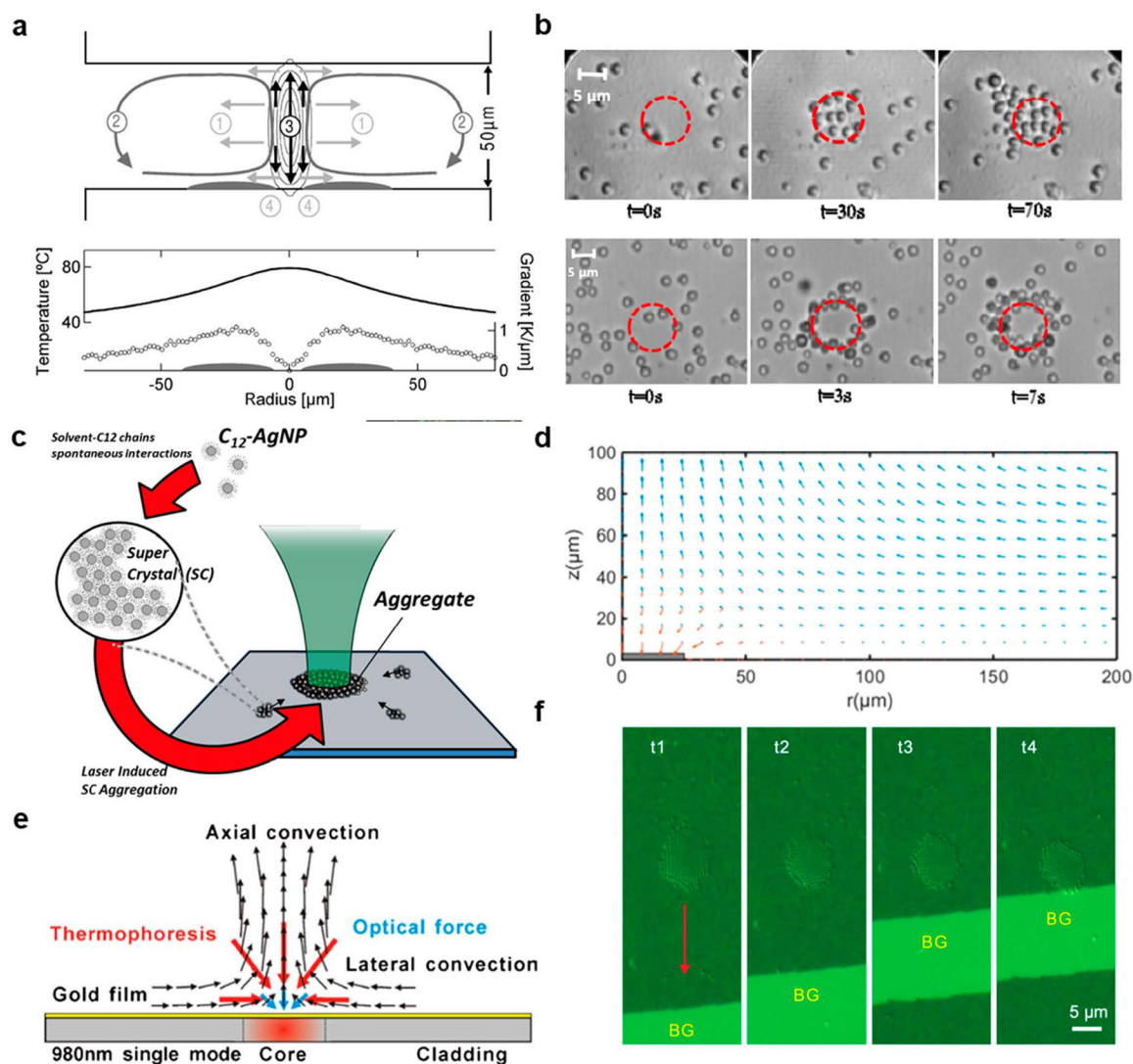
Figure 19.
Optical manipulation based on natural convection combined with thermophoresis. (a) Schematic showing the formation of ring-shaped particle assemblies based on the interplay of thermophoresis and natural convection. Adapted with permission from ref 302. Copyright 2002 American Physical Society. (b) Particle accumulation around the laser spot at an incident power of 0.8 mW (top) and 6 mW (bottom). Adapted with permission from ref 68. Copyright 2015 The Optical Society. (c) Schematic showing the formation of supercrystals based on negative thermophoresis and natural convection. (d) Simulated velocity field around the aggregation. Blue and red arrows correspond to the contribution of natural convection and thermophoresis, respectively. Adapted with permission from ref 288. Copyright 2018 American Chemical Society. (e) Schematic showing the long-range trapping mechanism based on natural convection, negative thermophoresis, and optical force. Adapted with permission from ref 307. Copyright 2015 The Optical Society. (f) Optical images showing the manipulation of assembled PS particles by moving the laser spot. BG, bare glass. Adapted with permission from ref 77. Copyright 2015 Springer Nature.
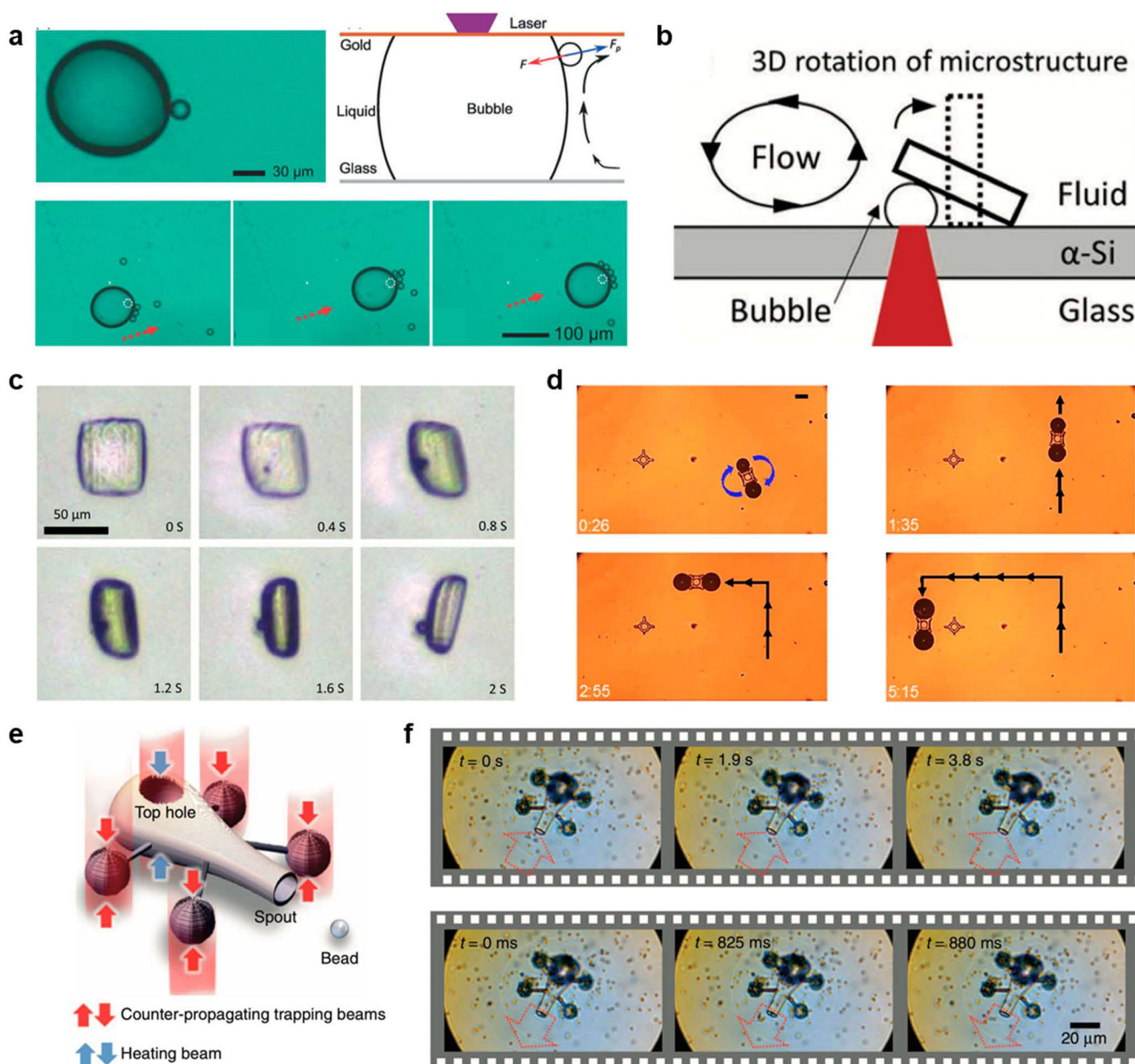
Figure 20.
Optical trapping and transport based on optothermal bubbles. (a) Illustrated working mechanism and optical images of particle manipulation via optothermal bubbles. Adapted with permission from ref 318. Copyright 2014 The Royal Society of Chemistry. (b) Working principle and (c) optical images of out-of-plane rotation of microstructures based on optothermal microbubbles. Adapted with permission from ref 320. Copyright 2019 Wiley-VCH. (d) Optical images showing the manipulation of a hydrogel microstructure based on the independent movements of two microbubbles. Scale bar: 100 μm. Adapted with permission from ref 322. Copyright 2017 Springer Nature. (e) Schematic of a vehicle-like microstructure or microrobot. It can move with full six degrees of freedom by controlling four trapping beams (red arrows). A heating laser beam (blue arrow) propagates through

the top hole to irradiate the deposited metallic layer on the hole wall for the generation of optothermal bubbles. (f) Optical images show the loading and unloading of particles based on optothermally controlled Marangoni convection at the bubbles inside the hole of the robot. Adapted with permission from ref 324. Copyright 2016 Springer Nature.
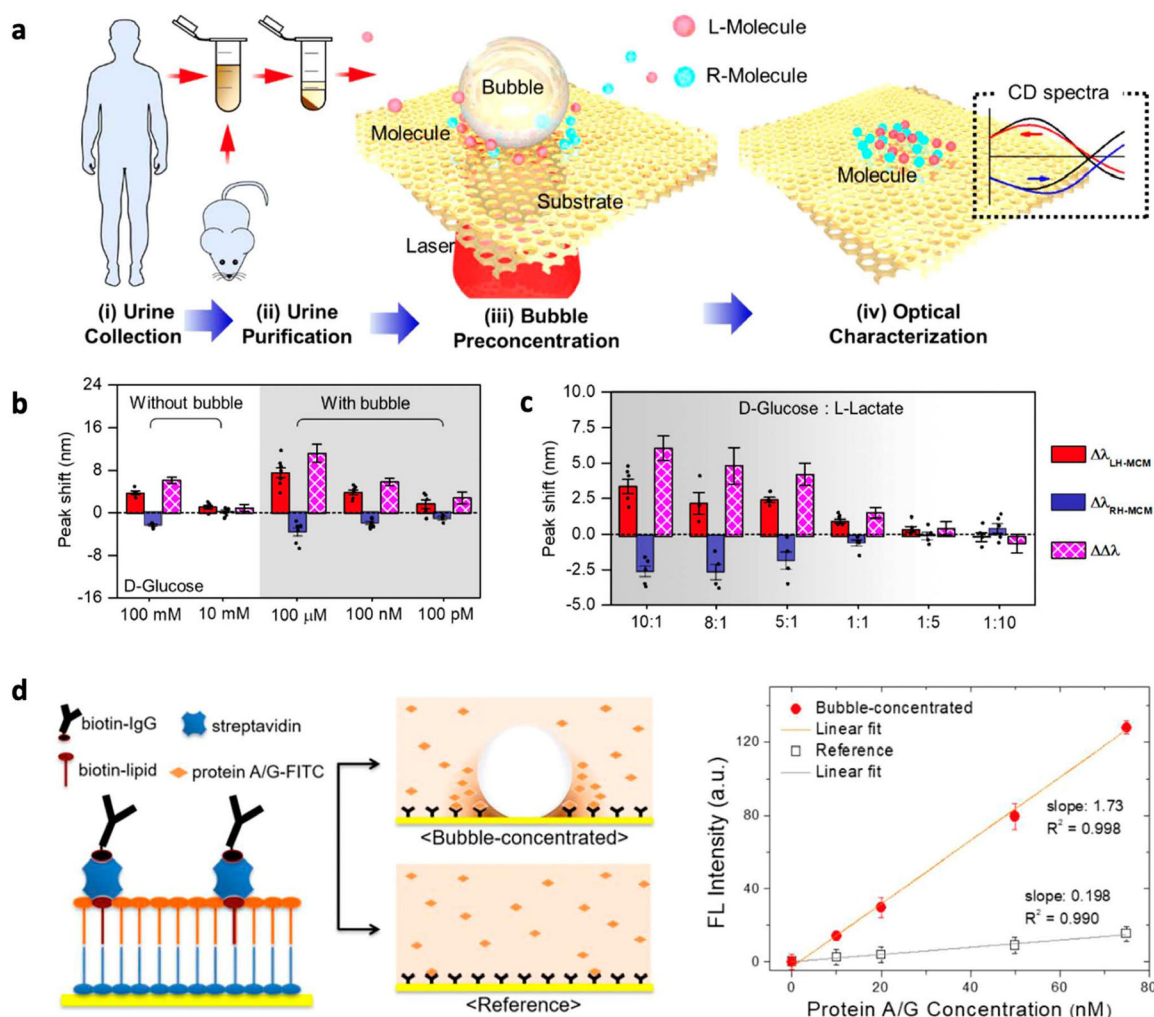
Figure 21.
Optical accumulation and printing of biomolecules based on optothermal bubbles for enhanced biosensing. (a) Schematic showing the working mechanism of optothermal-bubble-assisted chiral sensing on the plasmonic moiréchiral metamaterials. (b) CD spectral shifts (λ) and dissymmetry factors (λ) of D-glucose without or with bubble-assisted accumulation at different concentrations. (c) CD spectral shifts (λ) and dissymmetry factors (λ) of D-glucose and L-lactate mixtures of varying ratios with the bubble-enabled accumulation. Adapted with permission from ref 341. Copyright 2021 American Chemical Society. (d) Schematic (left) and corresponding fluorescence (FL) intensity (right) showing the bubble-enhanced surface capture and sensing of proteins. For each FL measurement, the bubble accumulation lasted for 1 min while the reference sample was incubated for 30 min. Adapted with permission from ref 339. Copyright 2020 American Chemical Society.
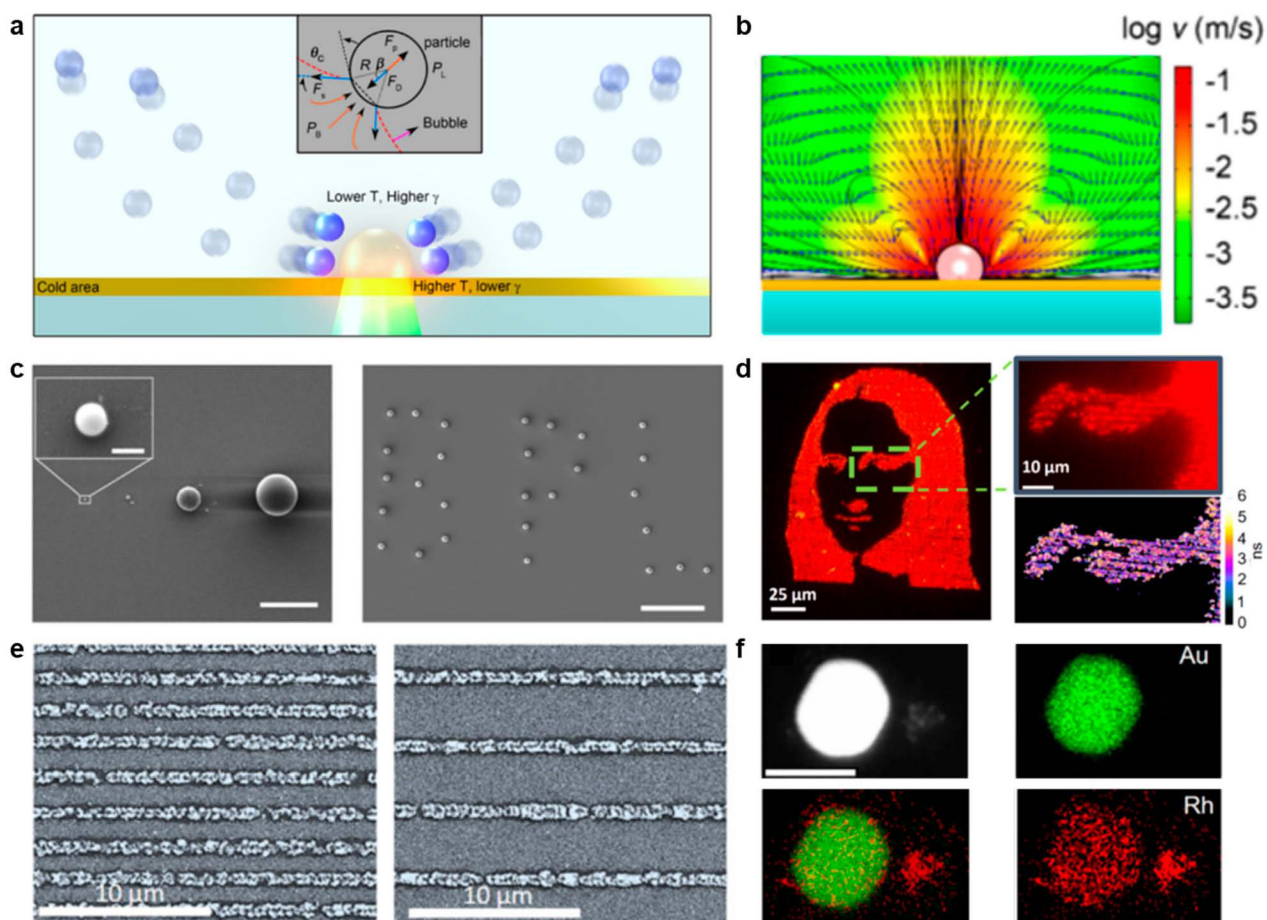
Figure 22.
Optical printing and synthesis of functional materials based on optothermal bubbles. (a) Schematic illustrating the mechanism of bubble printing. (b) Simulated velocity distribution of a Marangoni convective flow around a 1 μm bubble. (c) Printing single PS particle with different sizes (left) and patterning multiple particles into complex patterns (right). Adapted with permission from ref 217. Copyright 2016 American Chemical Society. (d) Bubble-printed "Mona Lisa" pattern of red quantum dots with fluorescence lifetime mapping. Adapted with permission from ref 347. Copyright 2017 American Chemical Society. (e) Scanning electron micrographs of rhodium–gold nanoalloys with 2 μm (left) and 4 μm (right) interline spacing. (f) High-resolution transmission electron micrographs along with 2D energy-dispersive X-ray spectroscopic mapping of the nanoalloys. Adapted with permission from ref 357. Copyright 2019 Cell Press.
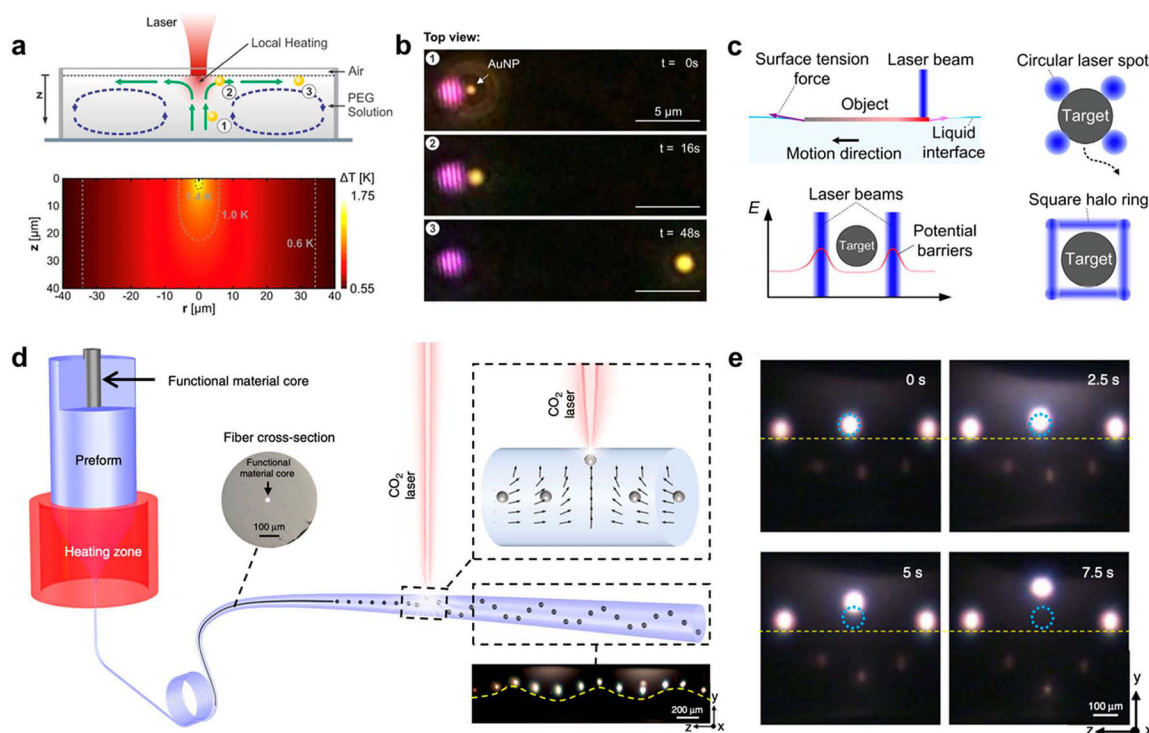
Figure 23.
Optical trapping and transport based on Marangoni convection at pre-existing interfaces under light irradiation. (a) Schematic of the working principle (top) and temperature distribution (bottom) of particle manipulation at the air–solution interface. (b) Dark-field optical images showing the motion of a single 80 nm Au nanoparticle driven by Marangoni convection. Adapted with permission from ref 359. Copyright 2018 The Royal Society of Chemistry. (c) Schematic showing the working principle of trapping and manipulation of small objects via ringlike laser patterns. The laser patterns create potential barriers to trap objects on the liquid–air interface. Adapted with permission from ref 360. Copyright 2021 Elsevier. (d) Schematic showing the working principle of in-fiber particle manipulation based on Marangoni convection occurring at the cladding–core interface. (e) Optical images showing the particle motion guided by the laser beam. Adapted with permission from ref 361. Copyright 2019 Springer Nature.
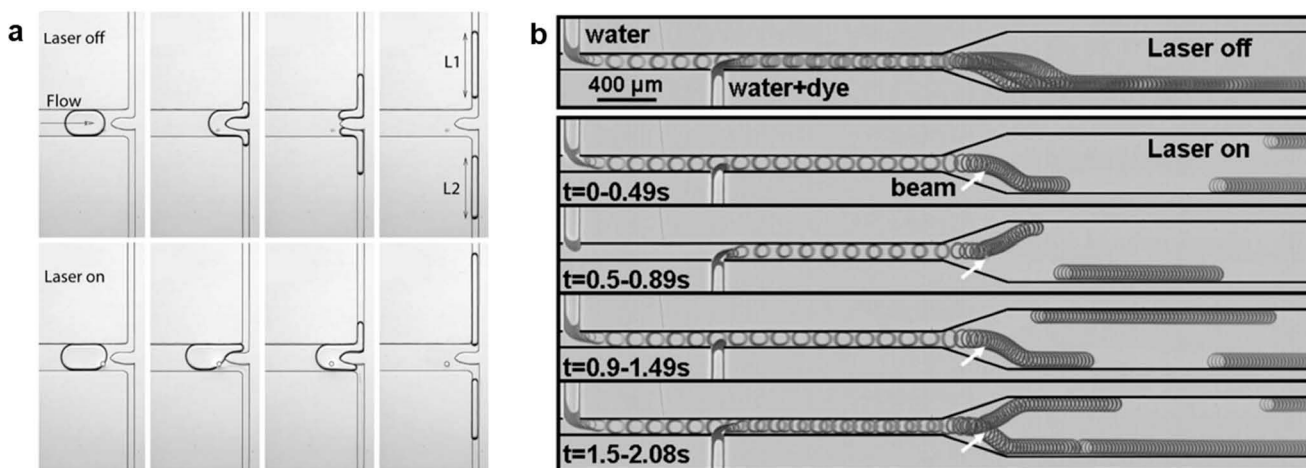
Figure 24.
Optical manipulation of droplets based on Marangoni convection. (a) Optical images showing how Marangoni convection controls the division of droplets. With the heating laser off, the droplet was divided evenly into two daughter droplets (top). With the heating laser on, two uneven daughter droplets were generated (bottom). Adapted with permission from ref 367. Copyright 2007 The Royal Society of Chemistry. (b) Sorting of pure water and water–dye droplets based on optothermally induced Marangoni effect at the droplets. Each of the images was obtained by superimposing ~200 frames of individual images. Adapted with permission from ref 369. Copyright 2008 American Institute of Physics.
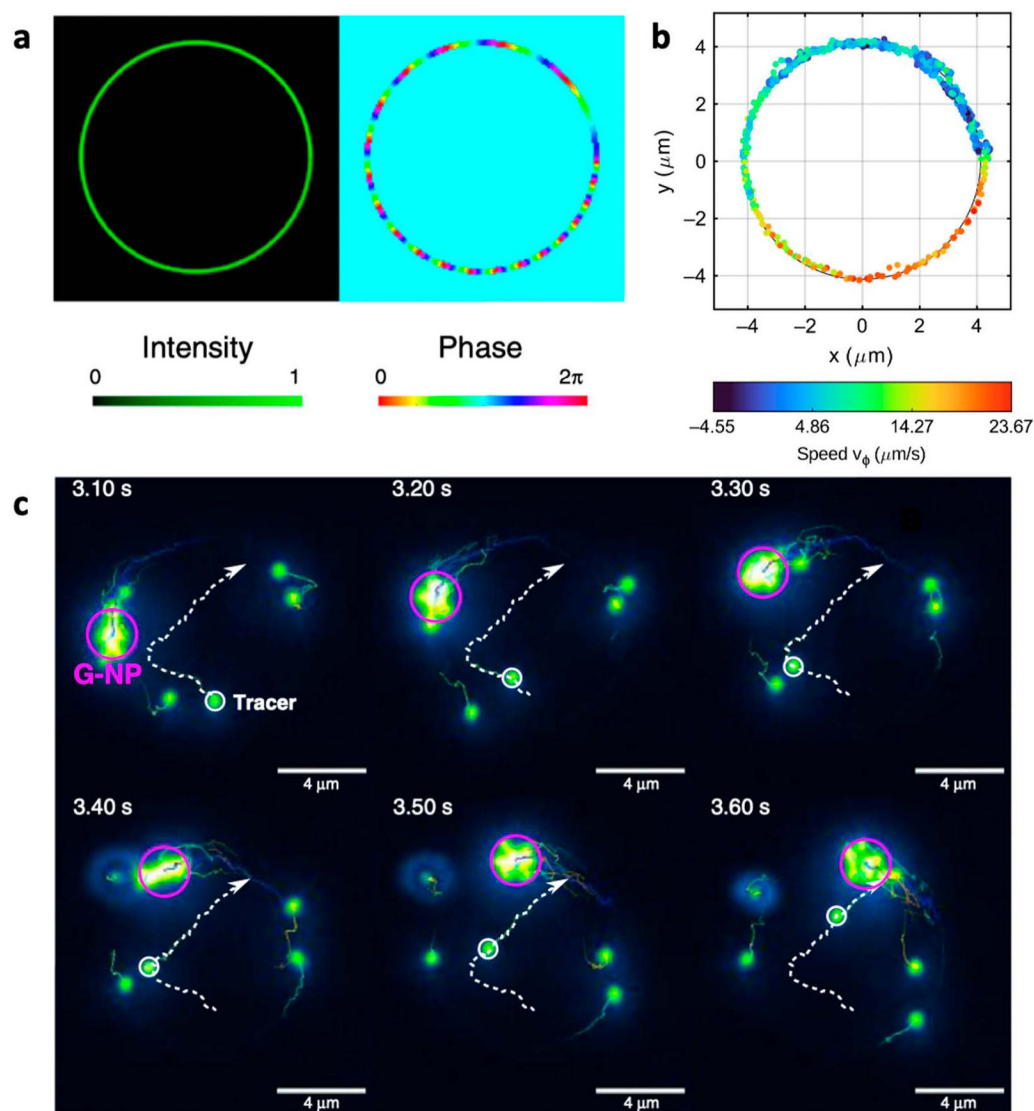
Figure 25.
Optothermal assembly of AuNPs based on structured-light irradiation coupled with Marangoni convection. (a) Intensity (left) and phase (right) distribution of the structured incident laser beam. (b) Trajectories and velocities of single AuNPs powered by structured light. (c) Dark-field optical image showing the formation and transport of a group of AuNPs. The white dashed line indicates the trajectory of a trace particle. Adapted with permission from ref 41. Copyright 2020 Springer Nature.
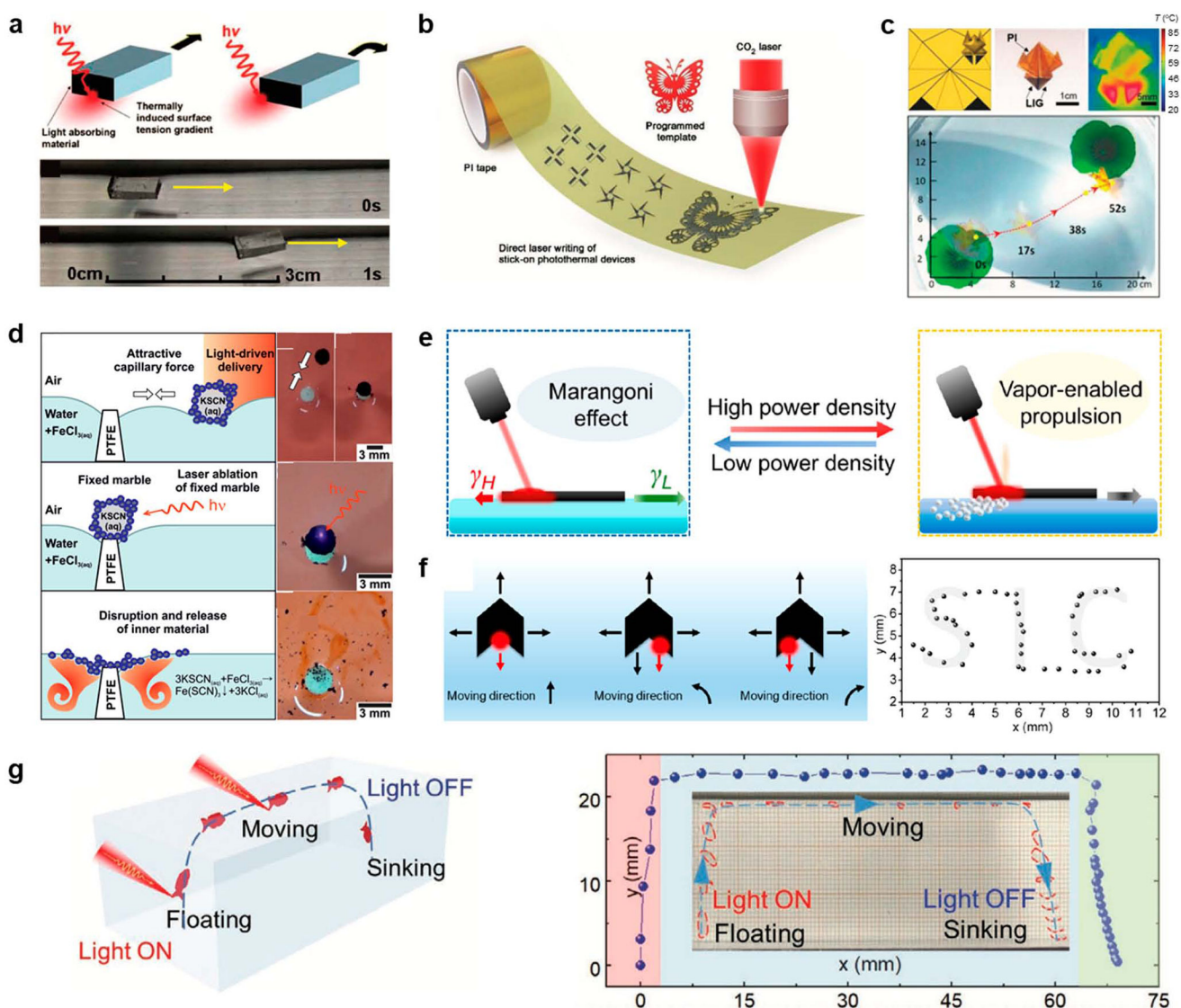
Figure 26.
Optothermal Marangoni swimmers. (a) Working principle and directional motion of optothermal Marangoni swimmers composed of a PDMS block with one side coated with vertically aligned carbon nanotube forests. Adapted with permission from ref 377. Copyright 2009 American Chemical Society. (b) Schematic showing the direct laser writing on the PI tape for the fabrication of optothermal Marangoni swimmers. (c) Origami template, optical image, thermography image, and directed movement of a 3D origami froglike swimmer powered by focused sunlight. Adapted with permission from ref 382. Copyright 2021 Wiley-VCH. (d) Schematics and optical images showing delivery, fixing, and disruption/release of the liquid marble powered by NIR laser irradiation. Adapted with permission from ref 376. Copyright 2016 Wiley-VCH. (e) Schematic showing the dual-mode propulsion of the optothermal-paper-based swimmer. (f) Schematic and trajectory showing directional control of the swimmer by manipulating the laser beam position. Adapted with permission from ref 380. Copyright 2020 American Chemical Society. (g) Schematic and experimental

demonstration of an optothermal swimmer with 3D motion. Adapted with permission from ref 381. Copyright 2021 Wiley-VCH.
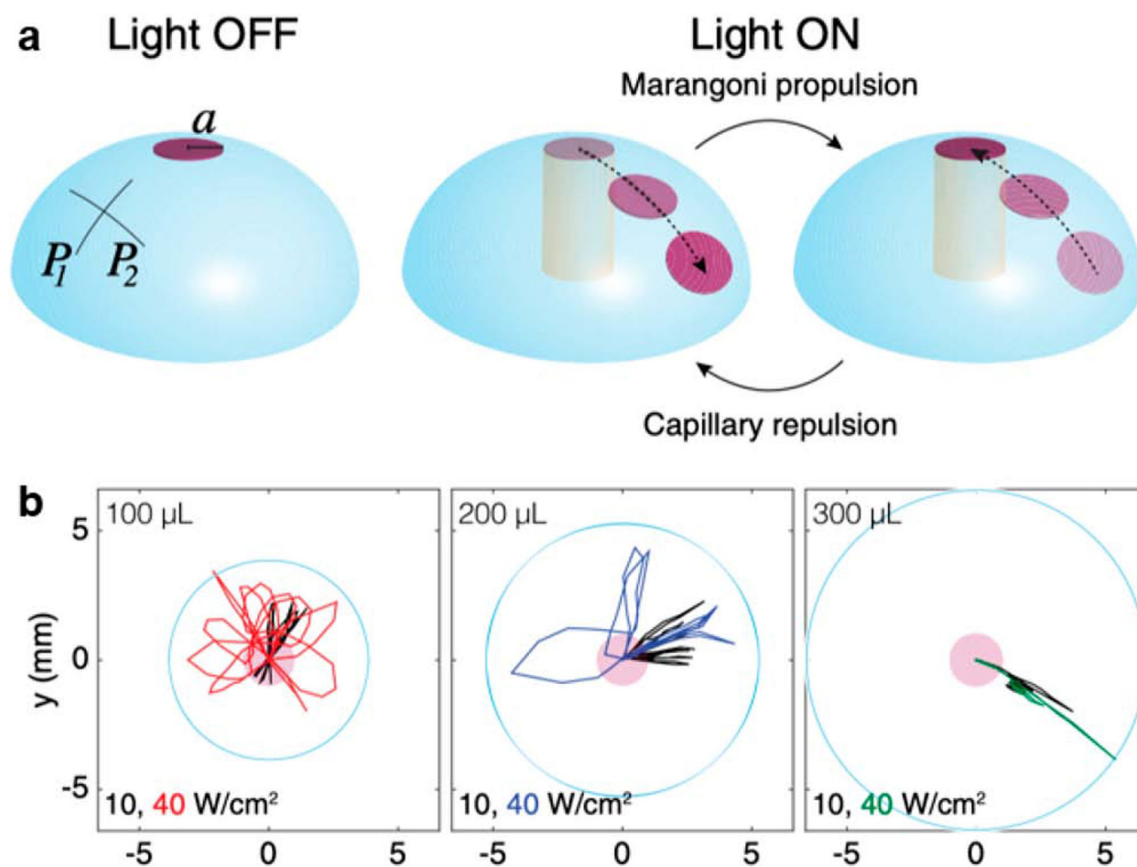
Figure 27.
Opto-thermocapillary oscillators. (a) Schematic showing the working principle of the oscillation of a gel disc under laser irradiation. (b) Top-view trajectories of the illuminated gel disc under different laser intensities and droplet volumes. Adapted with permission from ref 383. Copyright 2018 American Physical Society.
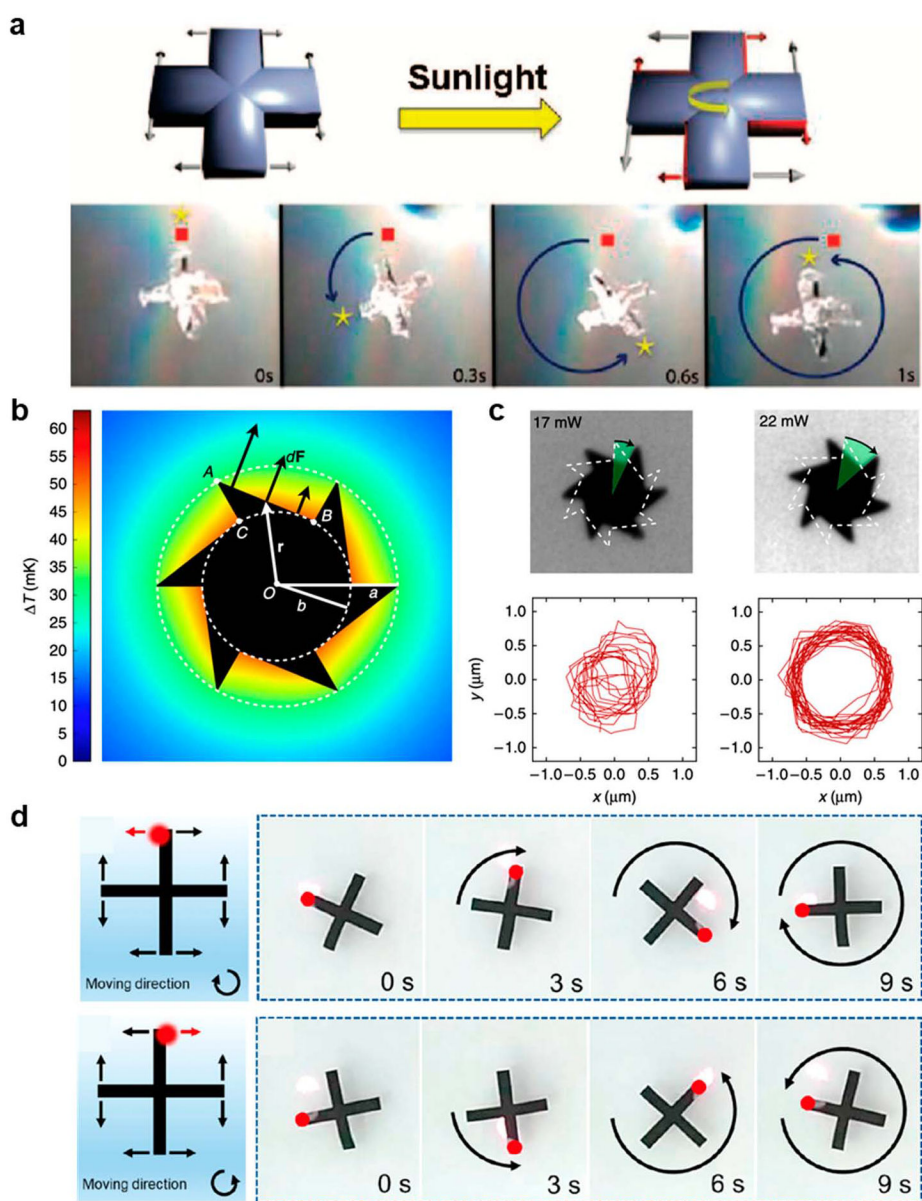
Figure 28.

Optothermal Marangoni rotors. (a) Schematic and optical images showing the rotation of a cross-shaped Marangoni rotor with light-absorbing material embedded on the clockwise face of each fin. Adapted with permission from ref 377. Copyright 2009 American Chemical Society. (b) Simulation of the temperature distribution at the light-irradiated rotor. A, B, and C represent different intersection points, respectively, while a and b are the outer and inner radii of the rotor, respectively. (c) Trajectories of the rotational rotor driven by laser beams with different powers. Adapted with permission from ref 256. Copyright 2015 Springer Nature. (d) Clockwise (top) and counterclockwise (bottom) rotation of the cross-shaped rotor at the liquid–air interface. Adapted with permission from ref 380. Copyright 2020 American Chemical Society.
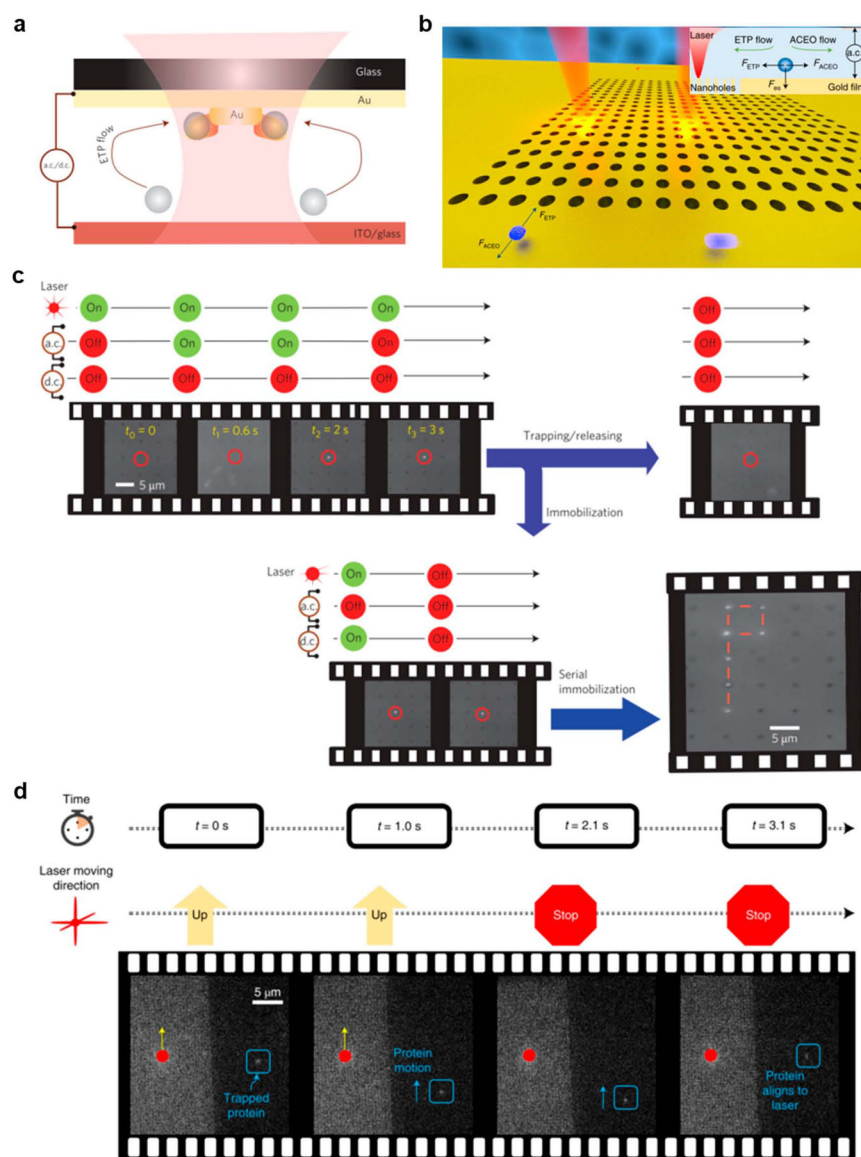
Figure 29.
ETP-flow-assisted optothermal tweezers. (a) Schematic and working principle of hybrid ETP nanotweezers. (b) Schematic of the optothermo-electrohydrodynamic tweezers. The inset demonstrates the forces acting on the particle. ACEO flow, ac electro-osmotic flow. (c) Trapping, releasing, and immobilization of a single nanoparticle using hybrid ETP nanotweezers. (d) Sequential images showing the dynamic manipulation of a single protein molecule. The red dots indicate the laser positions. (a, c) Adapted with permission from ref 155. Copyright 2016 Springer Nature. (b, d) Adapted with permission from ref 78. Copyright 2020 Springer Nature.
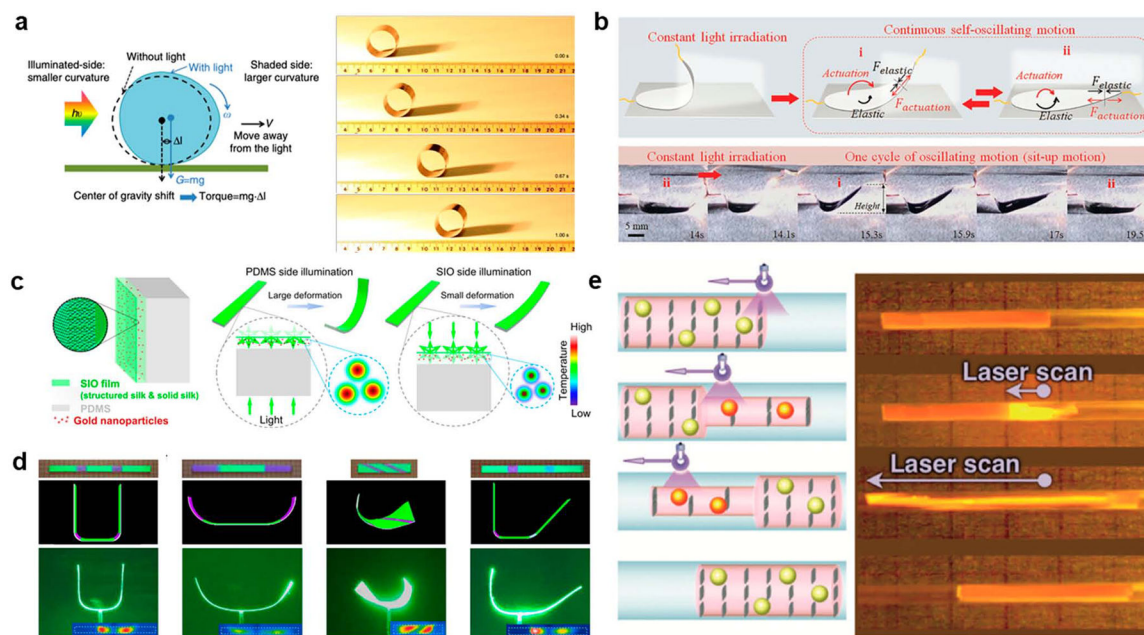
Figure 30.
Optothermal actuators, motors, and robots based on thermal expansion. (a) Schematic (left) and optical images (right) showing the directional motion of a cylindrical motor upon tilted laser irradiation. Adapted with permission from ref 402. Copyright 2014 Springer Nature. (b) Schematic (top) and optical images (bottom) showing the self-sustained oscillation of a CNT/PDMS optothermal actuator via the self-shadowing effect. Adapted with permission from ref 395. Copyright 2020 Wiley-VCH. (c) Schematic showing the composition of the silk PC/PDMS bimorph structure and its tunable optothermal deformation. (d) Schematic (top) and optical images (bottom) showing the programmable deformation by patterning the silk PCs on PDMS layers. The insets are the temperature profiles at the bimorph structures upon laser irradiation. Adapted with permission from ref 80. Copyright 2021 Springer Nature. (e) Schematic (left) and optical images (right) showing the crawling of a titanate nanosheet/AuNP/PNIPAM composite in a tube upon laser scanning. Adapted with permission from ref 396. Copyright 2018 Wiley-VCH.
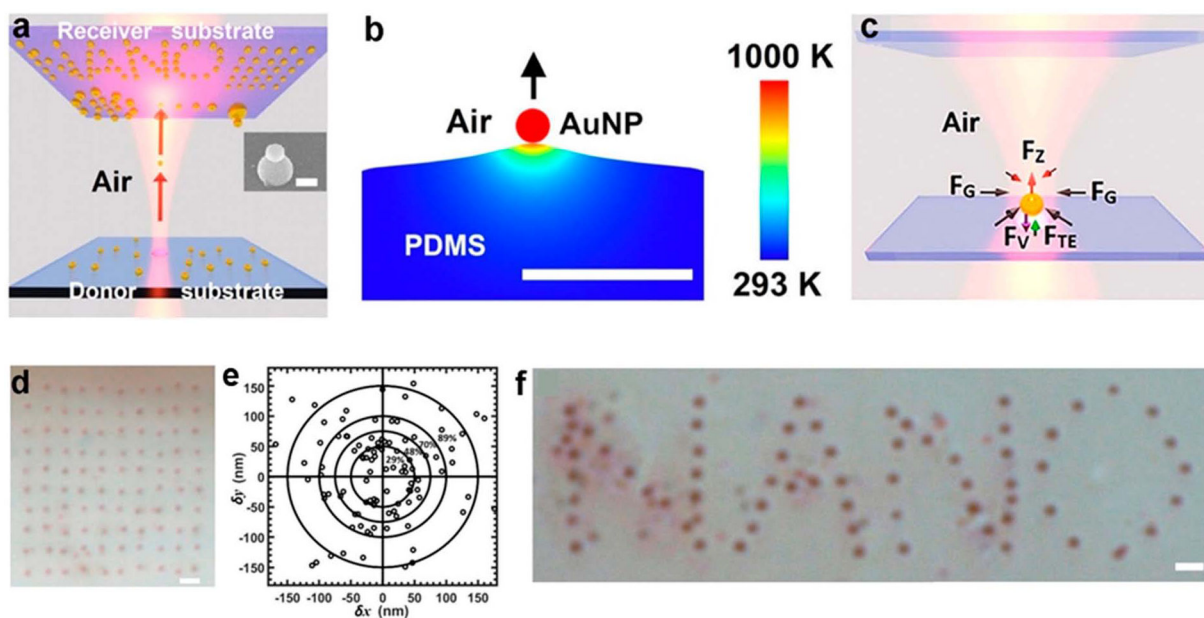
Figure 31.
Out-of-plane optical manipulation on solid substrates. (a) Schematic showing the concept of opto-thermomechanical nanoprinting. (b) Simulated temperature distribution and thermal expansion of the PDMS substrate under laser heating of a 100 nm AuNP. Scale bar: 500 nm. (c) Force analysis for out-of-plane nudging. (d) Array (10×10) of 100 nm Au nanoparticles printed on a glass substrate. Scale bar: 1 μm. (e) Position errors in X and Y direction of each Au particle in the 2D array. (f) Optical image of the printed "NANO" pattern. Scale bar: 1 μm. Adapted with permission from ref 414. Copyright 2020 American Chemical Society.
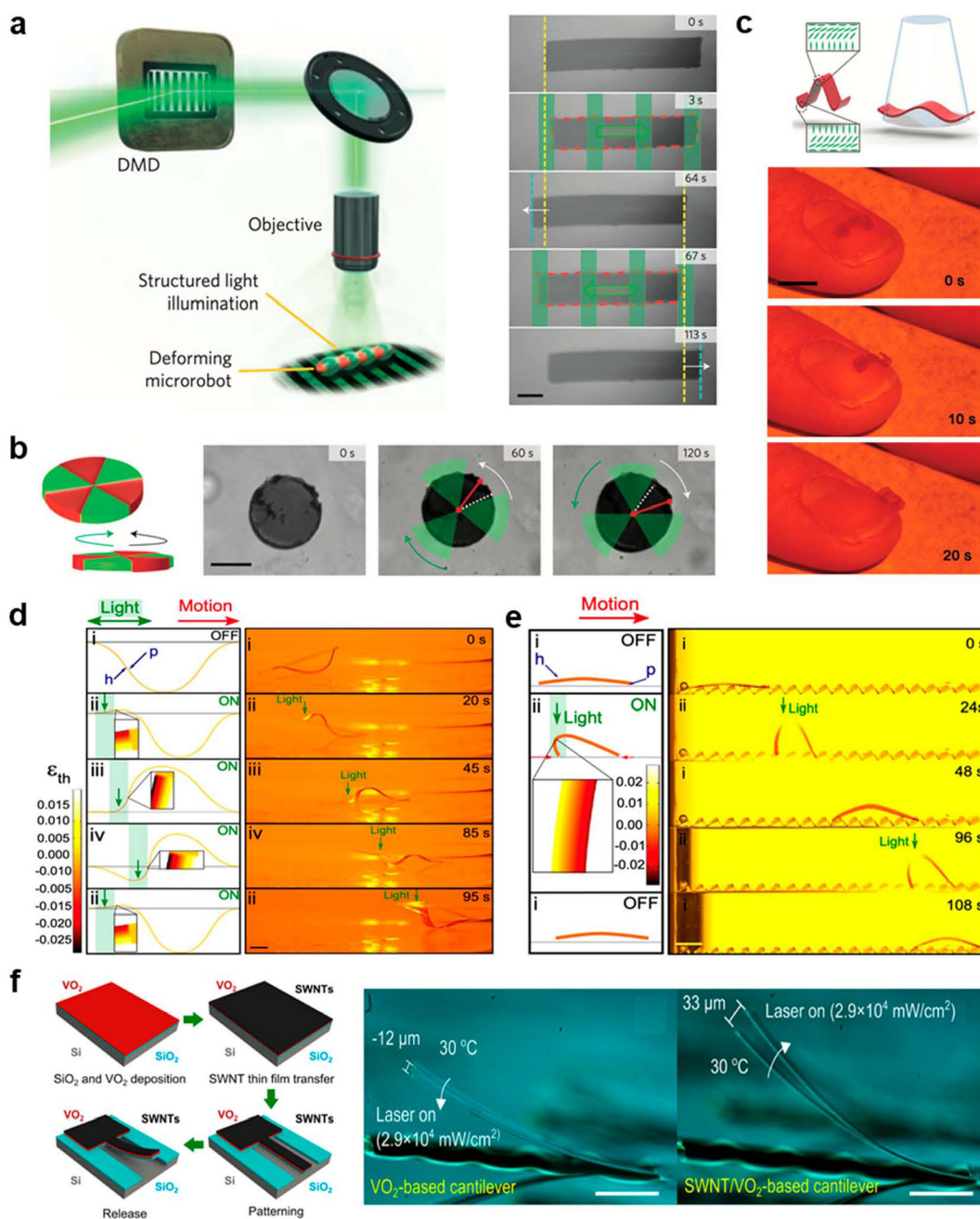
Figure 32.
Optothermal actuators and robots based on phase-transition-induced shape deformation.
(a) Schematic (left) and optical images (right) showing the back-and-forth crawling of
an azobenzene-doped LCE microrobot under a spatiotemporally modulated laser beam.
(b) Schematic (left) and optical images (right) showing the rotation of a LCE disc in an
azimuthal-wave light field. Scale bars: 200 μm. Adapted with permission from ref 257.
Copyright 2016 Springer Nature. (c) Schematic (top) and optical images (bottom) showing
the walking of a LCE paper on the nail of a human finger upon temporally modulated
light irradiation. Scale bar: 5 mm. Adapted with permission from ref 421. Copyright

2018 Wiley-VCH. (d, e) Schematic (with the insets showing thermal strain profiles) and optical images showing the underwater (d) crawling and (e) walking of a liquid-crystal gel paper. Scale bars: 4 mm. Adapted with permission from ref 426. Copyright 2020 National Academy of Sciences. (f) Schematic (left) showing the fabrication process and structure of CNT/VO$_2$ bimorph actuators driven by the optothermal phase transition of VO$_2$ (left) and optical images showing the amplitude difference in the optothermal oscillation of VO$_2$ and CNT/VO$_2$ bimorph actuators (right). Adapted with permission from ref 435. Copyright 2015 American Chemical Society.
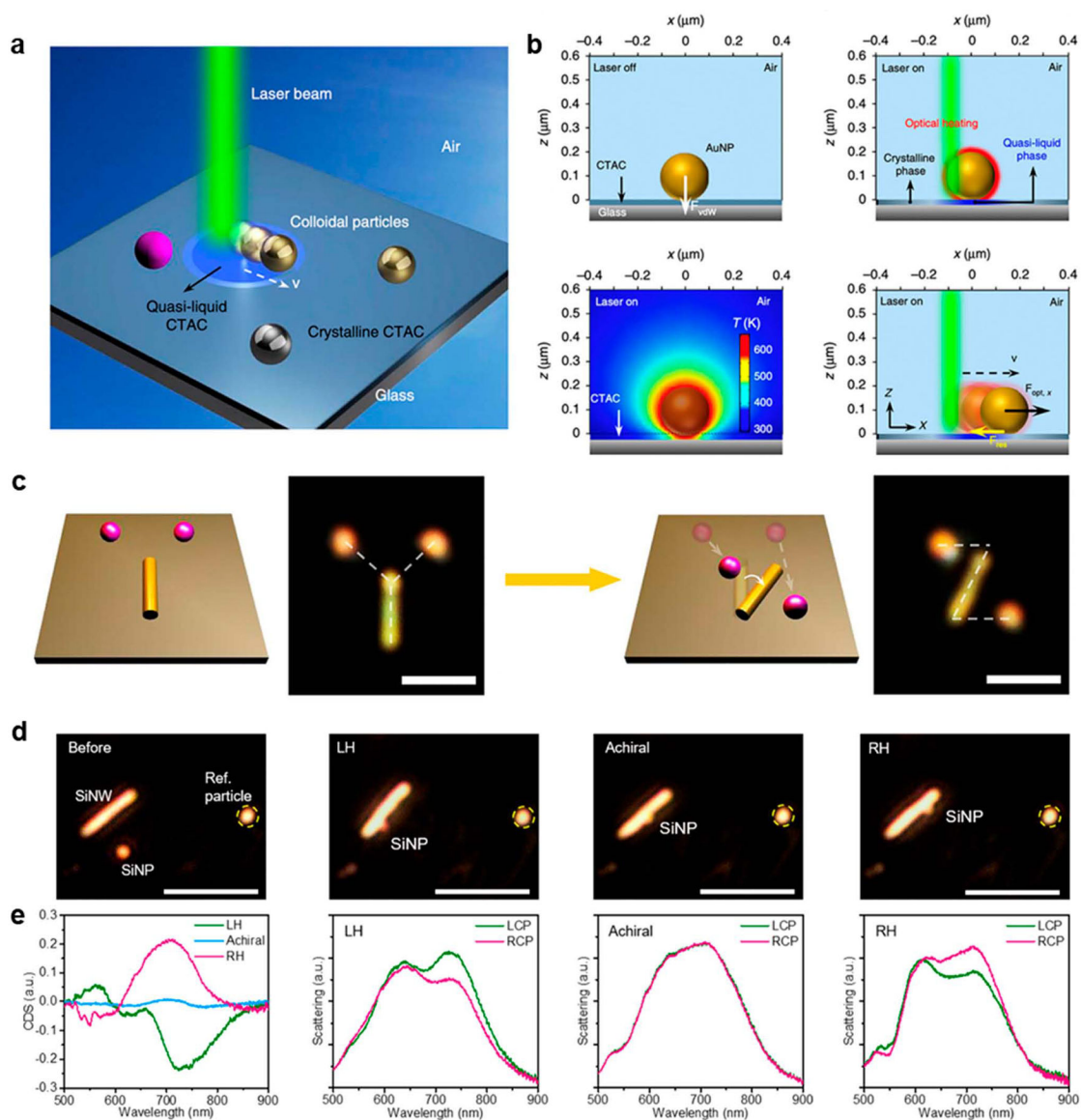
Figure 33.

In-plane optical manipulation on solid substrates. (a) Schematic of OPN on a solid substrate. (b) Working principle of OPN. (c) Schematic and optical images illustrating the reconfigurable patterning of two 500 nm Si nanoparticles and one Au nanowire. Scale bar: 3 μm. Adapted with permission from ref 412. Copyright 2019 Springer Nature. (d) Dark-field images showing the reconfigurable assembly of left-handed (LH) structure, achiral structure, and right-handed (RH) structure in sequence from the dispersed building blocks. (e) Measured optical scattering spectra of the structures in (d) under two types of circularly polarized light (i.e., LCP, left-handed circularly polarized light; RCP, right-handed circularly polarized light) and the corresponding circular differential scattering (CDS) spectra (i.e., $S_{RCP}-S_{LCP}$). Adapted with permission from ref 437. Copyright 2021 American Chemical Society.
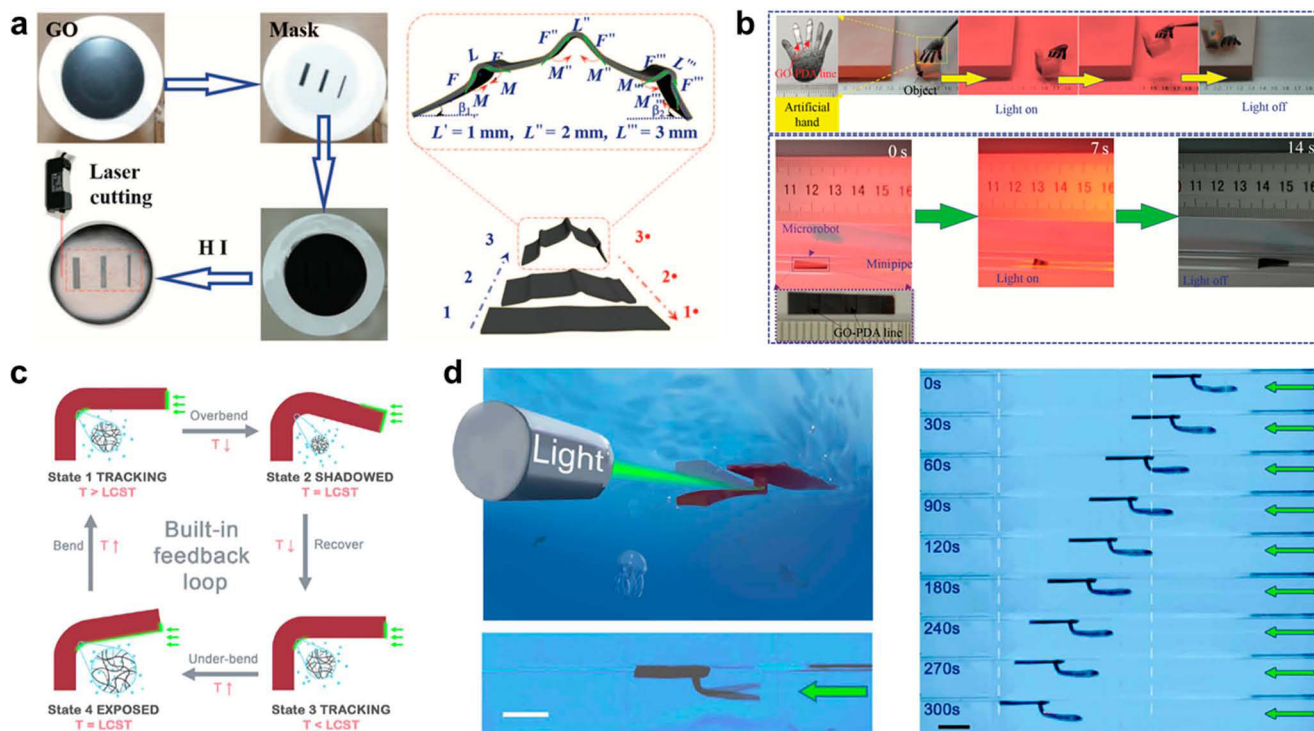
Figure 34.

Optothermal robots based on the shape deformation of materials with temperature-sensitive water sorption and desorption. (a) Schematics showing the fabrication of GO-PDA/rGO papers as walking robots and the mechanical model of the walking behavior. (b) Optical images showing the gripping (top) and crawling (bottom) of the GO-PDA/rGO paper-based robots upon periodic on/off laser irradiation. Adapted with permission from ref 443. Copyright 2015 American Association for the Advancement of Science. (c) Schematic showing the working principle of a self-sustained optothermal oscillator arising from a built-in feedback loop enabled by the self-shadowing effect of the AuNP-embedded PNIPAM hydrogel. LCST, lower critical solution temperature. (d) Schematic and optical images showing the swimming of a soft robot powered by the optothermal self-sustained hydrogel oscillator under constant light irradiation. Adapted with permission from ref 389. Copyright 2019 American Association for the Advancement of Science.
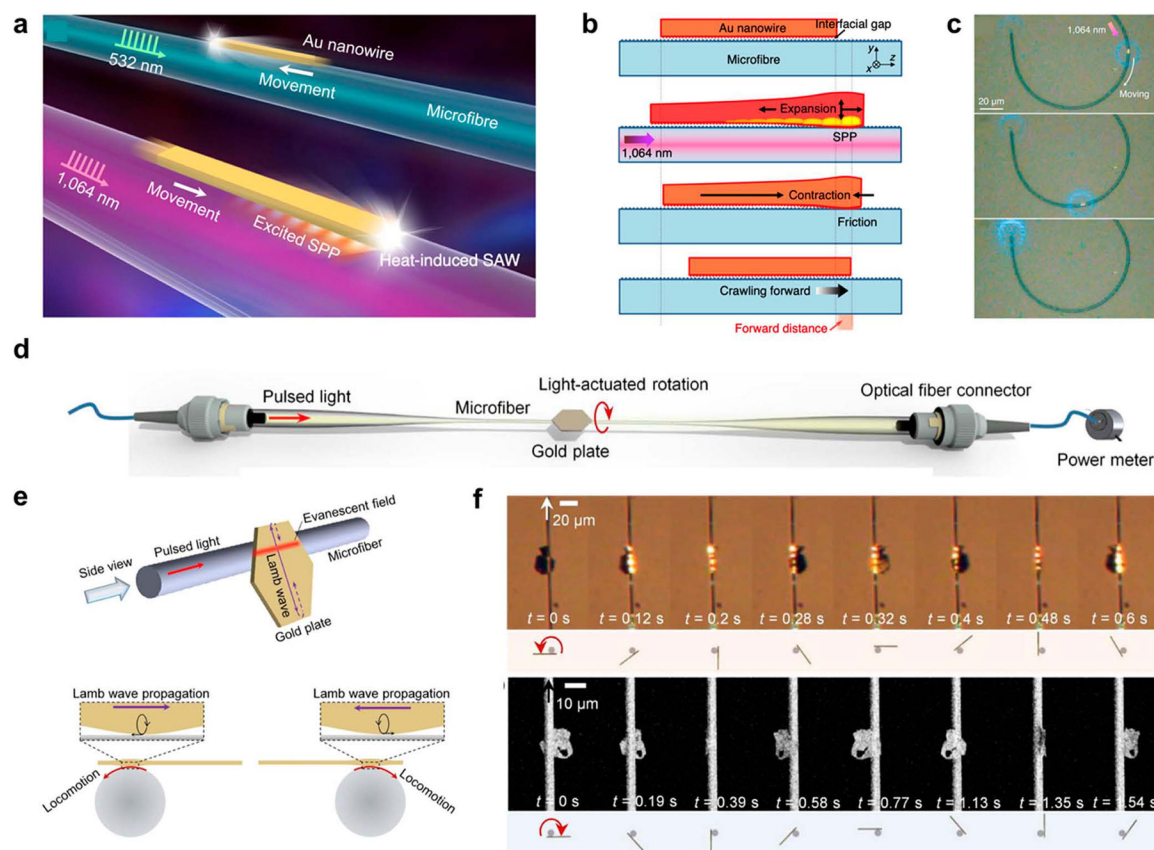
Figure 35.
Crawling and rotation of metal nanostructures driven by optothermally induced surface acoustic waves in nonliquid environments. (a) Schematic showing the crawling of Au nanowires on a microfiber powered by a pulsed laser with different wavelengths. SPP, surface plasmon polaritons. (b) Working mechanism of the Au nanowire's crawling. (c) Optical images showing the movement of a Au nanowire on a C-shaped fiber. Adapted with permission from ref 168. Copyright 2021 Springer Nature. (d) Schematic showing light-actuated rotation of a Au nanoplate around a microfiber. (e) Working mechanism of the Au nanoplate's rotation. The Lamb wave is one type of SAW generated when the thickness of the nanoplate is smaller than the wavelength of the incident light. (f) Optical images and scanning electron micrographs showing the clockwise and anticlockwise rotation of a Au nanoplate around a microfiber. Adapted with permission from ref 454. Copyright 2019 American Association for the Advancement of Science.

Table 1.

Summary of Heat-Mediated Optical Manipulation Techniques

general manipulation mechanisms	manipulation modes	specific working principles	heat sources	manipulation environments	target objects	pros and cons	refs
thermophoresis	tweezing	dynamic heating of ring-shaped nanostructures	substrate	liquid	objects with positive D_T	avoid potential thermal damage × lack dynamic control	208, 210, 212
		interfacial-entropy-driven negative D_T	substrate	liquid	objects with charged surfaces	allow for stable and dynamic tweezing × work in solvents with low ionic strength only	214, 221
		optical cooling	substrate	liquid	objects with positive D_T	avoid potential thermal damage × have limited operational wavelength	98
	swimming	asymmetric optical heating via the structural design of objects	object	liquid	objects with asymmetric light-absorbing response	achieve biocompatible and 3D manipulation × have challenge in directional control	179, 180, 203
		asymmetric optical heating via programmed illumination	object	liquid	objects with homogeneous light absorptivity	allow easy orientational control × are difficult for nanosized objects	10
thermoelectricity	tweezing	spatial separation of ions and surface-charge modification	substrate or object	liquid	all colloidal particles	have low operational power × require additional ions	62, 146, 224
	assembly	interparticle binding by depletion attraction	substrate	liquid	all colloidal particles	are capable of reconfigurable assembly at single-object resolution × have relatively low throughput	225, 230
	swimming, rotation	thermoelectric field by asymmetric optothermal response of the object	object	liquid	Janus particles	achieve directional swimming with two modes × require feedback control	235
diffusiophoresis	assembly	concentration gradients by secondary solutes	substrate	liquid	all colloidal particles	have relatively large working range × require additional solutes × have low accuracy	14, 237
	swimming	concentration gradients by decomposition of binary mixtures	object	liquid	Janus particles	have low working temperature work in 3D × require specific mixtures	181, 241
	rotation	synergy of diffusiophoretic forces and optical forces	object	liquid	objects with randomly distributed absorbing components	possess high rotation speed × require specific mixtures	255
		diffusiophoretic torques by asymmetric heating	object	liquid	objects with asymmetric shapes and absorbing coating	have controllable rotation direction × require specific mixtures	262
photophoresis	pulling, trapping	difference in temperature distribution of objects	object	gas	objects with low absorptivity	work in gaseous medium achieve long-range manipulation × require special design of light in general	276, 281, 282

general manipulation mechanisms	manipulation modes	specific working principles	heat sources	manipulation environments	target objects	pros and cons	refs
natural convection	tweezing	difference in thermal accommodation coefficients of objects	object	gas or liquid	objects with nonuniform thermal accommodation coefficients	work in gaseous medium; are applicable for macroscopic objects; × are relatively more difficult to achieve	285, 287
	assembly	rapid delivery of objects for enhanced optical trapping	substrate	liquid	all colloidal particles	promote trapping efficiency of other optical tweezers; × are not able to solely trap single particles	292, 293
		fast convection-induced accumulation by self-heating	object	liquid	plasmonic nanoparticles	favor free-of-substrate patterning with high throughput; × have low accuracy	295
		fast convection-induced accumulation by external heating sources	substrate or medium	liquid	all colloidal particles	are able to synergize with thermophoresis; × have low accuracy	300, 302
Marangoni convection	tweezing	trapping by optothermal bubble(s)	substrate	liquid	all colloidal particles	demand less on the medium; × have relatively low trapping accuracy; × work for microscale particles in general	318, 322, 324
		particle transport by surface tension at planar fluid–fluid interface	medium or object (liquid droplet)	fluid–air–liquid or liquid–liquid interface	all colloidal particles	operate at low temperature; × are difficult to control the moving direction	359–361
	assembly	fast accumulation by an optothermal bubble	substrate	liquid	all colloidal particles	are capable of continuous printing of objects on substrates; × risk thermally damaging objects	217, 334, 347
		fast accumulation via heated plasmonic nanoparticles	object	liquid	plasmonic nanoparticles	× operate at high temperature	41
	swimming	nudging at the air–liquid interface	object	air–liquid interface	objects with light-absorbing components	work on macroscopic objects; × risk disturbance by surfactants	377, 380, 382
	rotation	asymmetric nudging due to the asymmetric absorbing coatings	object	air–liquid interface	objects with asymmetric coatings	work on macroscopic objects; × risk disturbance by surfactants	256, 377
		asymmetric nudging due to the asymmetric illumination	object	air–liquid interface	nonspherical absorbing objects with rotational symmetric shapes	work on macroscopic objects; × risk disturbance by surfactants; × require dynamic control of light position	380
ETP flow	tweezing	rapid delivery of objects for enhanced plasmonic trapping	substrate	liquid	all colloidal particles	have high flow velocity; × require external electric fields	155
		synergy of the ETP flow and electro-osmotic flow	substrate	liquid	all colloidal particles	are applicable for sub-10 nm objects; have trapping sites away from the laser spot; × require external electric fields	78
	assembly	fast accumulation via ETP flow	substrate	liquid	all colloidal particles	have tunable interparticle spacing; × require external electric fields	387
shape deformation	walking, crawling, oscillating	macroscopic asymmetric shape deformation via asymmetric thermal expansion	object	gas	macroscopic objects with asymmetric CTEs or hydrogels doped	have facile fabrication process; × are difficult to operate in liquid	80, 395, 396

general manipulation mechanisms	manipulation modes	specific working principles	heat sources	manipulation environments	target objects	pros and cons	refs
	nudging, printing	out-of-plane nudging by optical force and thermal-expansion force from substrates	object or substrate	on solid substrate without liquid	with nanosheets with thermally modulated electrostatic repulsion all colloidal particles	3D patterning at sub-100 nm accuracy × work with relatively low throughput	413, 414
	walking, crawling, swimming, oscillating	macroscopic asymmetric shape deformation via inhomogeneous phase transition of objects	object	gas or liquid	macroscopic liquid crystals or shape-memory structures	function in both liquid and gas × possess relatively complicated fabrication process	257, 421, 435
	nudging, assembly	in-plane nudging by local phase transition of solid substrate and optical scattering forces	object or substrate	on solid substrate without liquid	colloidal particles that interact strongly with light	enable reconfigurable 2D patterning at nanoscale accuracy × work with relatively low throughput	412, 437
	walking, swimming, oscillating	macroscopic asymmetric shape deformation via asymmetric water sorption and desorption of hydrogels	object	gas or liquid	macroscopic materials with considerable hydrophilic groups	function in both liquid and gas × require specific humidity in gas or liquid medium for operation	389, 443
	crawling, rotation	lattice expansion and contraction (surface acoustic wave) of objects	object	gas	plasmonic objects	work on nanosized particles × require pulsed laser with selective optical wavelengths	168, 454